Applied Physics Reviews

REVIEW ARTICLE | SEPTEMBER 19 2025

Creation and microscopic origins of single-photon emitters in transition-metal dichalcogenides and hexagonal boron nitride

Special Collection: Quantum Light

Amedeo Carbone ; Diane-Pernille Bendixen-Fernex de Mongex ; Arkady V. Krasheninnikov ; Martijn Wubs ; Alexander Huck ; Thomas W. Hansen ; Alexander W. Holleitner ; Nicolas Stenger ; Christoph Kastl

Check for updates

Appl. Phys. Rev. 12, 031333 (2025)
https://doi.org/10.1063/5.0278132

View Online
Export Citation

Articles You May Be Interested In

Noble-transition-metal dichalcogenides-emerging two-dimensional materials for sensor applications

Appl. Phys. Rev. (July 2023)

Strain engineering of the transition metal dichalcogenide chalcogen-alloy WSSe

J. Appl. Phys. (June 2024)

Predicting the structure and stability of oxide nanoscrolls from dichalcogenide precursors

APL Mater. (January 2025)

02 July 2026 15:24:17

AIP Advances
Why Publish With Us?
21DAYS average time to 1st decision
OVER 4 MILLION views in the last year
INCLUSIVE scope
Learn More
AIP Publishing

AIP Publishing

Applied Physics Reviews REVIEW pubs.aip.org/aip/are

Creation and microscopic origins of single-photon emitters in transition-metal dichalcogenides and hexagonal boron nitride

Cite as: Appl. Phys. Rev. **12**, 031333 (2025); doi: 10.1063/5.0278132
Submitted: 28 April 2025 · Accepted: 3 September 2025 ·
Published Online: 19 September 2025

View Online Export Citation CrossMark

Amedeo Carbone,[1,2,3] Diane-Pernille Bendixen-Fernex de Mongex,[4] Arkady V. Krasheninnikov,[5] Martijn Wubs,[1,2] Alexander Huck,[6] Thomas W. Hansen,[4] Alexander W. Holleitner,[3,7,8,a)] Nicolas Stenger,[1,2,b)] and Christoph Kastl[3,7,8,c)]

AFFILIATIONS

[1]Department of Electrical and Photonics Engineering, Technical University of Denmark, 2800 Kgs, Lyngby, Denmark
[2]NanoPhoton—Center for Nanophotonics, Technical University of Denmark, 2800 Kgs, Lyngby, Denmark
[3]Walter Schottky Institute, Technical University of Munich, Am Coulombwall 4a, 85748 Garching, Germany
[4]Nanolab—National Centre for Nano Fabrication and Characterization, Technical University of Denmark, 2800 Kgs, Lyngby, Denmark
[5]Institute of Ion Beam Physics and Materials Research, Helmholtz-Zentrum Dresden-Rossendorf, 01328 Dresden, Germany
[6]Center for Macroscopic Quantum States (bigQ), Department of Physics, Technical University of Denmark, 2800 Kgs, Lyngby, Denmark
[7]Munich Center for Quantum Science and Technology (MCQST), Schellingstr. 4, 80799 Munich, Germany
[8]TUM International Graduate School of Science and Engineering (IGSSE), Boltzmannstr. 17, 85748 Garching, Germany

Note: This paper is part of the Special Topic, Quantum Light.
[a)]**Electronic mail:** holleitner@wsi.tum.de
[b)]**Electronic mail:** niste@dtu.dk
[c)]**Author to whom correspondence should be addressed:** christoph.kastl@wsi.tum.de

ABSTRACT

We highlight recent advances in the controlled creation of single-photon emitters in van der Waals materials and in the understanding of their atomistic origin. We focus on quantum emitters created in monolayer transition-metal dichalcogenide semiconductors, which provide spectrally sharp single-photon emission at cryogenic temperatures, and the ones in insulating hBN, which provide bright and stable single-photon emission up to room temperature. After introducing the different classes of quantum emitters in terms of band-structure properties, we review the defect creation methods based on electron and ion irradiation as well as local strain engineering and plasma treatments. A main focus of the review is put on discussing the microscopic origin of the quantum emitters as revealed by various experimental platforms, including optical and scanning probe methods.

© 2025 Author(s). All article content, except where otherwise noted, is licensed under a Creative Commons Attribution (CC BY) license (https://creativecommons.org/licenses/by/4.0/). https://doi.org/10.1063/5.0278132

TABLE OF CONTENTS

I. INTRODUCTION 1
II. CLASSES OF OPTICALLY ACTIVE DEFECTS 3
III. FUNDAMENTALS OF IRRADIATION ENGINEERING 4
IV. STRAIN ENGINEERING 5
V. PLASMA TREATMENT 7
VI. ION IRRADIATION 8
VII. ION IMPLANTATION 9
VIII. E-BEAM IRRADIATION 11
IX. X-RAY AND UV IRRADIATION 13
X. MICROSCOPIC NATURE OF THE EMITTERS 13
A. For hBN 13
B. For TMDCs 17
XI. TOWARD ATOMISTIC CONTROL AND CHARACTERIZATION 19
XII. CONCLUSION AND OUTLOOK 19
A. Outlook and future directions 20
B. Toward a systematic and predictive framework . . . 20

I. INTRODUCTION

On-chip sources of single photons are important building blocks for applications in quantum communication, computing, simulation,

02 July 2026 15:24:17

© Author(s) 2025

and metrology.[1–3] Single-photon emitters (SPEs) in layered bulk and two-dimensional (2D) van der Waals (vdW) materials, originally discovered in atomically thin semiconductors,[4–9] insulators,[10] and vdW heterostructures,[11] are being explored as an emerging solid-state platform,[12–17] which is complementary to established technologies, such as semiconductor quantum dots[18] or color centers in diamond.[19] Layered vdW materials promise not only ease of hybrid integration but also opportunities for monolithic integration[14,20] into larger photonic circuits, for example, waveguides,[9,21,22] cavities,[23,24] microlenses,[25] detectors,[26] or electronic circuits.[27] In initial studies, SPEs were randomly discovered at the edges or folds of crystals,[4–8] suggesting that mechanical strain plays a major role in their creation or activation, not only making them distinct from other solid-state SPEs but also offering the possibility to create and tune their properties via strain fields.[28–31] Recent advances in methods for creating quantum emitters, for example, using irradiation[32–41] and strain engineering,[42–56] have opened a route for scalable, nanoscale integration of SPEs with unparalleled positioning accuracy.[36,38,44,45,57,58]

To date, the scientific debate about the atomistic origin of single-photon emission in vdW materials has not been conclusively settled for many of the experimentally observed emission lines, despite a decade of extensive research. Defects are commonly assumed to play an essential role in enabling single-photon emission,[43,59–63] and their atomic structure can be inferred, in particular, for monolayer transition-metal dichalcogenides (TMDCs), from atomic resolution microscopy, such as scanning tunneling microscopy (STM), non-contact atomic force microscopy (AFM), or aberration-corrected scanning transmission electron microscopy (STEM),[58,62,64–69] as well as from atomistic calculations based on *ab initio* approaches, such as density functional theory (DFT).[70–76] Nevertheless, establishing a direct link between the atomic structure and the optical signature of defects has proven to be difficult. In particular, the microscopic nature of quantum emitters present in hexagonal boron nitride (hBN) is still largely under debate, despite many attempts to compare *ab initio* calculations with experiments.[66,77–82] From a theoretical point of view, predicting the optical properties of defects in a periodic crystal is very demanding. To describe excitonic effects *ab initio*, solving the Bethe–Salpeter equation (BSE) is required with a so-called *GW* correction on top of the electronic structure calculated within the framework of the "conventional" DFT with local or semi-local exchange and correlation functionals. For defects or heterostructures, these calculations require rather large supercells,[74,83] which in turn means that large computational resources are needed to converge the exciton energies to about 10–100 meV.[71,72,75,84] Exciton–phonon coupling, which is especially relevant for room-temperature emitters in hBN, can be included using effective models,[80,85] although full *ab initio* methods are emerging as well.[86–88] Additionally, many optically active defects or defect complexes exhibit charged states resulting in structural modification via, for example, the Jahn–Teller effect,[70,89–92] which at present are difficult to properly account for in *ab initio* calculations. Finally, while the emission spectrum from a single defect is easily detectable, its optical absorption spectrum, which is usually the quantity that *ab initio* calculations predict, is more difficult to access experimentally. In this respect, photoluminescence excitation (PLE) spectroscopy is a suitable tool to gain insights into absorption properties, excited states (ES), and vibronic structure of single defects.[80,93,94] Cavity-enhanced absorption spectroscopy of He ion-irradiated MoS_2 reported quantitative measurements of defect-related sub-gap absorption down to 10^{12} defects/cm^2, which still translates into about 10^3 defects probed within a typical laser spot.[95] By contrast, early reports in GaAs achieved already single-defect sensitivity: cross sections as low as $\sigma \approx 1 \times 10^{-18}$ cm^{-2} could be measured by monitoring current (fluctuations) in vertical tunneling structures upon sub-gap excitation,[96] similar to recent photocurrent experiments on MoS_2/hBN/graphene and strained WSe_2 heterostructures.[97,98]

When aiming to correlate atomic structure and optical functionality, the mismatch in length scales between the actual structure (few Ångstroms) and the spatial resolution in a typical far-field optical experiment (hundreds of nanometers) presents a formidable experimental challenge. Statistical photon counting provides robust, yet not perfect, evidence whether a given emission line stems from a single physical object.[99] It is not perfect because different atomic defects or multiple emission lines with varying emission power may be present within the typical size of a far-field optical detection spot. In this context, optical near-field[100–102] and cathodoluminescence (CL) spectroscopy[82,103] are powerful techniques to investigate quantum emitters in 2D materials beyond the diffraction limit, enabling, for example, the correlation of local strain fields and single-photon emission. Yet, a direct experimental link between the atomic structure of defects, defect-associated electronic states, and their optical emission spectrum will ultimately be necessary to unambiguously establish their atomistic structure–function relationships.[104]

Here, we review recent advances in the controlled creation of SPEs in vdW materials and in the understanding of their atomistic origin. We focus on quantum emitters created by irradiation engineering in direct bandgap TMDC semiconductors, which provide spectrally sharp single-photon emission at cryogenic temperatures, and in insulating hBN, which provide bright and stable single-photon emission up to room temperature. Due to the accelerated expansion of this research field in the past years, we do not aim for completeness. For the present work, we discuss selected representative examples that emphasize irradiation engineering and microscopic origin of single-photon emission. Additionally, we refer the reader to other reviews focusing on different aspects of quantum emitters in van der Waals materials, such as integration into photonic structures,[13,20] electrical control and optoelectronic integration into quantum light-emitting devices,[27] tunability of single-photon emission via strain and electric fields,[105] magneto-optical properties, engineering and coherence of spin defects,[106,107] and integration of 2D material-based quantum emitters into photonic platforms, with a focus on deterministic placement, coupling efficiency, and device scalability for quantum technologies,[3] the role of strain engineering,[108] exciton dynamics and excitonic quantum light generation in vdW heterostructures,[109] in-depth analysis of intrinsic and extrinsic defects in hBN,[110] and computational discovery of defect-based quantum emitters.[111,112] The review is structured as follows. To begin with, we introduce different classes of optically active emitters based on localized exciton states emphasizing the roles of deep vs shallow states, different exciton binding energies, and varying local potentials in the exciton localization and single-photon emission process (Sec. II). We discuss the fundamentals of irradiation engineering of lattice defects in thin vdW materials (Sec. III). Next, we review selected examples of quantum emitters as generated by local strain engineering, where vdW materials provide opportunities to create and tailor SPEs in ways not possible in traditional bulk

02 July 2026 15:24:17

© Author(s) 2025

material systems (Sec. IV). Plasma treatment provides a simple means to introduce optically active defects or defect complexes near the material surface on a large scale (Sec. V). Ion irradiation (Sec. VI) is commonly exploited for the creation of positioned SPEs, either based on the local introduction of single point defects into the host crystal or on the local patterning/sputtering of the host material. Although ion implantation is a powerful workhorse for color center creation in bulk materials, only a few works to date discuss the ion implantation of functional impurities into 2D and quasi-2D vdW materials (Sec. VII). By contrast, electron beam irradiation (Sec. VIII) has attracted significant interest as a simple approach for site-selective creation or activation of single-photon emitters. As an example of non-charged particle irradiation, Sec. IX highlights focused x-ray and UV-light irradiation as a tool to both introduce and spectroscopically interrogate defect states in 2D semiconductors. In the last part, we emphasize the importance of carefully identifying the atomistic origin of SPEs both in hBN and TMDCs (Sec. X). Section XI highlights recent advances toward the correlation of optical properties and structure at the atomic scale, and in an outlook, we address current and future challenges of SPEs in 2D vdW materials (Sec. XII).

II. CLASSES OF OPTICALLY ACTIVE DEFECTS

In hBN, both single-photon emitters and spin defects are mostly associated with deep-level color centers. In TMDCs, however, multiple mechanisms, such as defect-bound excitons and strain localization are relevant, often simultaneously, as discussed in the following. Color centers are typically related to states inside the bandgap due to vacancies, impurities, or complexes thereof that give rise to significant sub-gap absorption, thereby changing the apparent color of the crystal (hence the name color center). If the in-gap states are located sufficiently deep inside the gap, the optical properties of the defect can be understood in an atomic-like picture [Fig. 1(a)]. To first order, interactions with electronic states in the conduction and valence bands can be neglected in this case because of the separation of energy scales (on the order of eV) and because of the localization of the defect states (on the order of a unit cell or less). The localized electrons form a ground state (GS) and several possible excited states (ES), whereby the electron configuration is dictated by group theoretical considerations and exclusion principles according to the symmetries of the defect and the host crystal.[113,114] Direct excitation of the defect into one of the higher-lying excited states can be achieved by efficient absorption of photons at an energy below the optical gap of the host crystal. Single-photon emission then typically occurs from one of the lower-lying excited states after intra-defect relaxation processes and according to the symmetry-allowed dipole selection rules.[114] Single-photon emission can often be observable up to room temperature in wide-gap materials, including hBN. The energy of the absorption and emission lines can be significantly (on the order of eV) below the energy of the bandgap of the host material. Additionally, color centers often have a spin-dependent fine structure that allows control of spin transitions with suitable radio frequency or microwave fields. This enables optically detected magnetic resonance (ODMR) measurements[115–118] or coherent excitation and readout of spin states, e.g., for the V_B^- defect in hBN.[119,120] In general, color centers interact very efficiently with local vibronic excitations (or local phonon modes), in particular for heavy impurities or defects with large structural distortions. For hBN, this often results in complex emission spectra with multiple series of phonon sidebands below the zero-phonon line.[80,85,121,122]

By contrast, Fig. 1(b) illustrates the case of a shallow impurity level, such as a donor (or acceptor) in 2D semiconducting TMDCs. A bound electron–hole pair (or exciton) can localize to a shallow donor site via the mutual Coulomb interaction between the electron in the conduction band (blue), the hole in the valence (red), the donor electron (gray), and last but not least the screened core of the donor impurity (square). In the simplest model, the interaction is described in an effective mass approximation, implying that the formed particle complex delocalizes sufficiently over multiple unit cells.[123] In contrast to color centers, direct excitation of bound-exciton states via sub-gap absorption is inefficient, although it is in principle detectable down to the limit of a single-bound exciton.[96] Rather, free excitons are excited by band-to-band transitions, and at low temperatures, they will subsequently localize to the impurity sites via diffusion processes. In low-temperature luminescence spectra, bound excitons manifest as sharp emission lines at energies of approximately 10–100 meV below the free exciton emission. D^0X denotes excitons bound to neutral donors, while D^+X denotes excitons bound to ionized donors, leaving behind the

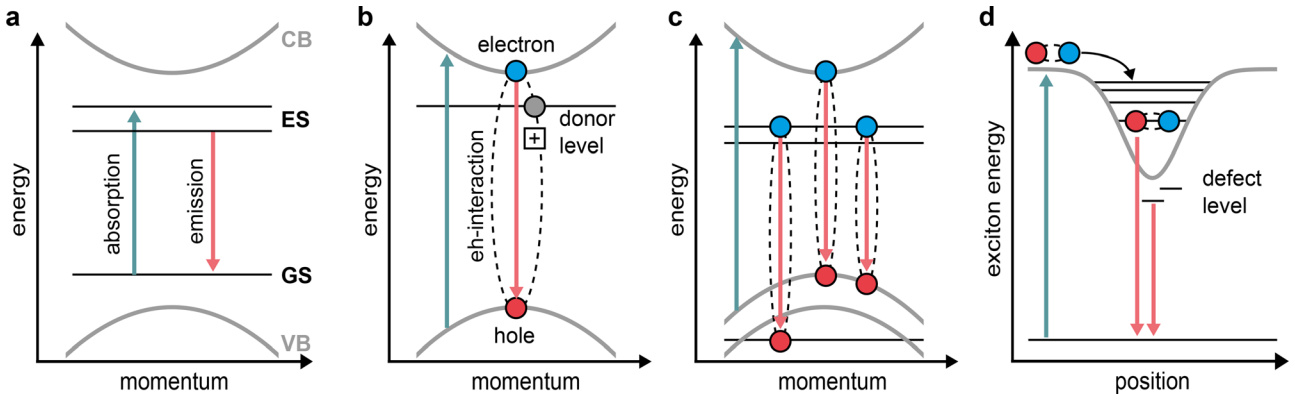


FIG. 1. Quantum emission from defects. (a) Color centers derived from deep in-gap states with ground state (GS) and multiple excited states (ES). The color center is directly addressable in absorption or emission. (b) Shallow donor or acceptor states localize excitons into bound complexes by mutual electron–hole interactions. (c) Defect-localized excitons can hybridize both to deep in-gap states and to shallow extended band states. (d) Local strains or moiré potentials trap excitons. Point defects may facilitate radiative recombination and single-photon emission.

02 July 2026 15:24:17

© Author(s) 2025

positively charged core. Along these lines, the notation for acceptor-bound states is A^0X (neutral) and A^-X (charged), although the latter is often considered energetically unstable.[123] For traditional bulk semiconductors, such as III–V materials, the binding energy scales as $E^b_{D^+X} < E^b_{D^0X} < E^b_{A^0X}$. For 2D vdW semiconductors, Ref. 124 provides extensive calculations covering monolayer MoS_2, WS_2, $MoSe_2$, and WSe_2. Note that, in general, the binding energy E^b of the defect-bound complex is not equivalent to the energy difference ΔE between the free exciton emission and the defect-bound exciton emission, because radiative recombination and dissociation may not necessarily result in the same final state. For example, Ref. 124 calculates for D^+X in monolayer $MoSe_2$ $\Delta E = 100$ meV and $E^b_{D^+X} = 6.5$ meV. This distinction resolves the apparent contradiction between the experimentally observed large detuning of the emission energy between defect-bound and free excitons, which can be on the order of 200 meV, and the small thermal activation energy of the defect emission (i.e., the binding energy of the complex), which is typically on the order of 10 meV.[125] Furthermore, these values exemplify that single-photon emission from excitons bound to shallow impurities, as demonstrated for example in Ref. 126 for dilute Nb impurities in WS_2, necessarily requires low temperatures, because otherwise free excitons will not localize onto the defect site.

In 2D TMDCs, the reduced dielectric screening results in large exciton binding energies on the order of a few hundred meV.[127] For carriers localized onto a defect site, the large exciton binding energy complicates a clear distinction between shallow and deep levels, since excitonic states can mix contributions from different levels over a large energy scale. In this case, *ab initio* calculations may provide model-free insights into the optical properties of the defects. For instance, Fig. 1(c) sketches the level scheme of MoS_2 with sulfur vacancy defects, as calculated by DFT with GW corrections,[62] comprising both occupied quasi-resonant defect levels overlapping with the spin–orbit split valence band and unoccupied in-gap states below the conduction band. In this case, BSE calculations predict a manifold of possible exciton states with a varying admixture of tightly localized defect vs more extended band states, as depicted conceptually in Fig. 1(c), and with transition energies up to 700 meV below the free exciton.[73]

Finally, spatial variations of the free exciton energy due to strain fields[128] and variations of the local dielectric environment[129] play an important role in exciton localization and corresponding single-photon emission in the case of 2D TMDCs. Local strain potentials may induce effective potential wells for excitons at mesoscopic length scales[130] with typical confinement energies on the order of a few meV due to renormalization of both bandgap and exciton binding energy with strain.[128,131] These strain fields can effectively guide single excitons into quantized, quantum-dot-like states at low temperatures, which in turn emit single photons upon radiative recombination Fig. 1(d). Although the microscopic origin of the single-photon emission has not been unambiguously resolved, both experimental and theoretical evidence suggests that atomic point defects play an important role in the recombination process. For example in monolayer WSe_2, calculations predict that strain locally shifts the exciton states into resonance with in-gap defect states resulting in inter-valley hybridization, efficient filling, and subsequent radiative decay from the defect state.[45,59] Note that moiré potentials in heterostructure can localize excitons at similar length and energy scales with a corresponding single-photon emission at low temperatures.[11]

III. FUNDAMENTALS OF IRRADIATION ENGINEERING

Irradiation with energetic particles, such as ions or electrons, is one of the most powerful and established techniques to tune material properties by introducing defects or impurities in a controllable manner.[132–137] Depending on the energy and type of the particle, as well as on the morphology and electronic properties of the irradiated material, different mechanisms of energy transfer from the projectile to the target are responsible for the formation of atomic defects [Figs. 2(a) and 2(b)]. Furthermore, the evolution of the system after impact of the particle, which includes any subsequent annealing and interaction with the environment, also strongly affects the final resulting types and concentrations of defects. For 2D materials, interaction with the environment can substantially change defect types and/or their concentration, as any unsaturated bonds at the surface tend to become passivated, for example by picking up other atoms, molecules, or radicals from the environment.[138]

For electron irradiation, the three main mechanisms for defect creation are the knock-on (or ballistic) damage, inelastic interactions due to electronic excitations and ionization, and beam-induced chemical etching, as illustrated in Figs. 2(c)–2(e).[32,139–141] Moreover, defects can also appear due to simultaneous contributions of several of these mechanisms.[142,143] The Coulomb interaction between the incoming electrons and the atomic nuclei results in elastic energy transfer from the electron to the recoil atom [Fig. 2(c)]. The minimum electron energy required to cause displacement of atoms is referred to as the electron knock-on displacement threshold energy. The latter is related through the relativistic binary collision formula to the recoil atom

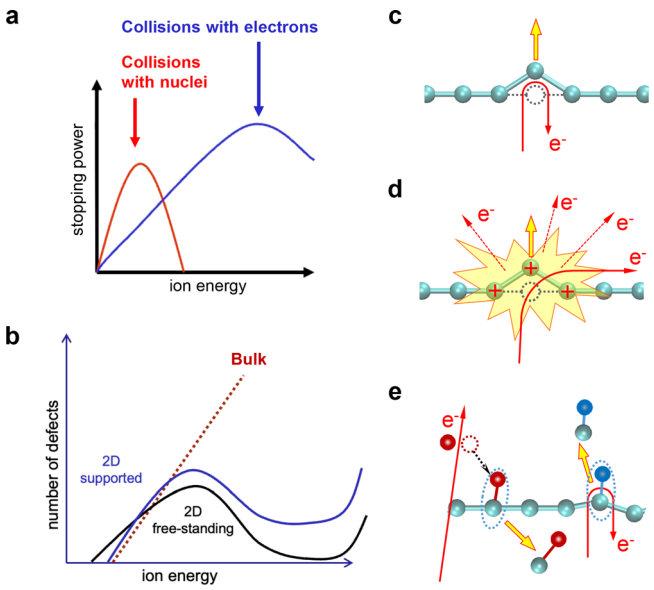


FIG. 2. Fundamentals of the irradiation-mediated engineering of 2D materials. (a) Schematic illustration of energy loss per unit length (stopping power) of the ion, with the main loss mechanisms being dependent on ion energy. (b) Sketch of the number of defects produced in a bulk system, a free-standing, and a supported 2D material by energetic ions as a function of ion energy. (c) Knock-on damage production mechanism upon electron irradiation, e.g., in the TEM. (d) Excitation/ionization damage production mechanism. (e) Beam-induced chemical etching and adatom-mediated damage production upon electron irradiation.

02 July 2026 15:24:17

© Author(s) 2025

displacement threshold energy, which is the minimum kinetic energy the recoiling atom should acquire to leave its position without immediate recombination. It depends both on the mass of the recoil atom and its chemical binding energy. At typical electron energies (60–300 keV) used in transmission electron microscopy (TEM), the energy transfer can be high enough for knock-on damage. With regard to semiconducting and insulating 2D materials, such as TMDCs and hBN, formation of defects has also been reported[142,144–149] at electron energies well below the knock-on threshold, which indicates that other damage mechanisms are active as well. For 2D MoS_2, a combination of electronic excitations and elastic scattering can in principle give rise to the displacement of atoms at rather low-electron energies.[147] Electronic excitations/ionizations [Fig. 2(d)] alone cannot result in the formation of defects in an ideal crystal with high-electron mobility due to a quick delocalization of the excitation.[142] Different physical processes contribute to inelastic energy transfer, including electronic excitations, ionization of target atoms, or electron–phonon coupling.[150] Beam-induced etching mechanisms [Fig. 2(e)] are very relevant to atomically thin targets, despite their comparably weak interaction with the electron beam, and they are active both in hBN[151] and TMDCs.[146,147] For example, degradation of 2D $MoTe_2$ in an oxygen partial pressure above 10^{-7} Torr was shown by *in situ* TEM, while MoS_2 was found to be inert to electron irradiation under oxygen environment on the time scales of the experiment.[146] Most likely, etching is the dominant channel of defect production under the electron beam in the SEM (typical energy is 1–30 keV), although charge accumulation in the material or the substrate followed by Coulomb explosion can also give rise to the appearance of defects.[152] Furthermore, adatoms present on the surface can also enhance the cross section for ballistic damage,[153] as new bonds formed between the material atoms and adatoms can decrease local in-plane bonding. For $MoTe_2$, the presence of hydrocarbons accelerated the etching by up to a factor of forty, which was attributed to break up and oxygen release from the complexes.[146] Breakup of hydrocarbon molecules, which can be ubiquitous in the TEM or SEM column, also gives rise to the deposition of amorphous carbon or other organic materials on top of the sample.[154,155] Deposition can proceed very fast at low-electron energies, as the cross section for the breakup of the molecules increases with decreasing electron energy.[156]

For ion irradiation,[132,157] nuclear stopping dominates in the case of relatively slow and heavy ions [Fig. 2(a)], and it originates from collisions and corresponding energy transfer between the ion and the nuclei of the atoms in the target governed by screened Coulomb interactions. By contrast, electronic stopping is a result of inelastic collisions between the moving ion and the electrons in the target, and it is important at high ion energies and/or for light ions. The crossover between nuclear and electron stopping depends on the ion mass. For hydrogen ions (protons) and helium ions, electronic stopping always dominates. Yet, defect production can still be caused through knock-on damage, as the amount of energy deposited through excitations may not be sufficient to displace atoms, especially in highly conductive systems.

Plasma treatment can be considered as a low-energy ion irradiation. Plasmas typically achieve fluences much larger than those achieved by irradiation with ion beams, with the drawback that control over the fluence of ions and their energy distribution is limited. Impurities can be introduced into 2D materials directly by ion implantation[158–164] or foreign atoms can fill vacancies created by energetic particles.[165,166]

The reduced dimensionality of 2D materials affects their response to ion bombardment [Fig. 2(b)]. Due to the planar geometry of the target and its thinness, the ion loses only a fraction of its energy, and the development of collisional cascades is suppressed. As a result, the number of defects produced in few-layer 2D materials will first increase with ion energy above a certain threshold, but will then drop at higher energies due to a smaller probability for the ion to displace an atom.[167] In particular for free-standing sheets, higher-energy ions should go through the 2D system without producing much damage.[168] Defects in 2D materials can appear again when the electronic stopping power is high enough to locally ionize and "melt" the material.[169] This stands in contrast to bulk systems, where the total number of defects is proportional to ion energy, but defects appear deeper in the sample with increasing ion energy. The situation may be different for supported 2D materials. At low ion energies (below 100 eV), the substrate should decrease the amount of damage created by the energetic ions. On the other hand, for ions with medium energies [for example, He and Ne ions with energies above 10 keV in a helium ion microscope (HIM)], the production of defects in the 2D material can be governed by the backscattered ions and atoms sputtered from the substrate rather than by direct ion impact.[58,162,170] For implantation into 2D materials, the ion energy should be relatively low (a few tens or at most hundreds of eVs), much lower than what is used for ion implantation into bulk materials.

IV. STRAIN ENGINEERING

We start by reviewing briefly key works on strain-induced localization of quantum emitters in 2D materials since they represent the first demonstration of site-selective creation of quantum emitters in the field. Strained 2D materials are also commonly used in combination with irradiation engineering as discussed in Sec. VIII. Local variations of strain have been discussed as the origin for quantum light emission in TMDCs since their first observations.[4–8,43–45,57] Strain variations often occur naturally due to wrinkles, folding, or bubbles beneath the layer. Inhomogeneous strain profiles from such corrugations facilitate the mesoscopic confinement of single excitons due to modifications of both bandgap and exciton binding energy.[109] Upon radiative recombination, the trapped excitons thus create single photons at locations predefined by the nanostrain. In particular, nanobubbles with sizes on the order of 10–100 nm can form during the dry stamping process for the transfer of TMDCs.[174] Using near-field optical microscopy and hyperspectral imaging, the formation of doughnut-shaped trapping potentials and their correlation to localized exciton emission was clearly demonstrated for such nanobubbles in monolayer WSe_2[100] [Figs. 3(a) and 3(b)]. Through heating of a poly(methyl methacrylate) membrane (PMMA) in the TMDC transfer process, hydrocarbon-filled bubbles with sub-μm sizes can be formed in large quantities underneath TMDC layers with universal strain profile independent of the bubble size. Choosing the substrate material, the strain profile can be tuned, and with this, the emission wavelength is shown for MoS_2 and a range of substrate materials.[175] Strain in TMDCs can also be introduced deliberately and site-selectively by patterning of the substrates with nanopillars and subsequent positioning of (few-layer) TMDCs onto the nano-corrugated surface.[24,45,46,48–51,55,57,176–180] Although initially demonstrated for intralayer excitons in direct-gap monolayer TMDCs, pillar-driven strain engineering of SPEs can be extended to interlayer excitons in 2D heterostructures, such as $MoSe_2/WSe_2$ heterobilayers[181] or WSe_2 homobilayers.[182] Single-photon emission from 2D

02 July 2026 15:24:17

© Author(s) 2025

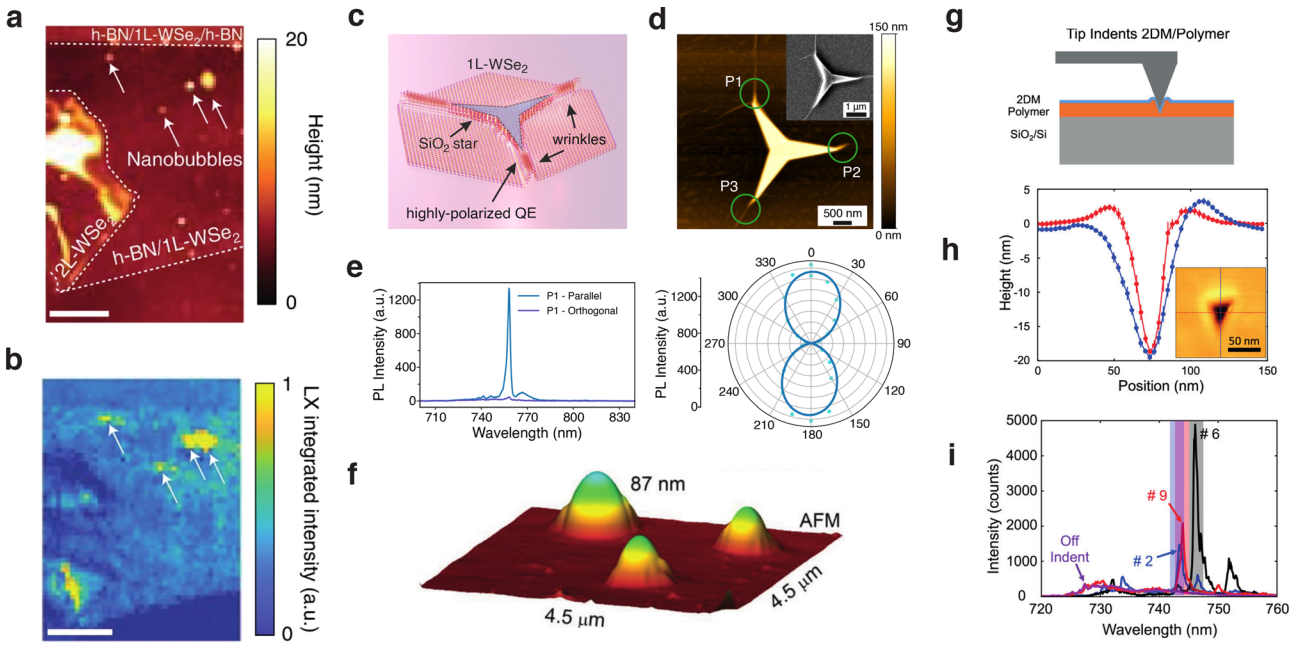


FIG. 3. Strain engineering of SPEs. (a) AFM topography and (b) integrated near-field PL (range 1.5–1.6 eV) image of exfoliated monolayer WSe_2 on top of hBN. The white arrows indicate that PL emission is spatially localized on nanobubbles sites. All scale bars, 500 nm. Reproduced with permission from Darlington *et al.*,[100] Nat. Nanotechnol. **15**, 854–860 (2020). Copyright 2020 Springer Nature. (c) Sketch and (d) AFM image (inset: SEM image) of monolayer WSe_2 on a star-shaped nanopillar. (e) (left) In-plane polarization-resolved PL spectrum and (right) corresponding polar plot (degree of polarization about 99%) taken from the P1 region in (d). Reproduced with permission from Paralikis *et al.*,[171] npj 2D Mater. Appl. **8**, 59 (2024). Copyright 2024 Authors, licensed under a Creative Commons Attribution Non Commercial License 4.0 (CC BY-NC). (f) AFM image of a region of a bulk WS_2 flake treated with H^+ irradiation, showing the formation of nanodomes. Reproduced with permission from Tedeschi *et al.*,[172] Adv. Mater. **31**, 1903795 (2019). Copyright 2019 WILEY-VCH Verlag GmbH & Co. KGaA, Weinheim. (g) Working principle of "quantum calligraphy": an AFM tip applies sufficient load to plastically deform a polymer underneath a 2D material, leaving a strain configuration. (h) Line profile of the strain configuration in (g). (i) PL spectra with SPEs generated by the local strain in (g). Reproduced with permission from Rosenberger *et al.*[173] ACS Nano **13**(1), 904–912 (2019). Copyright 2019 American Chemical Society.

heterolayers not only extends the tunability of the materials platform, but the large out-of-plane dipole moment of interlayer (localized) exciton transitions enables also electrical control of both emission energy and coupling to phonons.[182] Alternative methods for introducing local corrugations include the use of nanoparticles,[54] nanorods,[44] nanowires,[183,184] nano-antennas,[185] waveguides,[186] etched holes (for both WSe_2[43] and $MoSe_2$[52]) and trenches,[187] as well as strain tuning via application of an electrostatic field on a suspended monolayer.[188] By applying strain on $MoTe_2$ via nanopillar arrays, Zhao *et al.*[53] achieved single-photon emission up to 1550 nm (telecom C-band). It has been also shown that the emission wavelength of quantum light emitters localized on nanopillars can be tuned by applying an electric field with a few-layer graphene electrode.[176] Tuning of the emission wavelength can be also achieved via electrostatically actuated microcantilevers in SPEs as defined by utilizing nano-pyramid patterns[189] or via piezo-electric strain tuning along wrinkles.[28] Very recently, Wu *et al.*[190] exploited valley-spin locking in pillar-strained monolayer WSe_2 using a cross-circular polarization scheme to consistently reduce the background emission from free excitons and exciton complexes, thus achieving single-photon emission with improved purity.

Wrinkles in a hBN-TMDC bilayer structure placed on a patterned substrate have also been shown to be an optimal source of strain,[191] while strain induced with Au nanoparticles exhibits single-photon emission with temperature-dependent energy loss.[54] Similarly, Au tips[192] and star-shaped Au particles[191] were applied for WSe_2. Yet, another approach for local strain creation is based on a chemomechanical modification,[193] achieved with non-covalent surface modification with aryl diazonium chemistry.

The polarization and angular momentum of the emitted single photons can be defined by the symmetry of the local strain field [Figs. 3(c)–3(e)], using, for example, gold chiral nanoparticles[194] or patterned strain-mediating structures with elongated star-shaped structures.[171] Exploring the optical properties of the pattern-forming material together with their structure opens possibilities for modifying the dynamics of the emitter and the far-field radiation pattern. Radiative emission can thus be directly coupled to waveguide modes,[186] local cavity resonances,[24] or efficiently scattered to the far field with dielectric nano-antennas.[51,185]

Nanodomes with highly symmetric radial strain profiles can be generated controllably via H^+ irradiation [see Fig. 3(f)]. After penetration of the first layers, H^+ ions form molecular hydrogen in the first interlayer. TMDC material and dome size thus provide means to control the strain profile and the emission wavelength,[172] while capping with an hBN layer prevents dome deflation.[39] Yet, another approach for the site-controlled domes formation is the irradiation of polymer-supported vdW materials with low-energy electrons, where hydrogen is formed in the electron beam-induced degradation of the polymer.[195] Finally, nanometer-sized indentations carefully patterned with an

02 July 2026 15:24:17

© Author(s) 2025

atomic force microscope in a soft substrate, such as a spin-coated polymer layer, is another highly reproducible approach for exciton confinement via local strain modification[173,196–199] [see Figs. 3(g)–3(i)].

For hBN, SPEs were created by silica nanopillars,[200] nano-indentation,[201] and on nanoscale wrinkle sites.[202] Also, in this case, strong photoluminescence (PL) with good in-plane polarization and photon purity was observed. Furthermore, SPE creation and enhancement at the same time was achieved by employing gold-coated silicon pillars with an alumina spacer,[203] yielding a 10-fold PL enhancement and 2.46-fold reduction in lifetime. Notably, Chen *et al.*[204] employed Ag nanowire/hBN/graphene tunnel junctions to electrically drive strain-activated defect emission, although without reporting evidence of single-photon emission.

Depending on the type of defect and the band structure of the host material, strain may have different consequences on light emission. In semiconducting TMDCs, strain can funnel excitons which are subsequently trapped and recombine radiatively, often mediated by atomic defect states. By contrast, in wideband gap hBN, strain creates local electric fields and shifts the energy levels of intrinsic defects, thus allowing to modulate and fine-tune the optical emission spectrum. Furthermore, strain may also have an important impact on the defect creation process. In this context, first-principle calculations, for both hBN and TMDCs, predict that bi-axial strain changes the formation energy of defect structures, depending on the relative size of the impurity atom.[205]

V. PLASMA TREATMENT

There have been several reports on quantum emitter fabrication in hBN by plasma application, including Ar,[206,208] H_2,[206] or O_2 plasmas.[80,207] Typically, thin layers of hBN are mechanically exfoliated onto a substrate and then brought in contact to one of the mentioned plasmas to induce defects, while the activation of single-photon emission relies on a subsequent high-temperature thermal annealing [Fig. 4(a)]. Most reports have utilized an annealing temperature in the range of 750–900 °C for several minutes either in Ar gas,[207,208] N_2 gas[79] or even air[206] to suppress the fluorescence background in the photoluminescence spectra and to enhance the overall emitter stability. The characteristics of the corresponding quantum emitters vary both in spectral fingerprints [Fig. 4(b)] and in possible microscopic origins[80] (cf. Sec. X). Moreover, the energy of the zero-phonon line typically varies both with the type of plasma used and with the applied duration and power [Fig. 4(c)].[206,207] Nevertheless, plasma-induced quantum emitters in hBN have proven to exhibit very good quantum optical properties [Fig. 4(d)] and can be easily generated across a rather large spatial area of the exposed materials [Fig. 4(e)].[79,80,206–208] For TMDCs, there are several reports that Ar[209,210] or N_2[211] plasma

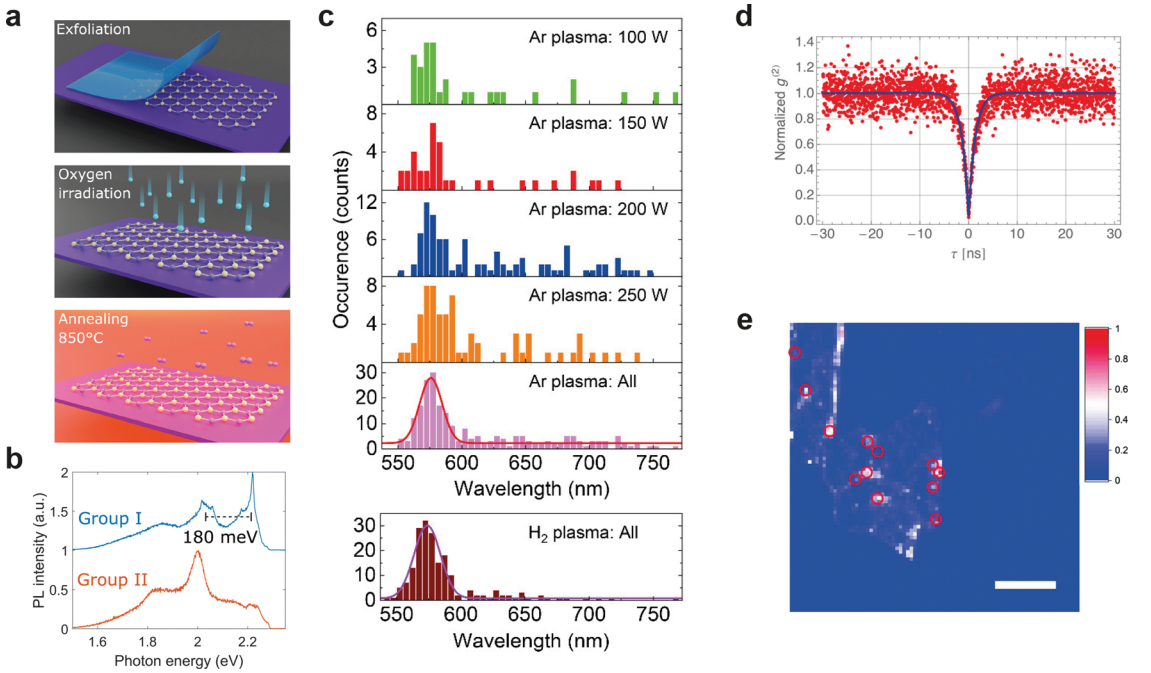


FIG. 4. SPEs in hBN as fabricated by plasma treatment. (a) Typical fabrication steps for creating SPEs in exfoliated hBN (top) based on an O_2-plasma treatment (middle) and subsequent high-temperature annealing in controlled atmosphere (bottom). (b) The luminescence of O_2-plasma treated hBN typically exhibits several lines, which can be grouped into distinct line shape categories (here Groups I and II as in Ref. 79) and which are red-shifted by ∼ 160–200 meV with respect to the zero-phonon line of the SPEs. Reprinted from Fischer *et al.*,[79] Science Advances **7**, 7138–7155 (2021). Copyright 2021 Authors, licensed under a Creative Commons Attribution Non Commercial License 4.0 (CC BY-NC) License. (c) Statistics of the zero-phonon line of emitters in hBN as treated with an Ar-plasma at certain plasma powers (top) and with a H_2-plasma (bottom). Reprinted with permission from Zeng *et al.*,[206] ACS Applied Materials & Interfaces **16**, 24899–24907 (2024). Copyright 2024 American Chemical Society. (d) Normalized second-order autocorrelation of an emitter in hBN fabricated by O_2-plasma treatment with $g^{(2)}(0) = 0.0034$.[47] Reprinted with permission from Vogl *et al.*,[207] ACS Photonics **5**, 2305–2312 (2018). Copyright 2018 American Chemical Society. (e) Luminescence map of SPEs (red circles) in hBN fabricated by an Ar-plasma with a characteristic random spatial distribution. Scale bar: 10 μm. Reprinted with permission from Xu *et al.*,[208] Nanoscale **10**, 7957–7965 (2018). Copyright 2018 Royal Society of Chemistry.

02 July 2026 15:24:17

© Author(s) 2025

exposure can generate luminescent defects as well. However, for all studies, the reported spectra are consistent with ensemble emission, and single-photon emission was not demonstrated.

VI. ION IRRADIATION

TMDC monolayers can be locally irradiated by a focused beam of He^+ ions to introduce defects, for example, by the help of a scanning helium ion microscope (HIM). The local crystal modification can act as a spatial trap for excitons in TMDC monolayers, as reported in a series of papers for different materials: MoS_2,[12,33,58,62,216–218] WS_2,[41] WSe_2,[40] $MoSe_2$.[219] In Ref. 216, it was shown how the introduced defects impact the vibrational, optical, and spin-valley properties in MoS_2 supported on a silicon oxide substrate. hBN encapsulation prior to irradiation revealed for the first time optically active defects with spectrally narrow emission lines near 1.75 eV, that is approximately 200 meV below the optical bandgap, which were later confirmed to be SPEs due to defects created at controlled positions in the MoS_2 layer.[33] The emitters show long-term stability over multiple cooling cycles,[12] although inhomogeneous broadening between different emitters exceeds the natural linewidth.[33] Individual defect sites positioned with an accuracy below 10 nm were observed with scanning tunneling microscopy, and pristine and oxygen-passivated sulfur vacancies were identified as the most abundant types of defect created by He-ion beam irradiation,[58] in agreement with estimates from SRIM simulations. The optical emission energies are consistent with pristine sulfur vacancies in monolayer MoS_2,[62] which are predicted to form localized exciton states, hybridized to extended band states [cf. Fig. 1(c)]. Spin characteristics, magnetic field-dependent photoluminescence, and dipolar emission patterns of these quantum emitters were studied in Refs. 212 and 218. A distinct advantage of the focused He^+ ion beam is that it allows creation of single-photon emitters at desired positions after encapsulation of the monolayer and after device fabrication[212] [Fig. 5(a)]. Helium ion irradiation has also been used to modify other monolayer TMDCs.[219] In monolayer WS_2 irradiated with a HIM, narrow photoluminescence peaks with energies below the exciton energies were identified as local defect states,[41] but no single-photon statistics have been demonstrated yet.

Other ion sources were explored as well. Focused Ga^+ ion beam exposure of monolayer WS_2 resulted in a strong modification of the photoluminescence even at locations far away (>10 μm) from the exposure sites due to redeposition of Ga ions,[220] suggesting that the heavy Ga ions are poorly suited for the generation of single-defect sites in TMDCs. Zhang *et al.*[37] systematically studied the impact of proton exposure on the excitonic properties of all the archetypical direct-gap monolayer semiconductors, namely, MoS_2, WS_2, $MoSe_2$, and WSe_2 [Fig. 5(b)]. In all cases, emission lines 100–200 meV below the free exciton with lifetimes beyond 1 ns were found, whereby the sulfides generally showed two orders of magnitude brighter defect emission than the selenides. As the underlying origin, chalcogen monovacancies were tentatively proposed, based on defect statistics gained from high-resolution STEM. A follow-up study elaborated in detail on the gate dependence of proton-induced emitters in $MoSe_2$ and suggested

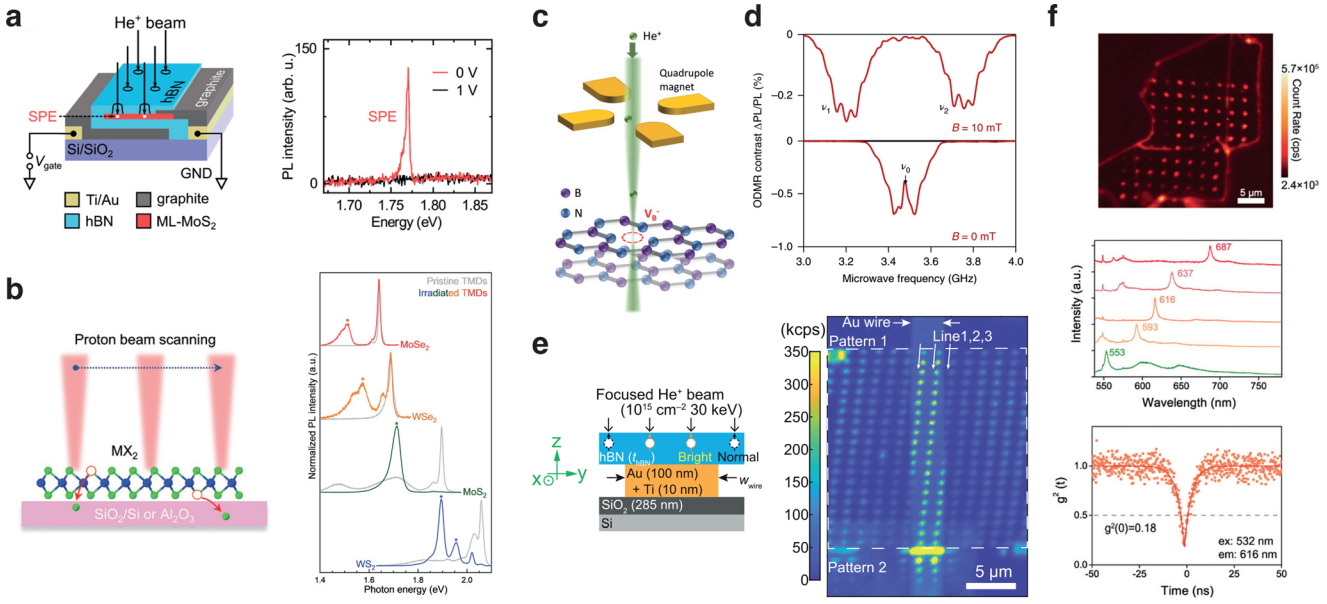


FIG. 5. Creation of SPEs utilizing ion irradiation. (a) With the focused ion beam, defects can be produced in TMDCs embedded in device structures. Reproduced with permission from Hötger *et al.*,[212] Nano Lett. **21**(2), 1040–1046 (2021). Copyright 2021 American Chemical Society. (b) A proton beam creates chalcogen vacancies in monolayer semiconductors. Reproduced with permission from Zhang *et al.*,[37] Adv. Opt. Mater. **10**, 2201350 (2022). Copyright 2022 Wiley-VCH GmbH. (c) Sketch of the highly focused ion beam that knocks out boron atoms in hBN. Reproduced with permission from Liang *et al.*,[213] Adv. Opt. Mater. **11**, 2201941 (2023). Copyright 2022 Wiley-VCH GmbH. (d) ODMR spectra of defects in hBN at vanishing and at finite magnetic fields. Reproduced with permission from Gottscholl *et al.*,[116] Nat. Mater. **19**, 540–545 (2020). Copyright 2020, under exclusive license to Springer Nature Limited. (e) Plasmonic enhancement of photoluminescence of defects in hBN created by a focused He^+ ion beam. Reproduced from Sasaki *et al.*,[214] Appl. Phys. Lett. **122**, 244003 (2023), with the permission of AIP Publishing. (f) Photoluminescence of an ion-irradiated array in hBN after thermal annealing, with associated PL spectra and second-order correlation functions. Reproduced with permission from Liu *et al.*,[215] Adv. Opt. Mater. **12**, 2302083 (2024). Copyright 2023 Wiley-VCH GmbH.

02 July 2026 15:24:17

© Author(s) 2025

bound excitons [cf. Fig. 1(b)] localized to neutral and negatively charged Se vacancies as the origin of the defect emission.[221] Note that none of the above studies experimentally demonstrated single-photon emission from the ion-induced defect state, but rather reported spectra consistent with optical emission from defect ensembles.

We now turn to irradiation studies on hBN. An important difference is that TMDCs are typically studied as monolayers, while defect emission from hBN crystals is most commonly studied in multilayer, bulk-like samples. Quite commonly, irradiated hBN samples exhibit broad luminescence peaks around 1.5 eV, which are attributed to charged boron vacancies (V_B^-). Although so far only ensemble luminescence has been reported from these defects, their spin-triplet ($S = 1$) ground state makes them promising for quantum sensing applications based on optically detected magnetic resonance (ODMR) schemes.[106,222] Intriguingly, V_B^- defects can also be used to manipulate nearby nuclear spins in hBN using the hyperfine interaction between nuclear spins and V_B^- electron spins,[223] similar to what has been done with NV centers in diamond.[224] The V_B^- defects can be created by many different methods, including irradiation [see Fig. 5(c)] with protons,[225,226] helium ions,[29,213–215,223,227–233] nitrogen ions,[222,231,234–237] gallium ions,[116,238] carbon ions,[231,239] oxygen plasma,[79,207] xenon ions,[236,240] argon ions,[230,231,236] or neutrons.[116,119,241–243] Alternative techniques that do not directly involve ion beams are neutron-driven nuclear transmutation doping,[244–247] transmutation doping,[22] femtosecond laser writing,[248] and AFM-induced damage.[249] Gottscholl *et al.*[116] first reported broad defect emission centered around 800 nm (1.5 eV) after irradiation with various particles (neutrons, lithium, and gallium ions). Careful analysis of ODMR experiments [Fig. 5(d)] identified the luminescent defects as V_B^- (cf. Sec. X).

For sensing applications, the creation of spin defects within a few atomic layers from the material surface may be advantageous.[236] In this context, low-energy He^+ ion implantation (200 eV–3 keV) was used to create shallow V_B^- defects integrated into gold plasmonic structures producing enhanced ODMR contrast (up to 50%) and enhanced brightness.[228] Sasaki *et al.*[214] report local magnetic field sensing with a hBN quantum sensor nanoarray, based on V_B^- defects created by helium irradiation directly on microfabricated gold wires [Fig. 5(e)]. The magnetic field created by current flow in the wires was resolved by an ODMR detection scheme with irradiated defect patches as small as 100 nm^2, thus demonstrating the potential for high spatial resolution imaging. Toward optimizing the creation process for V_B^-, Suzuki *et al.*[250] specifically compared high-temperature irradiation and post-irradiation annealing, with optimal ODMR contrast obtained at 500 °C and 500–600 °C, respectively. Finally, ion irradiation can also create V_B^- defects in hBN crystals with engineered nanophotonic environments.[228,251–253] V_B^- defects within nanophotonic bullseye structures revealed spectrally tunable narrowing of the otherwise broad photoluminescence spectrum.[226] Similarly, V_B^- defects were coupled to bound states in the continuum using a nanostructured hBN as a dielectric metasurface with spectral selectivity.[237,254] Experiments on V_B^- monolithically integrated into hBN nanobeam cavities provided evidence that the zero-phonon line of the V_B^- defect is located at 773 nm, which is otherwise obscured by strong inhomogeneous and phonon broadening of emission spectra.[253]

For V_B^-, an important consideration is the efficiency of the creation process, especially when its charged nature is taken into account. Guo *et al.*[231] estimated a lower bound for the generation probability around 10^{-3}% from the photon count pumped by a pulsed laser. Recently, Gong *et al.*[255] proposed to extract the V_B^- density by comparing the spin coherence time T_2 measured with two different schemes (XY-8 and DROID). Under the assumption that the splitting of the $m_s = \pm 1$ spin sublevels results predominantly from the interaction of V_B^- with the local electric field generated by nearby, randomly distributed charges (see also Sec. X), rather than from local strain effects, the defect density can be estimated from comparison of coherence time and splitting to numerical simulation. Support for the splitting-by-local-electric-fields hypothesis comes from a recent theoretical study[245] and from measurements showing that the E splitting vanishes in few-layer hBN, that is when such local electric fields are almost absent.[244] To date, the microscopic origin of the charge environment is not fully understood. Commonly, the charge density derived from such a model is assumed to be equal to the number of charged V_B^- defects. However, a recent work suggested that a phenomenological background charge should also be taken into account to improve the quantitative estimation of the V_B^- density created upon irradiation.[233]

Next, we focus on the irradiation engineering of other types of luminescent centers, where single-photon emission was demonstrated. In one of the first studies, from 2017,[29] a 100 nm-thick hBN flake was irradiated by He^+ ions in a He-ion focused ion beam (FIB) and then post-annealed in argon atmosphere at 1000 °C. Due to a reduction in background fluorescence, which was present in the as-prepared samples in the irradiated regions, SPEs near 2 eV could be resolved, and zero-phonon line (ZPL) tuning via strain up to 6 meV was demonstrated. The importance of annealing is evident in Ref. 215, where focused He^+ irradiation creates sites that display broad PL spectra, but no single-photon emission. Only after subsequent annealing to 1050 °C in an oxygen atmosphere, the exposed sites showed single-photon emission with energies ranging from 1.8–2.3 eV [Fig. 5(f)]. Note that the very high ion fluences of about 5×10^7 ions/spot used in the study resulted in substantial milling of the hBN over an approximately 100 nm wide circular patch. It is also worth mentioning three interesting nonstandard irradiation studies. In Ref. 240, optically active defects ensembles were created in hBN by combining a focused Xe-ion beam and subsequent DI-water etching. By using super-resolution optical microscopy combined with atomic force microscopy, the emitters were observed to be located at the rims of the etched patterns. Their broad spectra are centered at 830 nm, matching emission spectra typically associated with V_B^- defects in other studies. In the second study, Ref. 230, evidence of carbon-based luminescent defects (emitting at 2.15 eV) was reported after heterostructures comprising few-layer hBN covered with graphene on SiO_2 were irradiated from the top by 1 keV argon ions. Molecular dynamics simulations suggest that displaced carbon atoms could effectively be implanted into hBN, enhancing the likelihood of emission by carbon-based defects in hBN. In the third interesting nonstandard irradiation study, Ref. 256, the aim was again to create carbon-related color centers in a hBN flake, this time by first carbon irradiation (30 keV energy, 10×10^{14} ions/cm^{-2} fluence, and 30° incident angle), and then thermal annealing at 1297 K in argon atmosphere for 1 h, but they report only creation of V_B^- vacancies, thus far without clear signatures of single-photon emission.

VII. ION IMPLANTATION

Color centers or optically active impurities can be easily introduced in 2D materials during the growth process.[126,258] For example,

02 July 2026 15:24:17

© Author(s) 2025

in Ref. 259, carbon-related defects in monolayer hBN were created by chemical vapor deposition (CVD) synthesis at high temperature. However, toward the integration of quantum emitters into photonic structures, ion implantation can provide a more controllable approach for fabricating type-specific and site-specific color centers. Ion implantation is normally referred to as the process of directly introducing impurities (for example, carbon, nitrogen, boron, silicon, or other dopants) into a material by irradiation with the respective ion species.[158–164,260] Alternatively, impurities can be implanted indirectly upon irradiation with energetic particles by capturing displaced atoms into created vacancies.[165,166] For direct implantation of 2D materials, the ion energy should be relatively low (from a few tens to hundreds of eVs) to enable stopping and incorporation of the ions into the atomically thin target (see Sec. III). For graphene [Fig. 6(a)], doping via ion implantation was extensively studied,[159,160,162,163] and the successful implantation in monolayers was verified by atomic resolution high-angle dark field imaging (HAADF) with single-atom electron energy loss spectroscopy (EELS)[158] in STEM.

For implantation into hBN, so far the most attractive element has been—mostly without competition—carbon, because carbon is believed to be at the origin of many of the defect complexes studied.[66,77,80,115,117,118,230,257,259,261–273] For a more detailed discussion of possible candidates for the molecular structure of carbon-based defects, see Sec. X. Carbon-related luminescent defects are observed in hBN monolayers[259] and even in hBN nanotubes.[261] Moreover, site-specific electron microscopy imaging and EELS give further hints that carbon complexes are involved in photoluminescence (PL) emission.[66] In a pioneering study, Mendelson *et al.*[77] achieved injection of carbon inside hBN via both carbon incorporation during metal-organic vapor-phase epitaxy (MOVPE) growth and via irradiation with carbon ions at 10 keV (ion fluence 10^{13} ions/cm^2). Notably, for defects grown by carbon-doped MOVPE, they showed both photon antibunching and magnetic activity (positive ODMR contrast up to 0.06% with small zero-field spitting D). Concerning implantation, they irradiated both pristine MOVPE and exfoliated hBN with carbon (at 10 keV energy and 10^{13} ions/cm^2 fluence). After implantation, antibunched quantum emitters with narrowed ZPL as compared to carbon-doped MOVPE were obtained [see Figs. 6(b) and 6(c)], and their density scaled with the ion fluence. Control irradiation with silicon and oxygen created no SPEs but rather only boron vacancies. Interestingly,

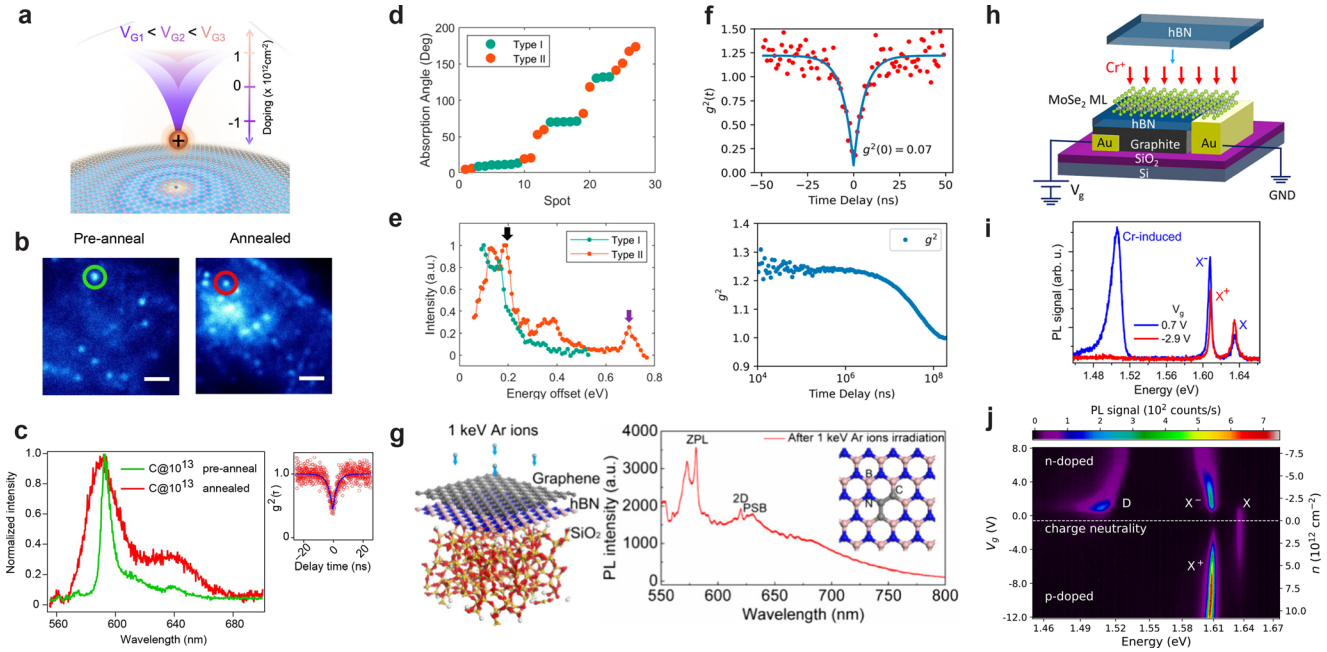


FIG. 6. Creation of SPEs utilizing ion implantation. (a) A positively charged ion is accelerated toward a target 2D lattice. Reproduced with permission from Telychko *et al.*,[164] Nano Lett. **22**(21), 8422–8429 (2022). Copyright 2022 American Chemical Society. (b) Integrated photoluminescence maps of carbon-implanted hBN films comparing pre-annealing and post-annealing conditions, with highlighted isolated SPEs. (c) PL spectra from the highlighted SPEs with an example g^2 measurement. Reproduced with permission from Mendelson *et al.*,[77] Nat. Mater. **20**, 321–328 (2021). Copyright 2020 Authors, under exclusive license to Springer Nature Limited. (d) PL absorption polarization characteristics and (e) photoluminescence excitation (PLE) spectra of $^{12}C^+$ implantation-generated emitters in hBN (divided in two groups). (f) Second-order autocorrelation (g^2) on a (upper) short and (lower) long timescale, highlighting the antibunching at $t = 0$. The experimental data are normalized by the coincidence rate at longer timescales. Reproduced with permission from Zhong *et al.*,[257] Nano Lett. **24**(4), 1106–1113 (2024). Copyright 2024 Authors, licensed under a Creative Commons Attribution 4.0 (CC BY) License. (g) (left) Graphical representation of carbon implantation inside the hBN achieved via low-energy (1 keV) argon-ion beam irradiation of a graphene/hBN stack. (right) PL spectra of carbon-related emitter in the graphene/hBN stack, with highlighted the proposed zero-phonon line (ZPL) and phonon sideband (PSB), and the 2D Raman mode of graphene. The inset is a scheme of the proposed defect molecular structure (C_BC_{N2}). Reproduced with permission from Ren *et al.*,[230] ACS Appl. Nano Mater. **7**(3), 3436–3444 (2024). Copyright 2024, American Chemical Society. (h) Sketch of the device fabricated in Ref. 144 (Cr-implanted $MoSe_2$ monolayer encapsulated in hBN and with a graphite backgate). (i) PL of the implanted device (at 10 K) as a function of the backgate voltage. (j) PL spectra as a function of the backgate voltage with marked the doping type and calculated carrier concentration n. Reproduced with permission from Bui *et al.*,[144] ACS Appl. Mater. Interfaces **15**(29), 35321–35331 (2023). Copyright 2023 Authors, licensed under a Creative Commons Attribution 4.0 (CC BY) License.

02 July 2026 15:24:17

© Author(s) 2025

subsequent annealing at 1000 °C broadened the PL peaks [see Figs. 6(b) and 6(c)] and suppressed the single-photon behavior indicating the formation of defect ensembles.

By contrast, Zhong *et al.*[257] combined $^{12}C^+$ irradiation (10 keV acceleration, 0° tilt angle, 10^{13} ions/cm^2 fluence under high vacuum) on commercial, exfoliated hBN with annealing in Ar gas at 900 °C for 30 min. They report the generation of SPEs with a strong correlation between optical dipole orientation and crystal direction. In particular, for one of the two types of emitters reported, the absorption dipole orientation takes only values 60° apart [see Fig. 6(d)]. The emitters exhibited highly repeatable excitation resonances in PLE and photon antibunching [see Figs. 6(e) and 6(f)]. Further control irradiation with $^{16}O^+$ confirmed that the reported emitters are not intrinsic defects, but rather induced by the carbon implantation process.

As an alternative approach, Ren *et al.*[230] present carbon-related color centers (with ZPL around 580 nm) generated in a graphene/monolayer hBN stack using 1 keV argon-ion implantation without subsequent annealing [see Fig. 6(g) for a representative sketch]. The created emitters overlap partly with Raman signatures from the graphene layer, but they generally show spectral features similar to the ones reported by Mendelson *et al.*[77] [see Fig. 6(c)] with long photostability, although no antibunching measurements were reported. The idea of carbon doping in hBN by bare momentum transfer could provide a reliable and site-selective way to generate position-controlled, carbon-based emitters in hBN, and constitute an alternative to carbon doping via annealing[79,262,274,275] or to heavy ion implantation.[276] Future steps might, for example, involve combining the two approaches from Mendelson *et al.*[77] and Ren *et al.*,[230] by using a thicker layer of carbon and/or employing carbon irradiation at the same time. In Ref. 277, an amorphous, 100 nm-thick carbon mask was placed in front of free-standing hBN flakes (with thicknesses between 10 and 100 nm) to decelerate incoming carbon ions (40 keV acceleration voltage, 2.5×10^{14} ions/cm^2). This approach achieved the creation of two classes of emitters distributed around 550 and 590 nm, showing high stability, a short lifetime around 1 ns, in-plane polarization in excitation, PL saturation, and photon antibunching. Currently, there are no experimental or simulated results on low-energy ion implantation into hBN. To this end, new works could be directed toward the optimization of the generation parameters. Remarkably, analytical potential molecular dynamics (APMD) simulations show that optimal parameters for carbon implantation into monolayer hBN are 50 eV ion energy combined with incident angles θ ranging from 20° to 40°.[265] Further works seem to be needed to optimize the irradiation parameters for efficient implantation of 2D and related materials with low-energy ion implantation.

We note that a very recent and pioneering work successfully created magnetically active quantum emitters in the 2 eV region by implantation. Specifically, they employed low-energy (2.5 keV) implantation of the magnetically active carbon isotope $^{13}CO_2$ into hBN.[278] ODMR measurements showed that two types of defects were formed with spin $S = 1/2$ and spin $S = 1$ states, and spin coherence times in the range of tens to hundreds μs. They used hyperfine magnetic coupling between electronic and nuclear spin in $^{13}CO_2$ to fingerprint the presence of carbon in the created emitters. This represents an interesting advance for the determination of the microscopic origins of defect-related quantum emitters with magnetic response in 2D materials.

For TMDCs, very few works have utilized ion implantation for the creation of optically active defects so far. Direct implantation into monolayer TMDCs is particularly challenging because of their increased structural sensitivity resulting in instability under implantation conditions and the tendency of high-energy ions to penetrate and stop inside the substrate. Therefore, efficient ion implantation into monolayers requires typically much lower ion energies than in conventional implantation processes (see Sec. III). Nevertheless, Bui *et al.*[144] successfully demonstrated implantation of low-energy $^{52}Cr^+$ ions (25 eV, 220 °C) directly into a monolayer $MoSe_2$ field effect structure [Fig. 6(h)]. The low-energy implantation resulted in a well-defined sub-gap PL [Fig. 6(i)], although no single-photon emission was observed. Since the defect PL was only present for the *n*-doped regime [Fig. 6(j)], the radiative recombination of a localized electron in a deep acceptor state with a free valence band hole was proposed (cf. Sec. II) as the potential origin. An alternative route, in particular to create quantum emitters in the telecom range with long coherence times, may be the implantation of rare-earth dopants, such as Er,[279] where the photophysics are dictated by internal transitions of the partially filled 4f-shell and are only weakly modified by the host crystal. In this context, a recent study reported evidence for narrowband PL emission in the telecom range with very long lifetime (4.5 ms at room temperature) after implantation of Er dopants into thick (above 200 nm) WS_2 flakes followed by annealing at 400 °C.[280]

VIII. E-BEAM IRRADIATION

As an alternative defect generation technique, focused electron irradiation has attracted widespread attention. The method makes use of the focused electron beam in standard scanning (transmission) electron microscopes where typical electron energies range from 1 keV to more than 100 keV. Depending on their kinetic energy, electrons introduce damage to the target material via knock-on damage, inelastic scattering, and beam-induced chemical etching (cf. Sec. III). Theoretical studies indicate that for MoS_2 and hBN[139] radiolysis and chemical etching are the primary factors causing damage at electron beam energies below 70 keV. In the latter case, electrons generate broadband electromagnetic fields that ionize the surrounding matter. Knock-on damage dominates at beam energies exceeding 90 keV for MoS_2 and 115 keV for hBN.[282] As noted in Sec. III, emitters in both MoS_2 and hBN have been experimentally created or activated below these theoretically estimated thresholds.

Prolonged focused electron beam irradiation at an energy of 15 keV, which is significantly below the knock-on damage threshold,[151] was shown to result in site-selective, room-temperature single-photon emission [Fig. 7(a)]. These sites emit photons with a characteristic blue emission spectrum centered at 440 nm [Fig. 7(b)].[35] An earlier cathodoluminescence study reported similar blue emitters,[103] which could be activated or deactivated under the electron beam irradiation and that appeared simultaneously with single-photon emission centers in the UV range.[283] More recent cathodoluminescence experiments[36] propose that blue emitters derive from UV-active defects, which are modified under the electron beam due to a bond-breaking-restructuring process of carbon-related defect complexes [Fig. 7(c)]. A more recent work from the same group suggests that the electron beam can generate electromigration of charged defects, leading to clustering and formation of B-centers[281] (see also Sec. X). Interestingly, electron beam irradiation (3 keV) was also reported to

02 July 2026 15:24:17

© Author(s) 2025

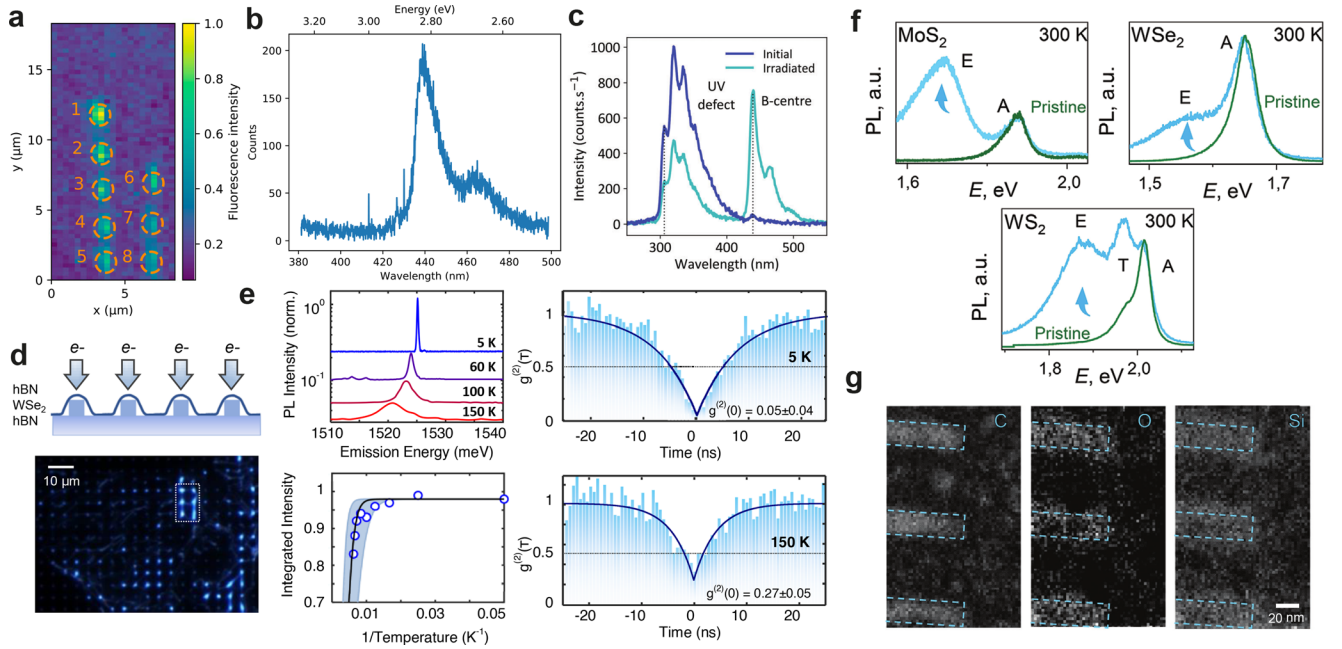


FIG. 7. Single-photon emission in hBN and TMDCs generated by electron beam irradiation. (a) PL map of a SPE array generated via extended e-beam exposure (15 keV) of hBN. (b) Associated PL spectrum of a given spot from the array in a exhibiting the ZPL and PSB of a blue emitter. Reproduced with permission from Fournier *et al.*,[35] Nat. Commun. **12**, 3779 (2021). Copyright 2021 Authors, licensed under a Creative Commons Attribution (CC BY 4.0) License. (c) CL spectra of UV and blue emission before and after the 300 s e-beam irradiation. The UV emission decreases, while the blue emission increases. Reproduced with permission from Nedic *et al.*,[281] Adv. Opt. Mater. **12**, 2400908 (2024). Copyright 2021 Authors, licensed under a Creative Commons (CC BY-NC-ND) License. (d) Combined e-beam and strain activation of SPE in WSe_2. (e) PL spectrum of a spot from the array in (d) for temperatures between 5 and 150 K. The PL peak quenches at 150 K. Associated second-order correlation functions at 5 and 150 K. Adapted with permission from Parto *et al.*,[38] Nat. Commun. **12**, 3585 (2021). Copyright 2024 Authors, licensed under a Creative Commons (CC BY) License. (f) PL spectra for multiple TMDCs showing a consistently E peak after e-beam irradiation. (g) EELS maps for C, O, and Si for MoS_2 sample in (f). The e-beam patterned arrays highlighted with blue-dashed lines exhibit how the C, O, and Si content is larger within these regions. Adapted with permission from Yagodkin *et al.*,[154] Adv. Funct. Mater. **32**, 2203060 (2022). Copyright 2022 The Author(s), licensed under a Creative Commons Attribution Non Commercial 4.0 (CC BY-NC) License.

result in the formation of position-controlled SPEs at 575 nm,[284] but to date, the results have not been reproduced independently.

In the context of single-photon emission in TMDCs, electron beam irradiation has so far been mostly used to introduce active defects sites in strain-patterned WSe_2.[38,63,171,285] Fig. 7(d) shows an example of a strain-patterned array of single-photon emitters in monolayer WSe_2 with emission lines around 1.55 eV [Fig. 7(e)], whereby the strain sites were activated by focused electron beam irradiation (100 keV). Notably, the latter study demonstrated single-photon statistics up to a temperature of 150 K. The rationale behind the electron beam activation process is to introduce locally in-gap defect states that serve as recombination centers for strain-localized (dark) exciton states (cf. Secs. II and X). Although single-photon emitters in WSe_2 were initially reported without any additional electron beam exposure,[4,6–8,42,286] several recent studies emphasize the benefit of using electron beam exposure to further optimize the emitter creation process.[38,63,171,285] Different defect creation mechanisms may prevail depending on the used electron energy (cf. Sec. III). Above the knock-on damage threshold,[38,171,285] creation of intrinsic defects, such as chalcogen vacancies, may be dominant, while below the knock-on damage threshold[61,63,154] chemical etching and electron beam-induced deposition may create both intrinsic and extrinsic defects, such as adsorbed or chemisorbed carbonaceous species, in the TMDC layer.

In this context, Ref. 154 revealed that electron beam exposure can alter the photoluminescence emission characteristics of MoS_2, WSe_2, and WS_2. After exposure, all materials exhibited a broad defect luminescence at energies below the bandgap-related exciton luminescence [Fig. 7(f)], notably at room temperature and without the demonstration of single-photon emission. For MoS_2, compositional analysis by EELS [Fig. 7(g)] further revealed a uniform Mo and S distributions, while significant C, O, and Si contents were detectable in the electron beam-exposed regions.[154] After mechanical cleaning by AFM,[287] the room-temperature defect luminescence disappeared. Both observations are consistent with an extrinsic contribution to the defect luminescence due to e-beam activated deposition of organic species, which can be omitted by encapsulating the TMDCs, e.g., in hBN before the beam exposure takes place.[154,217] For monolayer MoS_2, electron beam irradiation with 5 keV, i.e., far below the knock-on threshold, was recently shown to result in the formation of single-photon emitters,[148] whose spectral characteristics are consistent with vacancy-related SPEs created by 30 keV He-ion beam irradiation.[58,62,217] Importantly, the electron beam irradiation was found to be only effective on non-encapsulated samples suggesting beam-induced chemical etching or chemical modification of the exposed MoS_2 layer to be the dominant process of defect creation. The above discussion also highlights the need to carefully distinguish between creation of defect emitters,

02 July 2026 15:24:17

© Author(s) 2025

e.g., by the introduction of lattice defects, or the activation of defect emitters, e.g., by modifying the charge state of already existing defects.

IX. X-RAY AND UV IRRADIATION

So far, only very few attempts have been reported to locally generate defects and corresponding SPEs in TMDCs and hBN with the help of high-energy photon irradiation. Recently, the x-ray-based generation of sulfur vacancies was reported for monolayer MoS_2 [Fig. 8(a)],[288] which are consistent with the SPEs in the same material.[58,62] Soft x-ray irradiation leads to the emergence of distinct 3d Mo spectral features in the core-level photoemission spectra of MoS_2 associated with undercoordinated Mo atoms [Fig. 8(b)]. In particular, the photoemission spectra of the spin–orbit split doublet Mo $3d_{5/2}$ and Mo $3d_{3/2}$ [blue fits in Fig. 8(b)] and the corresponding appearance of an additional doublet shifted to lower binding energies (green) can be traced to the impact of the x-ray irradiation and to the presence of sulfur monovacancies (SV). Generally, similar spectral changes have been observed earlier for Ar and He bombardment,[290,291] thermal annealing,[292,293] and as-grown defective TMDCs.[294] Monitoring the binding energy of the Mo $3d_{5/2}$ core-level photoemission peak across the MoS_2 monolayers indicates the emergence of lateral space-charge regions associated with the local, x-ray-based generation of sulfur vacancies in MoS_2 [Fig. 8(a)]. Most likely, the sulfur monovacancies are locally generated via ionization-induced bond destabilization arising from the x-ray absorption within MoS_2 as well as inelastic scattering of secondary electrons emitted from the substrate.[288] The latter secondary process is also relevant for the generation of defects in TMDCs by charged particle beams (cf. corresponding sections above).

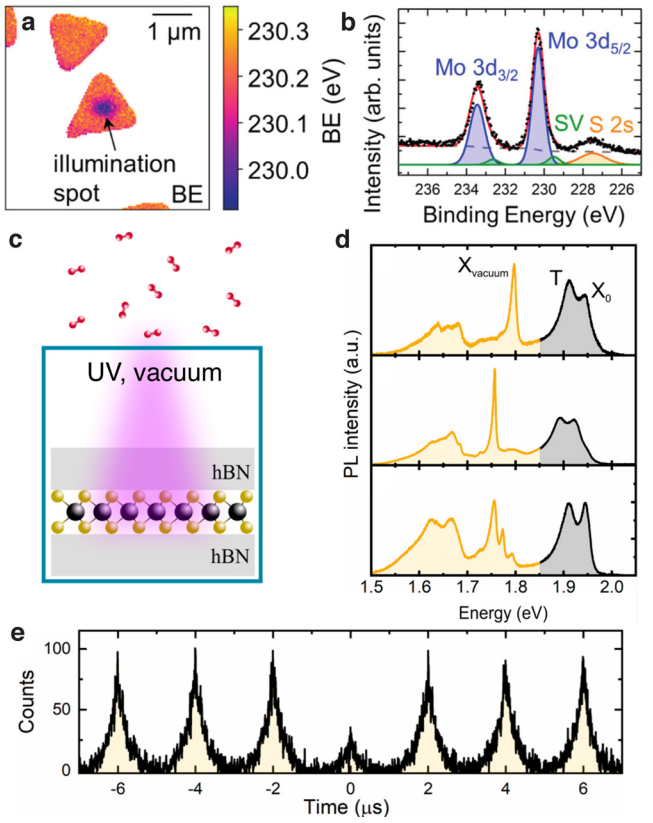


FIG. 8. Local generation of defects utilizing x-ray irradiation. (a) Map of the binding energy of the Mo $3d_{5/2}$ core-level photoemission peak after the illumination with a focused x-ray beam, indicating the local generation of defects. (b) Core-level photoemission spectra of the spin–orbit split doublets Mo $3d_{5/2}$/Mo $3d_{3/2}$ for an x-ray dose of 5 MJ/cm^2. The extracted contributions of the x-ray generated single-sulfur vacancies (SV) and disulfur vacancies (S 2s) are highlighted in green and yellow, respectively. Reprinted with permission from Grünleitner *et al.*,[288] ACS Nano **16**, 20364–20375 (2022). Copyright 2022 American Chemical Society. (c) Schematic of defect generation within a encapsulated monolayer under UV illumination in vacuum. (d) Representative spectra of defect emitters (yellow) created via UV illumination. (e) The defect emitters show single photon characteristics. Reprinted with permission from Wang *et al.*,[289] ACS Nano **16**, 21240–21247 (2022). Copyright 2022 American Chemical Society.

We further highlight a recent study, demonstrating that SPEs can be induced in monolayer MoS_2 by unfocused UV irradiation with a deuterium lamp over an extended period of time in vacuum [Fig. 8(c)].[289] Interestingly, the resulting spectral signatures [defect peak centered around 1.75 eV, Fig. 8(d)] are consistent with those reported for He-ion beam-irradiated samples (see Sec. VI) as well as thermally treated samples that are associated with the generation of pristine, unpassivated sulfur vacancies.[12,62,217,295,296] For defects created by UV irradiation of encapsulated samples in vacuum, a clear antibunching and corresponding single-photon emission was demonstrated [Fig. 8(e)]. Another recent study reported creation of defect emission in multilayer GaSe by UV laser (266 nm) irradiation, although without evidence for single-photon emission.[297]

X. MICROSCOPIC NATURE OF THE EMITTERS

A. For hBN

As mentioned in previous reviews,[78] the quantum emitters in hBN are typically categorized into four main families: the broad emission in the near-infrared (NIR), the sharper emission around 2 eV displaying identifiable phonon sidebands, the blue emitters with emission around 2.8 eV (the so-called B-centers), and finally the emission in the UV around 4.1 eV. There is strong evidence through photoluminescence excitation spectroscopy (PLE) and *ab initio* calculations that these four families of emitters are localized color centers with energies of their electronic states deep in the large optical gap (5.9 eV) of hBN. This situation corresponds to the atomic picture presented in Fig. 1(a). Efficient excitation of these deep electronic states is possible by exciting on resonance discrete vibronic states, i.e., electronic states dressed by the vibrations surrounding the emitter, as revealed by PLE measurements on NIR,[239] 2 eV,[80,93] and B-centers.[269] In this section, we focus on the emitters created by irradiation engineering and we attempt to relate the mechanism of creation to their proposed microscopic structure according to the published literature. Understanding the effect of particle irradiation on the atomic structure of hBN can shed light on the internal structure of emitters, a topic for which to date no unified consensus has been reached. Table I shows a survey of the main irradiation methods used and links them to the photophysical properties of the created emitters.

In general, identifying the microscopic nature of quantum emitters in multilayer hBN is challenging. Atomic resolution imaging techniques, such as transmission electron microscopy (TEM) and scanning tunneling microscopy (STM), often encounter non-ideal experimental conditions with hBN samples. Despite promising early attempts using TEM and cathodoluminescence,[82] TEM imaging faces difficulties due

02 July 2026 15:24:17

© Author(s) 2025

TABLE I. Table presenting photophysical information about quantum emitters created by irradiation engineering in hBN. For each category of emitters, the proposed defect complex structure is listed. N.A.: not available. DAP: donor–acceptor pair. Neutr.: neutrons. Graph.: graphene.

Irradiation method	Particle	Ref.	E_{ZPL} (eV)	FWHM (GHz)	Lifetime (ns)	$g^{(2)}(0)$	Proposed origin
Plasma and low-energy ion	He	228	≈1.5	N.A.	N.A.	N.A.	V_B^-
	O	299	≈1.91–2.25	2100–3100	0.55–0.8	0.14–0.23	N.A.
	O	79, 80	≈1.8–2.3	500 (10 K)	2	0.1–0.8	V_NC_B, C_2C_N, C_2C_B
	Ar, O	208	≈1.6–2.25	1660 (10 K)	2.4	0.1	V_BO_2
	Li, Ga, Neutr.	116	≈1.46	N.A.	1.2	N.A.	V_B^-
Ion irradiation	He, O, N, Xe, Ar	213, 233, 236, 300	≈1.5–1.55	38 k (5 K)[236]	0.77–1.028 [233]	N.A.	V_B^-
	Ga	34, 301	≈2–2.3	N.A.	N.A.	0.24, 0.33	$V_BO_N^-$[302]
	He	303	2.73, 2.86	N.A.	N.A.	N.A.	B_i
	Electrons	304	≈1.55	N.A.	N.A.	N.A.	V_B^-
	⋯	305	≈1.6–2.2	283–936	2.9–6.7	0.34–0.39	N_BV_N
E-beam	⋯	284	≈2.15	≈18 k	3–5	0.2–0.55	$(C_BC_N)^2(C_NC_B)^2$
	⋯	66	2.16	6800	N.A.	N.A.	Carbon cluster
	⋯	[35], 306, 307	≈2.85	0.75 (5 K)[307]	1.85	0.1–0.25	C_N^2, N^2, *trans*-C_4
	⋯	36, 308	≈2.85	≈2.2 (5 K) [308]	2.27 [308]	0.19	C_N^2, N^2, *trans*-C_4
	C	77	≈2	4424	2–6	<0.5	$V_BC_N^-$
Implantation	Ar on Graph./hBN	230	2.14	N.A.	N.A.	N.A.	C_BC_{N2}
	C	257	2.24	<36 (4 K)	4.4	0.07	DAP
	$^{13}CO_2$	278	2.1 and 1.8	≈25 k	N.A.	<0.5	$C_B^+C_N^0$-DAP C_BO_N

to the bulkiness of samples and the low atomic number Z of boron and nitrogen elements. The latter renders identifying atomic defects within atomic columns difficult, since the intensity of the detected signal is proportional to $Z^{1.8-1.9}$ resulting in poor contrast for single point defects in a multilayer sample. Additionally, correlating type and structure of defects with their photophysical properties simultaneously is problematic. Often, optical spectroscopy is used to detect quantum emitters, followed by TEM for atomic resolution characterization,[66,303] but the difference in spatial resolution between the two techniques makes it uncertain whether the same defects are predominantly probed in the different experiments. Sometimes different samples are used for optical and electron microscopy, further complicating direct correlation. To create a tunneling current, STM requires few-layer or monolayer hBN samples due to its large bandgap. Early studies using graphene-covered hBN[309] provided insights into defect charge states and electronic structures but, unlike a more recent work,[68] did not correlate these with optical measurements. In Sec. XI, we highlight recent developments combining STM and luminescence at the atomic scale that may tremendously accelerate the identification of the microscopic nature of SPEs in vdW materials.

Nevertheless, by combining multiple, complementary spectroscopic methods, the nature of some emitters in hBN was already clarified. Figure 9 sketches ball-and-stick models of defect structures occurring in hBN as discussed in the following. Combining photoluminescence and magnetic measurements, including ODMR and electron paramagnetic resonance spectroscopy (EPR), was used to pin-point the nature of the broadband emitters in the NIR with an emission peak centered around 800 nm wavelength.[116] Negatively

02 July 2026 15:24:17

© Author(s) 2025

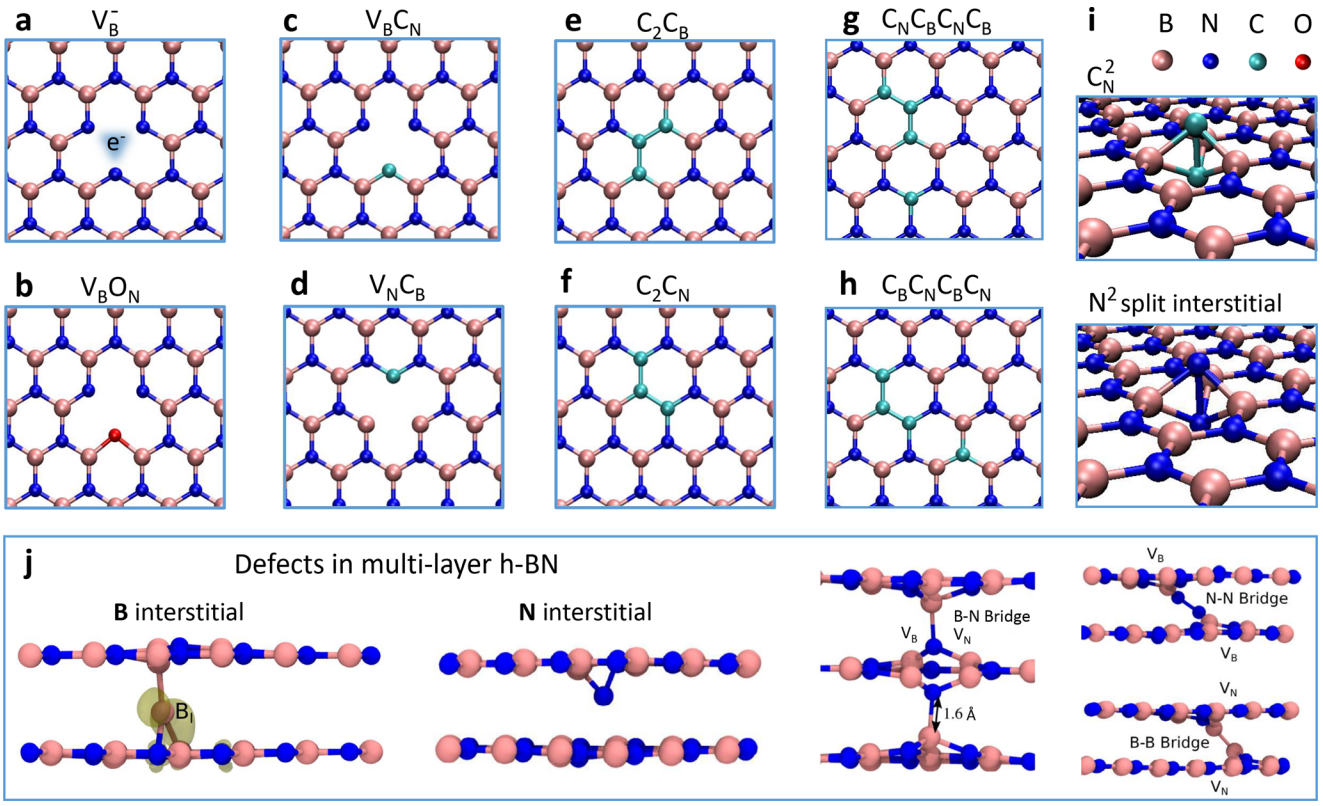


FIG. 9. Microscopic structure of several candidate defects for experimentally observed SPEs in mono- and multilayer hBN. (a) Charged boron vacancy. (b) Oxygen-vacancy center. (c)–(h) Examples of carbon-based centers. (i) Examples of split interstitial centers. (j) Examples of interlayer defect centers in multilayer hBN. The atomic models of the defect structures in (j) are taken from Ref. 298.

charged boron vacancies V_B^- [Fig. 9(a)] are now generally accepted to be responsible for this broadband NIR emission line. Furthermore, the broad luminescence spectrum featuring large phonon sidebands and the apparent absence of a zero-phonon line was related to the large electron–phonon coupling in V_B^- defects.[113] The comparably large Huang–Rhys factors above 3.5 explain that most of the emission is going through the phonon sidebands.[310] Ensembles of V_B^- are reliably generated via irradiation methods (see Sec. VI). It should be pointed out that the concentration of optically active defects may be substantially lower than what is expected just after irradiation. For example, boron vacancies may be neutral or doubly charged[298,311,312] due to charge transfer from other defects, or defect concentration can decrease due to the annealing of defects through annihilation of vacancies with interstitials, which are mobile at room temperature.[298,311] So far, V_B^- defects have been thoroughly characterized only as ensembles, since their low internal quantum efficiency hinders the detection and characterization of single defects.[235] Furthermore, the generation mechanism via irradiation engineering and the mechanism leading to the trapping of an electron by the boron vacancy is still under debate and will require further studies to be clarified.[233] Nonetheless, the V_B^- defect is considered to be one of the few hBN defects whose internal atomic structure and level scheme are well known, thanks to the extensive amount of studies conducted to date.[113,116,233,238,239,244,245,255,313] The system, possessing D_{3h} point symmetry, exhibits a spin-triplet ($S = 1$) ground state $^3A_2'$ and a corresponding spin-triplet excited state $^3E''$.[116,235] The ground state presents a so-called axial zero-field splitting $D_g \sim 3.47$ GHz between the spin sublevels $m_s = 0$ and $m_s = \pm 1$, with m_s electron spin projections along the c-axis of the hBN.[116] Likewise, the excited-state spin triplet has a zero-field splitting $D_e \sim 2.1$ GHz.[239,314,315] Additionally, a manifold of metastable singlet states (MS) is present, which can be populated from the excited state via intersystem crossing. Spin transitions between different m_s states are normally addressed by microwave pumping in ODMR experiments, where such transitions appear as strong resonances in ODMR spectra.[116] It is generally agreed that the splitting between those resonances depends on magnetic fields through the Zeeman effect,[116] whereas the residual splitting E (in the absence of external magnetic field) has recently been under debate. Originally, it was attributed to strain effects in the hBN,[116,231] but recent works discuss contributions from spin-sublevel mixing induced by a local electric field perpendicular to the c-axis.[244,245,255] Finally, each ODMR resonance is split sevenfold due to hyperfine interaction with the three surrounding ^{14}N $I = 1$ nitrogen nuclei.[116] It is assumed that only the excited state of the triplet system is optically active, while non-radiative decay paths are spin-dependent, that is, spins excited from the $m_s = \pm 1$ manifold decay radiatively less likely compared to the excited population of the $m_s = 0$ state. Therefore, V_B^- defects can be spin-polarized in the $m_s = 0$ spin sub-level within a few optical cycles.[116,234] Thanks to the

02 July 2026 15:24:17

© Author(s) 2025

fairly short lifetime of the metastable state (on the order of tens of nanoseconds[235,316]) the defect relaxes rather rapidly and can be re-pumped efficiently, despite its poor quantum efficiency. The V_B^- can therefore be optically initialized and coherently manipulated.[116,119] Typical spin-lattice relaxation times T_1 are on the order of tens of μs[119,228,231,256,317] and spin coherence times T_2 are around 100 ns,[120,228,255,256,317] with the possibility to be extended up to few μs.[120] Yet, the coherence time of V_B^- defects is limited by the nuclear spin bath of the hBN crystal, reducing their competitive edge against similar spin defects in 3D host systems.[318] A recent work using high-temperature annealing in oxygen reported quantum emitters with emission around 1.5 eV and very narrow linewidth.[319] If these emitters are paramagnetic, they could represent a good contender for spin-state manipulations on the single photon and emitter scale.

Next, we focus our discussion toward the origin of the SPEs observed around 2 eV. These emitters usually display an identifiable ZPL with clear phonon sidebands at energies around 160–170 meV below the ZPL. The phonon sidebands usually comprise both bulk optical phonon modes[85] and localized phonon modes.[80] Many types of elements and defect structures have been proposed as the microscopic origin of the ZPLs around 2 eV. This includes silicon,[267] oxygen [Fig. 9(b)],[267,302] and most prominently carbon [Figs. 9(c)–9(h)],[267,270,320–322] all of which are typically ubiquitous elements present around the hBN sample. A first systematic study involving the growth of hBN with MOVPE and MBE in carbon-rich environments as well as carbon implantation [cf. Fig. 6(b)] showed that carbon-based defects are the likely source for the emission observed around 2 eV.[77] In Ref. 267, the authors compared four different carbon-based structures with different charge and spin states, namely, C_B, C_N, V_BC_N [Fig. 9(c)], and V_NC_B [Fig. 9(d)]. The V_BC_N was identified as the most likely explanation of the observed luminescence spectra.[267] A further study prepared comparable quantum emitters in hBN via low-energy oxygen irradiation and subsequent annealing.[79] Fischer *et al.*[79] explained the formation of these carbon-based defect complexes by a two-step process. First, a low-energy ion irradiation amorphizes the top few layers of hBN. Then, the subsequent annealing in a carbon-rich environment leads to the formation of defects with substitutional carbon atoms, such as V_NC_B. An extension of this work, using the same irradiation-based method, compared low-temperature PL spectra with 26 optical transitions calculated from nine different defect complexes with different spin and charge states.[80] Their model used a novel combination of *ab initio* calculations with open quantum system theory (OQST), in particular the polaron model,[323] allowing an accurate description of the coupling of the electronic states with phonons in the presence of the electromagnetic field.[324] A statistical comparison of the theoretical spectral profiles for these 26 different optical transitions with the experimental data from 12 emitters in hBN suggested that C_2C_B [Fig. 9(e)], C_2C_N [Fig. 9(f)], and V_NC_B defect complexes match the experimental data best.[80] The above theoretical approach further allows modeling of photoluminescence excitation spectroscopy (PLE) maps,[80] which give crucial information about absorption properties and the electron–phonon coupling strength of the emitters.[93] When comparing the calculated PLE maps with experimental data, it was found that, in fact, C_2C_N and C_2C_B captured well the absorption spectra measured with PLE, with better agreement than V_NC_B. These results were in line with a comparable work using emitters in hBN produced by high-temperature annealing.[325] We note that calculations of C_2C_N lifetimes agree well with measurements on 2 eV emitters, showing nanosecond lifetimes (see Table I), while calculations on C_2C_B have shown two orders of magnitude longer lifetimes.[320] These works confined their comparison between experiments and theory to dimers and carbon trimers. More recently, four-atom structures were proposed as the microscopic origin of 2 eV emissions generated by electron beam irradiation.[284] Other even larger complexes, such as $C_NC_BC_NC_B$ [Fig. 9(g)] or $C_BC_NC_BC_N$ [Fig. 9(h)], were also proposed as the emitters generated by electron beam irradiation,[66] annealing at high temperatures,[326] or chemical vapor deposition.[327] More recently, a work employing pulsed laser deposition (PLD) combined with C-doping has proposed a trimer structure ($C_BC_NC_B$) for the reported SPEs (showing values for autocorrelation among the best ones for SPEs in hBN[273]) Thus, it seems that many different carbon complexes can be formed in the hBN lattice, thereby making the identification and controlled generation of 2 eV quantum emitters in hBN challenging. Further systematic studies are necessary and new methodologies need to be developed to identify the true microscopic nature of these emitters and to find ways to generate them on demand and site-selectively, ideally with high yield, specificity, and accuracy. Magnetically active quantum emitters in the 2 eV range have been now observed in samples synthesized in carbon-rich MOVPE.[115,264,328] As addressed in Sec. VII, a recent work reports the successful creation of apparently spin-active quantum emitters in the 2 eV region via low-energy implantation of CO_2 purified with the ^{13}C isotope.[278] *Ab initio* calculations compared with magnetic spectroscopy suggest that the microscopic origin of these defects are the so-called $C_B^+C_N^0$ donor–acceptor pair (DAP) and C_BO_N, respectively. This is, to our knowledge, one of the first works using magnetically active isotopes to fingerprint the presence of carbon in spin-active quantum emitters. Another interesting possibility is the oxygen-based defect complex,[302] which seems to match well the spectral profiles of quantum emitters generated by focused ion beams.[34] The complex V_BO_N [Fig. 9(b)] is supposed to be paramagnetic with an emission of the ZPL at 2 eV. ODMR and EPR measurements could be used to unambiguously identify these oxygen-based emitters.

We would also like to point to a recent work, suggesting that tape and organic solvent residues, which are commonly introduced during the exfoliation process of hBN, may lead to the formation of polycyclic aromatic hydrocarbons (PAHs).[329] In particular, during the so-called activation step at high temperature and in an inert atmosphere, such as argon, organic residues trapped below the hBN flakes can react to form PAH molecules. These are known to possess excellent quantum optical properties.[330] The challenge here is that spectra from PAHs show features similar to crystallographic defects in hBN, with an identifiable ZPL followed by a phonon sideband at 160–170 meV. Previous studies on CVD-grown hBN demonstrated that oxygen plays a key role in the photobleaching of such molecular emitters,[326] similar to laser-induced photobleaching of dye molecules.[331] Further research involving advanced cleaning processes to ensure the removal of all organic residues would be needed to clearly identify the contribution of PAH and crystallographic defects in the generation of 2 eV emitters.

The most promising quantum emitters generated in hBN in terms of quantum optical properties, such as photon purity $g^{(2)}(0)$ and coherence, are the B-centers.[35,36,103] They can be generated on demand and with high spatial resolution using keV electron beams. B-centers display a ZPL energy around 2.85 eV ($\approx$ 435 nm) with a linewidth on the order of a GHz,[269,308] which is even close to lifetime-limited on timescales shorter than their spectral diffusion.[307] They can be reproducibly created with the same ZPL energy and they possess good quantum optical

02 July 2026 15:24:17

© Author(s) 2025

properties,[308] with a high purity as well as a good quantum coherence.[269,307,332] Cathodoluminescence investigations seem to indicate that the generation of B-centers is correlated with the presence of emission at 4.1 eV,[36] as observed in previous works.[283,333–335] The emission at 4.1 eV could correspond to the presence of carbon impurities[333,334] or to the C_BC_N carbon dimer.[268,270,336,337] The exact formation mechanism of the B-centers is still unknown, but electrons with tens of keV can lead to radiolysis. The ionized electrons and radicals can react to form new defect complexes (see also Sec. VIII). Under the action of the electron beam, C_BC_N defect complexes present in the hBN lattice could react with interstitial boron atoms[81] and lead to the formation of the B-centers. A more recent work[281] points toward electron beam-induced electromigration of charged defects clustering together with native vacancies and interstitial atoms to form the B-center. Polarization-dependent measurements showed that the polarization of the emission is preferentially oriented along directions separated by 60°, which could correspond to the crystallographic orientations of the hBN lattice.[338] Regarding the microscopic nature of the B-centers, a recent investigation found a nonlinear Stark effect and the absence of a permanent dipole for these centers.[81] Due to symmetry arguments, this observation seems to indicate that the B-centers are consistent with split interstitial configurations[339] [Fig. 9(i)]. The formation of the B-centers has been related to the presence of the carbon-based emitters C_BC_N at 4.1 eV, so the split interstitial carbon structure seems to be a good candidate for this color center.[81] Even more recently, the same group generated B-centers in hBN and rhombohedral boron nitride (rBN) with a keV electron beam.[340] The blueshift observed experimentally between the ZPL of these emitters in hBN and those in rBN are well captured by DFT calculations[340,341] and hints toward a newly proposed defect complex, the *trans*-C4 configurations. Another research group created blue emitters[303] by keV Helium ion irradiations, but, in contrast to prior works on B-centers, they observed a new class of blue emitters with ZPL centered at 2.73 eV. Based on TEM imaging of the e-beam-irradiated samples, the study speculates that the emission around 2.73 eV is related to boron interstitial B_i intercalated between the hBN layers, which are sketched in Fig. 9(j) along with other possible interstitial configuration for multilayer hBN.

B. For TMDCs

In contrast to hBN, SPEs in 2D TMDCs exhibit rather low detrapping barriers (on the order of tens of meV) and require consequently cryogenic temperatures to be optically active. Their

TABLE II. Table gathering photophysical information about quantum emitters created by various methods in TMDCs and related materials. g-factors are quoted as absolute values. 1L: single layer, ML: multilayer, N.A.: not available.

Method	Material	Refs.	E_{ZPL} (eV)	FWHM (GHz)	Lifetime (ns)	$g^{(2)}(0)$	g-factor
Strain (intrinsic)	1L $MoSe_2$	286	1.58–1.62	36–97 at 4 K	N.A.	N.A.	3.8
	1L WSe_2	4–8	≈1.65–1.71	≈30	0.5–7	0.03–0.2 at 4 K	7–12
Strain pillar (SiO_2)	1L WSe_2	57, 190	≈1.51–1.7	≈43	3–12	0.01 (4 K)–0.09 (10 K)	N.A.
	ML GaSe	342	1.65–2.06	400–2000	4–6	0.3–0.5 at 3.5 K	N.A.
Strain pillar (Au)	1L WSe_2	46	≈1.59–1.7	240	0.7–3.7	0.3 at 3 K	N.A.
Strain (electrostatic)	1L WSe_2	188	1.57–1.67	220	2.6	0.4 at 4 K	N.A.
Strain gap (dielectric)	1L WSe_2	51	≈1.6–1.67	110	≈10–100	0.26 at 4 K	N.A.
Strain dome (H-implantation)	1L WS_2	39	≈1.9–1.97	≈200–1200	3–7	0.15–0.25 at 7 K	7–9
Strain dent (molding)	1L $MoSe_2$	52	≈1.58	40	0.2	0.3 at 1.8 K	4.1
Strain and e-beam	1L WSe_2	63	1.55–1.7	N.A.	N.A.	≈0.3 at 3.5 K	N.A.
	1L WSe_2	38	1.52–1.58	20	4–6	0.27 at 150 K	N.A.
	2L WSe_2	45	1.48–1.59	≈30	4.8	0.03 at 3.5 K	N.A.
Strain pillar (resist)	ML InSe	56	0.80–0.95	≈650	3–90	0.34–0.6 at 10 K	N.A.
	ML $MoTe_2$	53	0.8–1.1	800	22–160	0.06–0.18 at 11 K	3.6
Strain (AFM-indentation)	1L WSe_2	196	1.55–1.72	600	1–30	0.02–0.15 at 7 K	N.A.
	1L WSe_2	173	≈1.61–1.7	≈150	8	0.33–0.41 up to 60 K	N.A.
	1L WSe_2	197	1.58–1.69	≈100	≈2–8	0.3–0.4 at 4 K	N.A.
Low-energy e-beam	1L MoS_2	148	1.77–1.85	>170	N.A.	N.A.	0.95
UV irradiation	1L MoS_2	289	1.75–1.8	>550	100–140	0.05–0.42 at 5 K	N.A.
	1L $MoSe_2$	221	1.56	4000	10–20	Ensemble	N.A.
Proton irradiation	1L $MoSe_2$, MoS_2, WSe_2, WS_2	37	1.5–1.95	5800–9700	2–200	Ensemble	N.A.
Cr-implantation	1L $MoSe_2$	144	1.48–1.52	3500	14	Ensemble at 10 K	1.2
He-ion irr.	1L MoS_2	33, 98, 217, 218, 296	1.75–1.85	60	270–1730	0.23–0.44 at 1 K	0.1–1.3
Nb-doping	1L WS_2	126	1.92–1.93	75	80	0.27 at 4 K	10.4

02 July 2026 15:24:17

© Author(s) 2025

microscopic origin is mostly interpreted in terms of strain-localized, impurity-localized, or vacancy-localized excitons, although color centers based on deep levels with emission energies in the telecom range have been predicted for some of the large gap TMDCs[70] as well. Table II summarizes SPEs (and some other defect-associated emitters) in the most common TMDCs (MoS_2, $MoSe_2$, WSe_2, WS_2, $MoTe_2$) and some monochalcogenides (GaSe and InSe). Toward narrowing down the origin of the single-photon emission, particularly useful experimental fingerprints are the doping dependence and g-factor of the defect-related excitons. In strained WSe_2 and WS_2, large g-factors ($|g| \approx 8$–10) are found, and they are associated with dark exciton states. In turn, the single-photon emission is attributed to strain funneling and localization of dark excitons,[128] which hybridize with shallow trap states close to the conduction band [cf. Fig. 1(d)].[59] Due to strong localization at the defect sites, the optical selection rules are relaxed resulting in an effective brightening and radiative recombination of the dark states. Note that the experiments are consistent with an intrinsic origin of the defect states, such as shallow impurities or vacancies, but future studies might reveal the impact of possible extrinsic effects from, e.g., absorbed and chemisorbed molecules as well (cf. Sec. VIII). For strain-induced SPEs in $MoSe_2$ and $MoTe_2$, g-factors consistent with a bright exciton state were found ($|g| \approx 4$). In the case of unstrained 2D TMDCs with impurities, for example, Cr-implanted $MoSe_2$ and Nb-doped WS_2, the predominant origin of exciton localization appears to be donor/acceptor-bound excitons [cf. Fig. 1(b)]. Nevertheless, the measured g-factors can vary significantly from $|g| \approx 1$ for Cr-implanted $MoSe_2$[144] to $|g| \approx 10$ for Nb-doped WS_2,[126] which generally point to different admixtures of localized states and extended states in the radiative recombination process.[73] For Nb-WS_2, the exclusive incorporation of Nb on W-sites, as would intuitively be expected for a dilute metallic dopant, was verified by STEM enabling a detailed comparison of DFT-calculated electronic structure and single-particle g-factors. Calculations place the Nb-induced defect bands just below the valence band maximum resulting in significant defect-to-band hybridization. Based on the large g-factor, a likely scenario is a defect-induced brightening of a spin-forbidden transition involving a valence band state. Therefore, decay of neutral dark excitons bound to ionized Nb, denoted as $Nb^{-}X^{0}_{D}$, was proposed as the dominant radiative recombination pathway, leading to the observed SPE with $g \approx 10$. By contrast, for Cr-implantation of $MoSe_2$,[144] several different defect geometries, including Cr adatoms, Cr on Mo-sites, and Cr at Se sites with a Se adatom, are considered likely based on molecular dynamics simulations. In turn, an assignment of the optical transition based on the observed g-factor alone is difficult. Due to the absence of the defect emission for p-type doping in field effect devices, radiative recombination of an electron bound to a defect state with a valence band hole was tentatively proposed. The small negative g-factor of $g \approx -1.2$ may potentially be explained by a

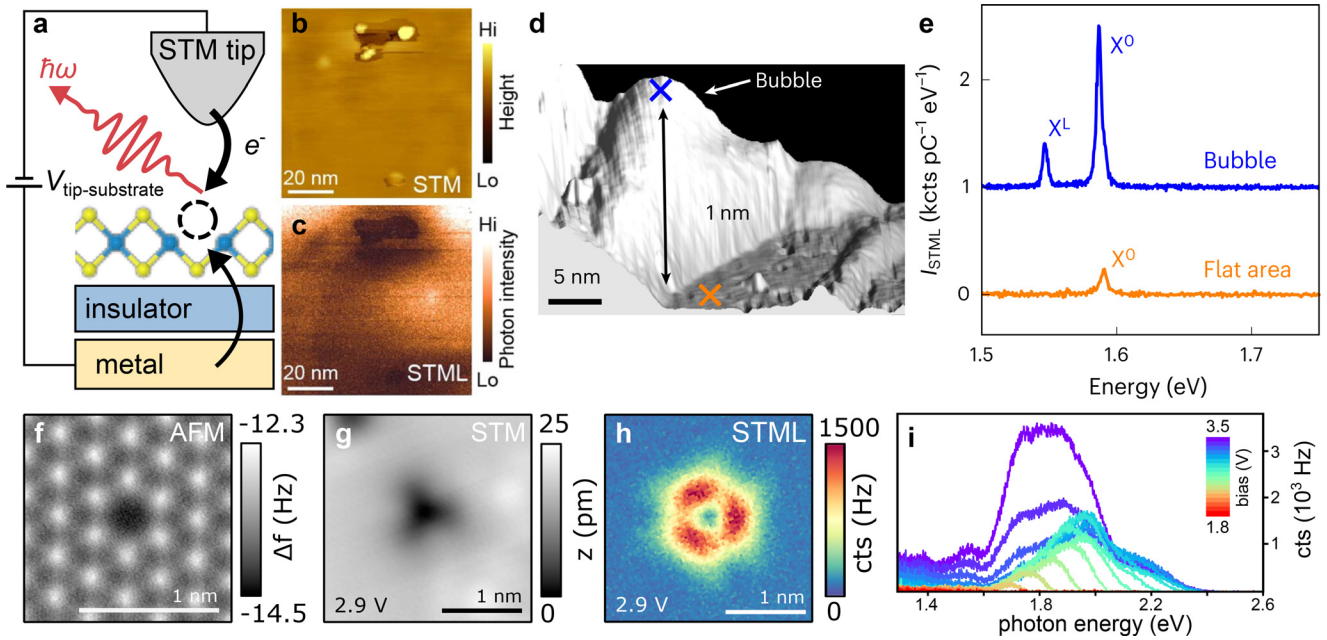


FIG. 10. Atomic-scale characterization of defect-based SPEs. (a) Schematic of scanning tunneling microscope-induced luminescence (STML). (b) STM topography of a WSe_2 monolayer with a hBN decoupling layer. (c) Topographic features correlate with nanoscale variations in STML. Reproduced with permission from Geng *et al.*[343] ACS Nano **18**, 8961–8970 (2024). Copyright 2024 American Chemical Society. (d) STM topography of a $MoSe_2$ monolayer with a graphite decoupling layer on Au(111). (e) The graphite provides sufficient decoupling to acquire STML spectra resolving both free X_0 and localized excitons X_L with nanoscale spatial resolution. Reproduced with permission from López *et al.*[344] Nat. Mater. **22**, 482–488 (2023). Copyright 2023, The Author(s), under exclusive license to Springer Nature Limited. (f) Non-contact AFM image of monolayer WS_2 directly placed on epitaxial graphene. The bright features denote the positions of the sulfur atoms with a single-sulfur vacancy at the center of the image. (g) STM image revealing the defect orbital of the sulfur vacancy. The tip-substrate voltage is 2.9 V. (h) STML mapping of a single-sulfur vacancy. The tip-substrate voltage is again 2.9 V. (i) Bias-dependent luminescence spectra. Due to the missing decoupling layer to the substrate, a fast plasmon-mediated emission process prevails over the slow recombination dynamics of the defect-localized exciton. Reproduced with permission from Schuler *et al.*,[64] Sci. Adv. **6**, eabb5988 (2020). Copyright 2020 Authors, licensed under a Creative Commons Attribution Non Commercial 4.0 (CC BY-NC) License.

02 July 2026 15:24:17

© Author(s) 2025

large g-factor for the electron acceptor level (compensating the large g-factor of holes near the valence band maximum), as would be case for Cr on a Mo site, or by a reduced g-factor of holes in the valence band due hybridization with the defect, as would be the case for Cr on a Se site. For proton or He-ion beam irradiation, experiments point toward a predominant creation of chalcogen vacancies[58,62,221] narrowing the discussion and theoretical modeling to these structures. For SPEs in He-ion exposed MoS_2, a vanishing valley polarization and a small positive g-factor (between +0.1 and +1.3) were measured experimentally.[296] Both observations were found to be consistent with exciton transitions where the presence of sulfur vacancies results in strong hybridization between defect and band states [cf. Fig. 1(c)] as calculated by BSE-GW calculations.[71,73] Moreover, the predicted optical absorption characteristics are consistent with photovoltage spectra as detected in corresponding vertical tunneling devices.[98] For proton irradiated $MoSe_2$,[221] a finite valley polarization was observed for the defect emitters. Therefore, band excitons which retain the valley character bound to deep acceptor levels introduced by selenium vacancies [cf. Fig. 1(b)] were proposed as the microscopic origin. The diversity of observation and interpretations for SPEs in both hBN and TMDCs highlight the importance of an unambiguous atomic-scale characterization, which we discuss in Sec. XI.

XI. TOWARD ATOMISTIC CONTROL AND CHARACTERIZATION

An emerging technique to correlate atomic structure and optical properties of defect-based SPEs is scanning tunneling microscope luminescence (STML) as sketched in Fig. 10(a). Electrons tunnel from the STM tip into local states in the 2D layer. In a simple picture, if the electrons are injected with sufficiently high excess energy, which is controlled by the tunneling bias $V_{\mathrm{tip-sample}}$, they can relax by emitting photons, which are then detected in the far field.[345,346] Following early works from around 1990[347,348] STML has achieved so far spatial imaging with atomic resolution,[349] vibronic coupling,[350,351] time-resolved luminescence,[352] and single-photon statistics.[353,354] A key challenge is detecting emission spectra which are specific to the molecular or defect structure in which electrons are being tunneled, because the junction between the metallic tip and the metal substrate forms a plasmonic cavity,[355] which can dominate the light emission process and spectral fingerprints. To overcome this limitation, a decoupling layer needs to be introduced between the localized state and the metal substrate [Fig. 10(a)]. In a simplified picture, the decoupling layer extends the lifetime of the excited electronic state in the molecule[356] or defect[357] by preventing fast tunneling into or quenching by the metal substrate, which in turn allows the sample-specific photon emission to prevail. For molecules, few-layer NaCl evaporated *in situ* is a common barrier layer.[356] For 2D TMDCs, hBN barriers can decouple the 2D layer and the defects therein from the metallic substrate, such as graphene[358] or Au.[343] Figures 10(b) and 10(c) compare topography and STM-induced electroluminescence of a WSe_2 monolayer decoupled from the substrate by a 10 nm-thick hBN layer and connected in a lateral fashion to a gold substrate. The spatial maps of the exciton electroluminescence exhibit nanoscale variations that correlate with the STM topography. Interestingly, efficient excitonic STML and nanoscale imaging were also achieved in monolayer $MoSe_2$ that was only weakly decoupled by few-layer graphite from a Au (111) substrate[344] [Figs. 10(d) and 10(e)]. This may be related to the strong oscillator strength and concomitant short radiative lifetime of free excitons in 2D TMDCs. The spectra clearly differentiate tip-induced luminescence from free excitons and excitons localized to nanoscale topographic features, such as bubbles. As a possible excitation mechanism for the electroluminescence, a many-body excited-state picture was proposed.[344,359] Electrons (holes) injected into the conduction (valence) band form a negatively (positively) charged excited-state resonance. The system can either directly relax back to the neutral ground state, where the electron (hole) tunnels into the substrate, or it can form an intermediate exciton state by binding a hole (electron) tunneled into the 2D layer from the substrate. Note that, due to the Coulomb interaction, the exciton state represents an intermediate energetic minimum. Now, the system can relax to the neutral ground state by emission of a photon. This picture highlights the importance of balancing the tunneling rates between tip-sample, for example by controlling the tip-sample and the tip-substrate distance, for example, by introducing a suitable decoupling layer. Toward the ultimate goal of identifying and controlling single-photon sources in 2D vdW materials by STML, Figs. 10(f)–10(i) depict experiments on single-sulfur vacancies in monolayer WS_2 on epitaxial graphene.[64] Non-contact atomic force microscopy using a CO-functionalized tip resolves a single lattice defect at a sulfur site [Fig. 10(f)]. The electronic spectroscopy by STM identifies the defect as a sulfur vacancy [Fig. 10(g)]. Mapping of the STML demonstrates efficient driving of electroluminescence by tunneling into the defect orbital [Fig. 10(g)]. However, the photon spectra indicate a dominant plasmonic light emission process, which is likely due to the absence of a decoupling layer and a rather long radiative lifetime, as measured for SPEs in MoS_2.[217] Despite the absence of a clear spectral fingerprint and of single-photon statistics, the latter examples highlight the progress toward a complete atomistic understanding of SPEs in 2D materials.

Similarly, significant progress toward correlating atomic structure and optical properties via (transmission) electron microscopy has been reported. For example, excitonic wavefunctions in an atomically thin heterostructure were reconstructed by precise low-energy electron loss spectroscopy.[360] Using STEM-based CL, multiple classes of stable quantum emitters were resolved in hBN.[82] The spatial resolution was demonstrated to be about 15 nm. While this still precludes the study of single defects with sub-nm precision, as discussed above for STM, it is sufficient to elucidate, for example, the role of nanoscale strain patterns on the optical properties of the quantum emitters.[82] For TMDCs, a recent work employed transmission electron microscopy combined with cathodoluminescence to generate, identify and optically address sulfur mono- and bivacancy defects in monolayer WS_2, although single-photon emission was not resolved[361] in CL. Due to the often complicated interplay of defect generation, imaging, and excitation via the electron beam, machine learning and artificial intelligence-based algorithms are being increasingly utilized to identify atomic-scale defects and to study their formation under the electron beam.[361–366] Recent advancements in algorithmic electron beam control have enabled the systematic targeting of individual atoms in monolayer TMDCs with few-picometer precision, facilitating the controlled creation vacancies.[367] This was achieved through a sparse, rapid, and dose-efficient scan combined with a fast algorithm ("atomic lock-on"), which together enable rapid lattice reconstruction while mitigating common issues such as scan distortions and sample drift.

XII. CONCLUSION AND OUTLOOK

In this review, we provided a broad overview of fabrication methods used to create quantum emitters in TMDCs and hBN. We covered

02 July 2026 15:24:17

© Author(s) 2025

various approaches, including strain engineering (Sec. IV), low-energy ion irradiation (Sec. V), high-energy irradiation methods (Sec. VI), ion implantation (Sec. VII), electron beam irradiation (Sec. VIII), and photon-based irradiation (Sec. IX). From a fundamental physics point of view, a key challenge remains the identification and understanding of the microscopic origin of the single-photon emission, which we discussed extensively in Secs. X and XI.

Irradiation techniques with charged particles such as ions or electrons offer nanometer-scale probe resolution, making them key tools for the site-selective creation of quantum emitters in 2D materials. These methods have successfully produced several classes of emitters in hBN—including those emitting in the near-infrared (NIR), around 2 eV, blue, and ultraviolet spectral regions—and predominantly NIR-emitting centers in monolayer TMDCs. In hBN, electron beam irradiation has been particularly effective in generating blue emitters with reproducible ZPL energies and precise spatial localization. Both high- and low-energy ion irradiation methods have consistently demonstrated the ability to create ensembles of magnetically active boron vacancy V_B^- centers. However, the site-controlled creation of quantum emitters with ZPLs around 2 eV remains a significant challenge. These 2 eV emitters are particularly promising due to their narrow ZPLs and well-defined phonon sidebands. Emitters formed through high-temperature annealing have even approached lifetime-limited linewidths—an essential requirement for indistinguishable single-photon sources.[368–370] Lifetime-limited quantum emitters at 2 eV have not yet been demonstrated using irradiation or strain-based techniques.

Oxygen plasma[371] and $^{13}CO_2$ implantation[278] revealed the existence of magnetically active emitters in the 2 eV range. More studies in this direction are needed to create spin-active 2 eV emitters on demand and with a higher yield for potential sensing and quantum memory applications. These efforts should be paired with advanced cleaning protocols, such as those from Neumann *et al.*,[329] to mitigate the formation of spurious molecular emitters arising from organic residues on hBN flakes during the different fabrication stages.[372] Recent theoretical[373] and experimental[374] studies have further indicated that 2D materials can serve as ideal hosts for molecule-based quantum emitters, highlighting the importance of surface cleanliness in order to differentiate crystallographic defects from molecular emitters. In the TMDC family, strain-induced single-photon emitters (SPEs) currently represent the most advanced and widely adopted platform. Ion beam engineering of SPEs has been particularly successful in MoS_2,[12] with promising progress now extending to other TMDCs.[37,221] Low-energy ion implantation (from tens to hundreds of eV) has also emerged as a promising technique, especially for introducing impurity—and impurity–vacancy complexes,[70,375] with initial experimental demonstrations under way.[144]

Potential applications would benefit from further refinements of the spatial and spectral precision of the emitter creation process. For example, while strain-induced emitters in WSe_2 are created quite consistently and with high yield in the NIR spectral range, the ZPL of different emitters still exhibits statistical inhomogeneous broadening of about 30 meV. Regarding the positioning accuracy of strain-induced emitters, Ref. 45 reports a direct correlation between the location of the patterned pillar and the observed quantum emission to better than 120 nm, while other studies often quote the size of pillars or strain indents as estimates of the positioning accuracy (typical values are 300 nm[38,197]). By contrast, atomically resolved studies of focused He-ion beam-irradiated MoS_2 demonstrated a spatial precision better than 9 nm for the creation of single point defects, yet without a direct correlation to the location of optical emission.[58] The optically active single-photon emitters created in the latter way are consistently produced, also using other methods,[148,289] but a statistical broadening within ensembles of such emitters of about 30 meV is still present.[12,217] With respect to the reproducibility of the ZPL, blue emitters at 435 nm (2.85 eV) created by electron beam irradiation of hBN exhibit the most consistent results so far.[35,36] Spatial positioning of these emitters is further verified to be better than 300 nm.[35] Notably, a very recent work employing a focused He-ion beam demonstrated a very narrow statistical distribution of ZPL for a potentially different class of blue emitters at 433 nm (2.86 eV) and 454 nm (2.73 eV) with an inhomogeneous broadening as low as 0.1 nm (0.7 meV).[303]

A. Outlook and future directions

Future research should address the critical issue of coherence loss, particularly due to phonon interactions.[80,94,285] Non-perturbative treatments of electron–phonon coupling[323,376,377] are essential to enable phonon suppression schemes, such as the swing-up of quantum emitter population (SUPER) excitation scheme.[378–380] Moreover, the development of quantum emitters operating at telecom wavelengths remains a priority for integration into fiber-based quantum networks. While strain-induced emitters in $MoTe_2$ have demonstrated telecom emission,[53] recent work has also reported single-photon emission from strained InSe multilayers.[56] High-throughput theoretical frameworks and curated color center databases[74,272,375] could significantly accelerate the identification of defect complexes with optimal optical and magnetic properties across the vast configuration space of 2D and vdW layered materials. Despite rapid experimental progress, the microscopic origin of many quantum emitters in hBN and TMDCs remains poorly understood, as discussed in Sec. X. Establishing this foundational knowledge is critical for enabling on-demand, site-selective fabrication of quantum emitters with properties comparable to those in III–V semiconductors. A clear understanding of emitter structure will inform strategies for improving brightness, purity, and indistinguishability, while also enabling precise modeling of environmental coupling and the rational design of pulsed excitation schemes like SUPER. Special attention must be paid to fabrication artifacts, such as those arising from tape transfer processes and solvent residues. Based on the report by Neumann *et al.*,[329] we advocate for transparent reporting of fabrication protocols, rigorous substrate cleaning, and standardized reference tests to suppress parasitic emitters. On the theoretical front, models incorporating thermal broadening[380–382] and phonon-induced decoherence[324] will be essential to guide the development of emitters with robust performance at elevated temperatures.

B. Toward a systematic and predictive framework

The controlled creation of quantum emitters in 2D materials via irradiation and strain engineering remains a promising yet largely empirical field. Realizing its full potential will require a transition to systematic, theory-guided strategies.[74,111,112,272,375] To date, numerous irradiation approaches—including electron and ion beams—have been deployed to produce emitters in hBN and TMDCs with varying outcomes. Electron beams in the tens of keV range have yielded emitters with near-Fourier-limited linewidths,[307,383] whereas ion beams provide

02 July 2026 15:24:17

© Author(s) 2025

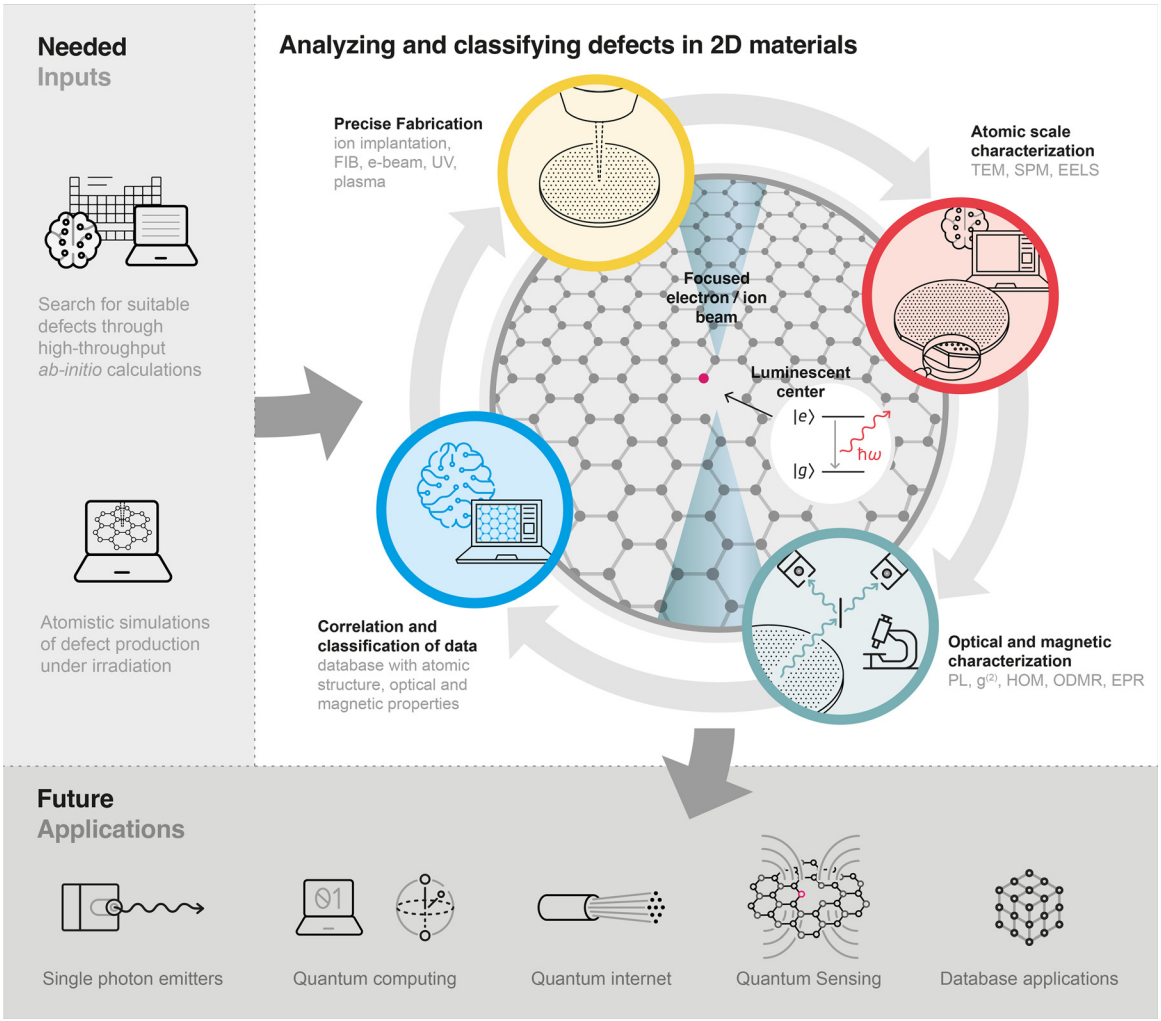


FIG. 11. Toward a systematic and predictive Framework. Schematic illustration of a theory-guided strategy for the controlled generation of quantum emitters in 2D materials like hBN and TMDCs for future quantum applications. FIB: focused ion beam. UV: ultraviolet. TEM: transmission electron microscope. SPM: scanning probe microscopy. EELS: electron energy loss spectroscopy. PL: photoluminescence. $g^{(2)}$: second-order correlation function for photon statistics measurements. HOM: Hong–Ou Mandel setup for photon indistinguishability measurements. ODMR: optically detected magnetic resonance. EPR: electron paramagnetic resonance.

high creation yields and remain the most widely used method. However, most discoveries have emerged through trial and error. A more predictive methodology is needed, integrating high-throughput *ab initio* calculations, atomistic simulations, and detailed experimental characterization (see Fig. 11). Such an interdisciplinary approach would enable the targeted design of emitters with engineered quantum optical and magnetic features. Research should expand beyond traditional defects (e.g., carbon, vacancies, and oxygen) to include novel dopants identified by deep-learning-assisted screening. For example, rare-earth elements like erbium could offer telecom emission[280] and enhanced coherence through shielded inner-shell transitions. Defects with large zero-field splitting may also enable long-lived spin coherence, a valuable asset for quantum memory applications. Ion implantation remains the most promising avenue for introducing such engineered defects. Given the ultrathin nature of 2D materials, the implantation process must be carefully optimized—considering kinetic energy, incidence angle, and substrate effects—to ensure dopant incorporation rather than transmission or backscattering (see Sec. III). Reactive-gas-assisted focused beams may facilitate site-selective doping, while interstitial implantation represents a largely unexplored but potentially transformative approach with minimal environmental coupling. Implanting magnetic isotopes can offer the possibility to clarify the nature of the elements forming these emitters by changing on purpose their magnetic properties via hyperfine coupling, which can then be compared to predictions from *ab initio* calculations. Molecular dynamics simulations, including thermal effects and defect diffusion, are necessary to refine these techniques. Concurrently, *in situ* atomic-scale characterization—using STEM, STM, possibly supplemented by cathodoluminescence measurements—can correlate structural and optical properties.[82,344] Advanced techniques such as

02 July 2026 15:24:17

© Author(s) 2025

energy-filtered EELS and low-energy phonon mapping provide insight into defect composition and vibrational environments.[384–387] Machine learning, particularly convolutional neural networks, offers exciting prospects for identifying luminescent centers,[364,366,388,389] especially in low-Z materials such as hBN, where imaging resolution is inherently limited. Once identified, these emitters should undergo comprehensive optical characterization—ideally at the same locations used in structural analysis—requiring STEM-compatible sample holders to facilitate such correlative studies. Spectroscopic measurements of phonon sidebands should be compared to DFT and open quantum system models, which accurately capture phonon-induced decoherence effects.[80,94,324] Furthermore, second-order correlation and Hong–Ou–Mandel (HOM) interference experiments are essential for quantifying single-photon purity and indistinguishability—key metrics for quantum photonics.[390] Magnetic characterization via EPR and ODMR complements optical studies by providing insight into ground-state spin configurations and coherence. A further step, which is currently attracting growing attention in the 2D community, is the integration of luminescent centers in vdW materials into more complex, layered structures. The aim is to leverage the flat nature of 2D systems to fabricate more sophisticated heterostructures[391] in which the optical response of embedded quantum emitters can be modulated and further investigated upon application of a gate voltage and/or a tunneling/source-drain current.[42,370] The advantages are multiple. On the one hand, by applying a tunneling/source-drain voltage, it is possible to control the carrier population and the Fermi level of the material, thus injecting carriers into in-gap states[392–395]—including those that are typically not accessible by usual optical excitation[393,396]—with the potential to obtain quantum light emission by means of only voltage/current application, i.e., electroluminescence.[394,395,397,398] This strategy provides a pathway to access and explore the photophysics of new hidden, dark states in such materials,[396,399] provide a tool for probing the properties of already known classes of emitters,[98,312] and/or provide a knob for turning on/off emitters deterministically.[212,396,399] On the other hand, embedding of luminescent centers in electrically switchable devices can lead to the production of 2D light-emitting diodes (LEDs)[42,397,400] or on-demand single-photon sources, which can be turned on/off by means of current application. Several works have already addressed different aspects of device integration, both for TMDCs[98,212] and hBN.[312,394,398,401–403] Future efforts are expected to focus on advancing fabrication strategies and enhancing device performance under ambient conditions,[14] especially concerning minimizing the operation-induced device degradation.[403]

Finally, to streamline research and application, experimental data should be compiled in an open-access searchable database. Classification by defect type, emission wavelength, magnetic properties, and fabrication method will accelerate the integration of these emitters into scalable quantum photonic platforms. Such databases can also serve as training sets for machine learning models, enabling more accurate prediction, screening, and engineering of quantum emitters in 2D materials.

ACKNOWLEDGMENTS

A.W.H and C.K. thank the International Graduate School of Science and Engineering (TUM-IGSSE, Project BrightQuanDTUM), the Deutsche Forschungsgemeinschaft (DFG, German Research Foundation) via the Munich Center for Quantum Science and Technology No. (MCQST)-EXC-2111-390814868 and via the excellence cluster e-conversion No. EXC-2089/1-390776260, and the Munich Quantum Valley K6 as well as the One Munich Strategy Forum—EQAP. C.K. acknowledges funding by the European Union's Horizon Europe research and innovation program under Grant No. 101076915 (2DTopS). N.S. thanks the Novo Nordisk Foundation NERD Programme (Project QuDec NNF23OC0082957). N.S. and M.W. acknowledge the support from the Independent Research Fund Denmark, Natural Sciences (Project No. 0135-00403B) and from the Danish National Research Foundation through NanoPhoton—Center for Nanophotonics (Project No. DNRF147). A.H. acknowledges the NNF Biomag project (NNF21OC0066526) and the Danish National Research Foundation through the center for macroscopic quantum states (bigQ, Project No. DNRF0142). A.V.K. acknowledges funding from the German Research Foundation (DFG), projects KR 4866/9-1, and the collaborative research center "Chemistry of Synthetic 2D Materials" CRC-1415-417590517. D.P.B.F.M. and T.W.H. thank the Independent Research Fund Denmark, DFF-FTP (Project No. 4264-00065B).

AUTHOR DECLARATIONS

Conflict of Interest

The authors have no conflicts to disclose.

Author Contributions

Amedeo Carbone: Conceptualization (supporting); Data curation (lead); Formal analysis (lead); Investigation (lead); Visualization (lead); Writing – original draft (equal); Writing – review & editing (equal). **Diane-Pernille Bendixen-Fernex de Mongex:** Data curation (supporting); Formal analysis (supporting); Investigation (supporting); Validation (equal); Visualization (equal); Writing – original draft (equal); Writing – review & editing (equal). **Arkady V. Krasheninnikov:** Conceptualization (equal); Formal analysis (equal); Funding acquisition (equal); Project administration (equal); Supervision (equal); Writing – original draft (equal); Writing – review & editing (equal). **Martijn Wubs:** Conceptualization (equal); Formal analysis (equal); Funding acquisition (equal); Project administration (equal); Supervision (equal); Writing – original draft (equal); Writing – review & editing (equal). **Alexander Huck:** Conceptualization (equal); Formal analysis (equal); Funding acquisition (equal); Project administration (equal); Supervision (equal); Writing – original draft (equal); Writing – review & editing (equal). **Thomas W. Hansen:** Conceptualization (supporting); Funding acquisition (equal); Supervision (equal); Writing – original draft (supporting); Writing – review & editing (equal). **Alexander W. Holleitner:** Conceptualization (equal); Funding acquisition (equal); Investigation (equal); Project administration (equal); Supervision (equal); Writing – original draft (equal); Writing – review & editing (equal). **Nicolas Stenger:** Conceptualization (equal); Funding acquisition (equal); Project administration (equal); Supervision (equal); Validation (equal); Writing – original draft (equal); Writing – review & editing (equal). **Christoph Kastl:** Conceptualization (equal); Funding acquisition (equal); Project administration (equal); Supervision (equal); Writing – original draft (equal); Writing – review & editing (equal).

DATA AVAILABILITY

Data sharing is not applicable to this article as no new data were created or analyzed in this study.

02 July 2026 15:24:17

© Author(s) 2025

REFERENCES

[1]S. Rodt and S. Reitzenstein, "Integrated nanophotonics for the development of fully functional quantum circuits based on on-demand single-photon emitters," APL Photonics **6**, 010901 (2021).
[2]C. Couteau, S. Barz, T. Durt, T. Gerrits, J. Huwer, R. Prevedel, J. Rarity, A. Shields, and G. Weihs, "Applications of single photons to quantum communication and computing," Nat. Rev. Phys. **5**, 326–338 (2023).
[3]A. R. P. Montblanch, M. Barbone, I. Aharonovich, M. Atatüre, and A. C. Ferrari, "Layered materials as a platform for quantum technologies," Nat. Nanotechnol. **18**, 555–571 (2023).
[4]P. Tonndorf, R. Schmidt, R. Schneider, J. Kern, M. Buscema, G. A. Steele, A. Castellanos-Gomez, H. S. J. van der Zant, S. Michaelis de Vasconcellos, and R. Bratschitsch, "Single-photon emission from localized excitons in an atomically thin semiconductor," Optica **2**, 347 (2015).
[5]C. Chakraborty, L. Kinnischtzke, K. M. Goodfellow, R. Beams, and A. N. Vamivakas, "Voltage-controlled quantum light from an atomically thin semiconductor," Nat. Nanotechnol. **10**, 507–511 (2015).
[6]M. Koperski, K. Nogajewski, A. Arora, V. Cherkez, P. Mallet, J.-Y. Y. Veuillen, J. Marcus, P. Kossacki, and M. Potemski, "Single photon emitters in exfoliated WSe_2 structures," Nat. Nanotechnol. **10**, 503–506 (2015).
[7]Y.-M. He, G. Clark, J. R. Schaibley, Y.-M. He, M.-C. Chen, Y.-J. Wei, X. Ding, Q. Zhang, W. Yao, X. Xu, C.-Y. Lu, and J.-W. Pan, "Single quantum emitters in monolayer semiconductors," Nat. Nanotechnol. **10**, 497–502 (2015).
[8]A. Srivastava, M. Sidler, A. V. Allain, D. S. Lembke, A. Kis, and A. Imamoğlu, "Optically active quantum dots in monolayer WSe_2," Nat. Nanotechnol. **10**, 491–496 (2015).
[9]P. Tonndorf, S. Schwarz, J. Kern, I. Niehues, O. Del Pozo-Zamudio, A. I. Dmitriev, A. P. Bakhtinov, D. N. Borisenko, N. N. Kolesnikov, A. I. Tartakovskii, S. Michaelis de Vasconcellos, and R. Bratschitsch, "Single-photon emitters in GaSe," 2D Mater. **4**, 021010 (2017).
[10]T. T. Tran, K. Bray, M. J. Ford, M. Toth, and I. Aharonovich, "Quantum emission from hexagonal boron nitride monolayers," Nat. Nanotechnol. **11**, 37–41 (2016).
[11]H. Baek, M. Brotons-Gisbert, Z. X. Koong, A. Campbell, M. Rambach, K. Watanabe, T. Taniguchi, and B. D. Gerardot, "Highly energy-tunable quantum light from moiré-trapped excitons," Sci. Adv. **6**, eaba8526 (2020).
[12]K. Barthelmi, J. Klein, A. Hötger, L. Sigl, F. Sigger, E. Mitterreiter, S. Rey, S. Gyger, M. Lorke, M. Florian, F. Jahnke, T. Taniguchi, K. Watanabe, V. Zwiller, K. D. Jöns, U. Wurstbauer, C. Kastl, A. Weber-Bargioni, J. J. Finley, K. Müller, and A. W. Holleitner, "Atomistic defects as single-photon emitters in atomically thin MoS_2," Appl. Phys. Lett. **117**, 070501 (2020).
[13]S. I. Azzam, K. Parto, and G. Moody, "Prospects and challenges of quantum emitters in 2D materials," Appl. Phys. Lett. **118**, 240502 (2021).
[14]M. Turunen, M. Brotons-Gisbert, Y. Dai, Y. Wang, E. Scerri, C. Bonato, K. D. Jöns, Z. Sun, and B. D. Gerardot, "Quantum photonics with layered 2D materials," Nat. Rev. Phys. **4**, 219–236 (2022).
[15]S. Michaelis de Vasconcellos, D. Wigger, U. Wurstbauer, A. W. Holleitner, R. Bratschitsch, and T. Kuhn, "Single-photon emitters in layered van der Waals materials," Phys. Status Solidi B **259**, 2100566 (2022).
[16]S. Gupta, W. Wu, S. Huang, and B. I. Yakobson, "Single-photon emission from two-dimensional materials, to a brighter future," J. Phys. Chem. Lett. **14**, 3274–3284 (2023).
[17]A. B. Kaul, Y. Wang, A.-P. Li, X. Li, and X. Ma, "Single photon emitters in van der Waals solids for quantum photonics: Materials, theory and molecular-scale characterization probes," J. Phys. D: Appl. Phys. **58**, 123001 (2025).
[18]S. Hepp, M. Jetter, S. L. Portalupi, and P. Michler, "Semiconductor quantum dots for integrated quantum photonics," Adv. Quantum Tech. **2**, 1900020 (2019).
[19]M. Atatüre, D. Englund, N. Vamivakas, S.-Y. Lee, and J. Wrachtrup, "Material platforms for spin-based photonic quantum technologies," Nat. Rev. Mater. **3**, 38–51 (2018).
[20]M. Kianinia, Z.-Q. Xu, M. Toth, and I. Aharonovich, "Quantum emitters in 2D materials: Emitter engineering, photophysics, and integration in photonic nanostructures," Appl. Phys. Rev. **9**, 011306 (2022).
[21]F. Peyskens, C. Chakraborty, M. Muneeb, D. Van Thourhout, and D. Englund, "Integration of single photon emitters in 2D layered materials with a silicon nitride photonic chip," Nat. Commun. **10**, 4435 (2019).
[22]J. Li, E. R. Glaser, C. Elias, G. Ye, D. Evans, L. Xue, S. Liu, G. Cassabois, B. Gil, P. Valvin, T. Pelini, A. L. Yeats, R. He, B. Liu, and J. H. Edgar, "Defect engineering of monoisotopic hexagonal boron nitride crystals via neutron transmutation doping," Chem. Mater. **33**, 9231–9239 (2021).
[23]J. E. Fröch, C. Li, Y. Chen, M. Toth, M. Kianinia, S. Kim, and I. Aharonovich, "Purcell enhancement of a cavity-coupled emitter in hexagonal boron nitride," Small **18**, 2104805 (2022).
[24]O. Iff, Q. Buchinger, M. Moczała-Dusanowska, M. Kamp, S. Betzold, M. Davanco, K. Srinivasan, S. Tongay, C. Antón-Solanas, S. Höfling, and C. Schneider, "Purcell-enhanced single photon source based on a deterministically placed WSe_2 monolayer quantum dot in a circular Bragg grating cavity," Nano Lett. **21**, 4715–4720 (2021).
[25]J. A. Preuß, H. Gehring, R. Schmidt, L. Jin, D. Wendland, J. Kern, W. H. P. Pernice, S. M. de Vasconcellos, and R. Bratschitsch, "Low-divergence hBN single-photon source with a 3D-printed low-fluorescence elliptical polymer microlens," Nano Lett. **23**, 407–413 (2023).
[26]F. Najafi, J. Mower, N. C. Harris, F. Bellei, A. Dane, C. Lee, X. Hu, P. Kharel, F. Marsili, S. Assefa, K. K. Berggren, and D. Englund, "On-chip detection of non-classical light by scalable integration of single-photon detectors," Nat. Commun. **6**, 5873 (2015).
[27]L. Loh, J. Wang, M. Grzeszczyk, M. Koperski, and G. Eda, "Towards quantum light-emitting devices based on van der Waals materials," Nat. Rev. Electr. Eng. **1**, 815–829 (2024).
[28]O. Iff, D. Tedeschi, J. Martín-Sánchez, M. Moczała-Dusanowska, S. Tongay, K. Yumigeta, J. Taboada-Gutiérrez, M. Savaresi, A. Rastelli, P. Alonso-González, S. Höfling, R. Trotta, and C. Schneider, "Strain-tunable single photon sources in WSe_2 monolayers," Nano Lett. **19**, 6931–6936 (2019).
[29]G. Grosso, H. Moon, B. Lienhard, S. Ali, D. K. Efetov, M. M. Furchi, P. Jarillo-Herrero, M. J. Ford, I. Aharonovich, and D. Englund, "Tunable and high-purity room temperature single-photon emission from atomic defects in hexagonal boron nitride," Nat. Commun. **8**, 705 (2017).
[30]N. Mendelson, M. Doherty, M. Toth, I. Aharonovich, and T. T. Tran, "Strain-induced modification of the optical characteristics of quantum emitters in hexagonal boron nitride," Adv. Mater. **32**, 1908316 (2020).
[31]S. D. Patel, K. Parto, M. Choquer, N. Lewis, S. Umezawa, L. Hellman, D. Polishchuk, and G. Moody, "Surface acoustic wave cavity optomechanics with atomically thin h-BN and WSe_2 single-photon emitters," PRX Quantum **5**, 10330 (2024).
[32]A. V. Krasheninnikov and F. Banhart, "Engineering of nanostructured carbon materials with electron or ion beams," Nat. Mater. **6**, 723–733 (2007).
[33]J. Klein, M. Lorke, M. Florian, F. Sigger, L. Sigl, S. Rey, J. Wierzbowski, J. Cerne, K. Müller, E. Mitterreiter, P. Zimmermann, T. Taniguchi, K. Watanabe, U. Wurstbauer, M. Kaniber, M. Knap, R. Schmidt, J. J. Finley, and A. W. Holleitner, "Site-selectively generated photon emitters in monolayer MoS_2 via local helium ion irradiation," Nat. Commun. **10**, 2755 (2019).
[34]J. Ziegler, R. Klaiss, A. Blaikie, D. Miller, V. R. Horowitz, and B. J. Alemán, "Deterministic quantum emitter formation in hexagonal boron nitride via controlled edge creation," Nano Lett. **19**, 2121–2127 (2019).
[35]C. Fournier, A. Plaud, S. Roux, A. Pierret, M. Rosticher, K. Watanabe, T. Taniguchi, S. Buil, X. Quélin, J. Barjon, J.-P. Hermier, and A. Delteil, "Position-controlled quantum emitters with reproducible emission wavelength in hexagonal boron nitride," Nat. Commun. **12**, 3779 (2021).
[36]A. Gale, C. Li, Y. Chen, K. Watanabe, T. Taniguchi, I. Aharonovich, and M. Toth, "Site-specific fabrication of blue quantum emitters in hexagonal boron nitride," ACS Photonics **9**, 2170–2177 (2022).
[37]Z. Zhang, H. Liang, L. Loh, Y. Y. Y. Chen, Y. Y. Y. Chen, K. Watanabe, T. Taniguchi, S. Y. Quek, M. Bosman, A. A. Bettiol, and G. Eda, "Optically active chalcogen vacancies in monolayer semiconductors," Adv. Opt. Mater. **10**, 2201350 (2022).
[38]K. Parto, S. I. Azzam, K. Banerjee, and G. Moody, "Defect and strain engineering of monolayer WSe_2 enables site-controlled single-photon emission up to 150 K," Nat. Commun. **12**, 3585 (2021).
[39]S. Cianci, E. Blundo, F. Tuzi, G. Pettinari, K. Olkowska-Pucko, E. Parmenopoulou, D. B. L. Peeters, A. Miriametro, T. Taniguchi, K. Watanabe, A. Babinski, M. R. Molas, M. Felici, and A. Polimeni, "Spatially controlled single photon emitters in hBN-capped WS_2 domes," Adv. Opt. Mater. **11**, 2202953 (2023).

02 July 2026 15:24:17

© Author(s) 2025

[40]J. Howarth, K. Vaklinova, M. Grzeszczyk, G. Baldi, L. Hague, M. Potemski, K. S. Novoselov, A. Kozikov, and M. Koperski, "Electroluminescent vertical tunneling junctions based on WSe_2 monolayer quantum emitter arrays: Exploring tunability with electric and magnetic fields," Proc. Natl. Acad. Sci. U.S.A. **121**, e2401757121 (2024).
[41]A. Micevic, N. Pettinger, A. Hötger, L. Sigl, M. Florian, T. Taniguchi, K. Watanabe, K. Müller, J. J. Finley, C. Kastl, and A. W. Holleitner, "On-demand generation of optically active defects in monolayer WS_2 by a focused helium ion beam," Appl. Phys. Lett. **121**, 183101 (2022).
[42]C. Palacios-Berraquero, M. Barbone, D. M. Kara, X. Chen, I. Goykhman, D. Yoon, A. K. Ott, J. Beitner, K. Watanabe, T. Taniguchi, A. C. Ferrari, and M. Atatüre, "Atomically thin quantum light-emitting diodes," Nat. Commun. **7**, 12978 (2016).
[43]S. Kumar, A. Kaczmarczyk, and B. D. Gerardot, "Strain-induced spatial and spectral isolation of quantum emitters in mono- and bilayer WSe_2," Nano Lett. **15**, 7567–7573 (2015).
[44]J. Kern, I. Niehues, P. Tonndorf, R. Schmidt, D. Wigger, R. Schneider, T. Stiehm, S. Michaelis de Vasconcellos, D. E. Reiter, T. Kuhn, and R. Bratschitsch, "Nanoscale positioning of single-photon emitters in atomically thin WSe_2," Adv. Mater. **28**, 7101–7105 (2016).
[45]A. Branny, S. Kumar, R. Proux, and B. D. Gerardot, "Deterministic strain-induced arrays of quantum emitters in a two-dimensional semiconductor," Nat. Commun. **8**, 15053 (2017).
[46]T. Cai, J.-H. Kim, Z. Yang, S. Dutta, S. Aghaeimeibodi, and E. Waks, "Radiative enhancement of single quantum emitters in WSe_2 monolayers using site-controlled metallic nanopillars," ACS Photonics **5**, 3466–3471 (2018).
[47]M. Brooks and G. Burkard, "Theory of strain-induced confinement in transition metal dichalcogenide monolayers," Phys. Rev. B **97**, 195454 (2018).
[48]Y. Luo, G. D. Shepard, J. V. Ardelean, D. A. Rhodes, B. Kim, K. Barmak, J. C. Hone, and S. Strauf, "Deterministic coupling of site-controlled quantum emitters in monolayer WSe_2 to plasmonic nanocavities," Nat. Nanotechnol. **13**, 1137–1142 (2018).
[49]Y. Luo, N. Liu, X. Li, J. C. Hone, and S. Strauf, "Single photon emission in WSe_2 up 160 K by quantum yield control," 2D Mater. **6**, 035017 (2019).
[50]Q. Wang, J. Maisch, F. Tang, D. Zhao, S. Yang, R. Joos, S. L. Portalupi, P. Michler, and J. H. Smet, "Highly polarized single photons from strain-induced quasi-1D localized excitons in WSe_2," Nano Lett. **21**, 7175–7182 (2021).
[51]L. Sortino, P. G. Zotev, C. L. Phillips, A. J. Brash, J. Cambiasso, E. Marensi, A. M. Fox, S. A. Maier, R. Sapienza, and A. I. Tartakovskii, "Bright single photon emitters with enhanced quantum efficiency in a two-dimensional semiconductor coupled with dielectric nano-antennas," Nat. Commun. **12**, 6063 (2021).
[52]L. Yu, M. Deng, J. L. Zhang, S. Borghardt, B. Kardynal, J. Vučković, and T. F. Heinz, "Site-controlled quantum emitters in monolayer $MoSe_2$," Nano Lett. **21**, 2376–2381 (2021).
[53]H. Zhao, M. T. Pettes, Y. Zheng, and H. Htoon, "Site-controlled telecom-wavelength single-photon emitters in atomically-thin $MoTe_2$," Nat. Commun. **12**, 6753 (2021).
[54]M. von Helversen, L. Greten, I. Limame, C.-W. Shih, P. Schlaugat, C. Antón-Solanas, C. Schneider, B. Rosa, A. Knorr, and S. Reitzenstein, "Temperature dependent temporal coherence of metallic-nanoparticle-induced single-photon emitters in a WSe_2 monolayer," 2D Mater. **10**, 045034 (2023).
[55]S. Chen, C. Wang, H. Cai, L. Ma, Y. Qu, Z. Liu, S. Wang, J. Zhan, Q. Tan, B. Sheng, X. Liu, X. Wang, X. Zhang, J. Xu, W. Gao, and Q. Liu, "Realization of single-photon emitters with high brightness and high stability and excellent monochromaticity," Matter **7**, 1106–1116 (2024).
[56]H. Zhao, S. M. Hus, J. Chen, X. Yan, B. J. Lawrie, S. Jesse, A.-P. Li, L. Liang, and H. Htoon, "Telecom-wavelength single-photon emitters in multilayer InSe," ACS Nano **19**, 6911–6917 (2025).
[57]C. Palacios-Berraquero, D. M. Kara, A. R.-P. Montblanch, M. Barbone, P. Latawiec, D. Yoon, A. K. Ott, M. Loncar, A. C. Ferrari, and M. Atatüre, "Large-scale quantum-emitter arrays in atomically thin semiconductors," Nat. Commun. **8**, 15093 (2017).
[58]E. Mitterreiter, B. Schuler, K. A. Cochrane, U. Wurstbauer, A. Weber-Bargioni, C. Kastl, and A. W. Holleitner, "Atomistic positioning of defects in helium ion treated single-layer MoS_2," Nano Lett. **20**, 4437–4444 (2020).
[59]L. Linhart, M. Paur, V. Smejkal, J. Burgdörfer, T. Mueller, and F. Libisch, "Localized intervalley defect excitons as single-photon emitters in WSe_2," Phys. Rev. Lett. **123**, 146401 (2019).
[60]J. J. P. Thompson, S. Brem, H. Fang, J. Frey, S. P. Dash, W. Wieczorek, and E. Malic, "Criteria for deterministic single-photon emission in two-dimensional atomic crystals," Phys. Rev. Mater. **4**, 84006 (2020).
[61]G. Moody, K. Tran, X. Lu, T. Autry, J. M. Fraser, R. P. Mirin, L. Yang, X. Li, and K. L. Silverman, "Microsecond valley lifetime of defect-bound excitons in monolayer WSe_2," Phys. Rev. Lett. **121**, 57403 (2018).
[62]E. Mitterreiter, B. Schuler, A. Micevic, D. Hernangómez-Pérez, K. Barthelmi, K. A. Cochrane, J. Kiemle, F. Sigger, J. Klein, E. Wong, E. S. Barnard, K. Watanabe, T. Taniguchi, M. Lorke, F. Jahnke, J. J. Finley, A. M. Schwartzberg, D. Y. Qiu, S. Refaely-Abramson, A. W. Holleitner, A. Weber-Bargioni, and C. Kastl, "The role of chalcogen vacancies for atomic defect emission in MoS_2," Nat. Commun. **12**, 3822 (2021).
[63]D. D. Xu, A. F. Vong, D. Lebedev, R. Ananth, A. M. Wong, P. T. Brown, M. C. Hersam, C. A. Mirkin, and E. A. Weiss, "Conversion of classical light emission from a nanoparticle-strained WSe_2 monolayer into quantum light emission via electron beam irradiation," Adv. Mater. **35**, 2208066 (2023).
[64]B. Schuler, K. A. Cochrane, C. Kastl, E. S. Barnard, E. Wong, N. J. Borys, A. M. Schwartzberg, D. F. Ogletree, F. J. G. de Abajo, and A. Weber-Bargioni, "Electrically driven photon emission from individual atomic defects in monolayer WS_2," Sci. Adv. **6**, eabb5988 (2020).
[65]H. Park, Y. Wen, S. X. Li, W. Choi, G. Lee, M. Strano, and J. H. Warner, "Atomically precise control of carbon insertion into hBN monolayer point vacancies using a focused electron beam guide," Small **17**, 2100693 (2021).
[66]S. Singla, P. Joshi, G. I. López-Morales, S. Sarkar, S. Sarkar, J. Flick, and B. Chakraborty, "Probing correlation of optical emission and defect sites in hexagonal boron nitride by high-resolution STEM-EELS," Nano Lett. **24**, 9212–9220 (2024).
[67]W. Sohn, M. Kim, and H. W. Jang, "Atomic-scale insights into the 2D materials from aberration-corrected scanning transmission electron microscopy: Progress and future," Small Sci. **4**, 2300073 (2024).
[68]Z. Qiu, K. Vaklinova, P. Huang, M. Grzeszczyk, K. Watanabe, T. Taniguchi, K. S. Novoselov, J. Lu, and M. Koperski, "Atomic and electronic structure of defects in hBN: Enhancing single-defect functionalities," ACS Nano **18**, 24035–24043 (2024).
[69]O. L. Krivanek, M. F. Chisholm, V. Nicolosi, T. J. Pennycook, G. J. Corbin, N. Dellby, M. F. Murfitt, C. S. Own, Z. S. Szilagyi, M. P. Oxley, S. T. Pantelides, and S. J. Pennycook, "Atom-by-atom structural and chemical analysis by annular dark-field electron microscopy," Nature **464**, 571–574 (2010).
[70]S. Gupta, J.-H. Yang, and B. I. Yakobson, "Two-level quantum systems in two-dimensional materials for single photon emission," Nano Lett. **19**, 408–414 (2019).
[71]S. Refaely-Abramson, D. Y. Qiu, S. G. Louie, and J. B. Neaton, "Defect-induced modification of low-lying excitons and valley selectivity in monolayer transition metal dichalcogenides," Phys. Rev. Lett. **121**, 167402 (2018).
[72]S. Gao, H.-Y. Chen, and M. Bernardi, "Radiative properties of quantum emitters in boron nitride from excited state calculations and Bayesian analysis," npj Comput. Mater. **7**, 85 (2021).
[73]T. Amit, D. Hernangómez-Pérez, G. Cohen, D. Y. Qiu, and S. Refaely-Abramson, "Tunable magneto-optical properties in MoS_2 via defect-induced exciton transitions," Phys. Rev. B **106**, L161407 (2022).
[74]F. Bertoldo, S. Ali, S. Manti, and K. S. Thygesen, "Quantum point defects in 2D materials—The QPOD database," npj Comput. Mater. **8**, 56 (2022).
[75]A. Kirchhoff, T. Deilmann, and M. Rohlfing, "Excited-state geometry relaxation of point defects in monolayer hexagonal boron nitride," Phys. Rev. B **109**, 085127 (2024).
[76]M. Maciaszek, L. Razinkovas, and A. Alkauskas, "Thermodynamics of carbon point defects in hexagonal boron nitride," Phys. Rev. Mater. **6**, 014005 (2022).
[77]N. Mendelson, D. Chugh, J. R. Reimers, T. S. Cheng, A. Gottscholl, H. Long, C. J. Mellor, A. Zettl, V. Dyakonov, P. H. Beton, S. V. Novikov, C. Jagadish, H. H. Tan, M. J. Ford, M. Toth, C. Bradac, and I. Aharonovich, "Identifying carbon as the source of visible single-photon emission from hexagonal boron nitride," Nat. Mater. **20**, 321–328 (2021).
[78]I. Aharonovich, J.-P. Tetienne, and M. Toth, "Quantum emitters in hexagonal boron nitride," Nano Lett. **22**, 9227–9235 (2022).

02 July 2026 15:24:17

© Author(s) 2025

[79]M. Fischer, J. M. Caridad, A. Sajid, S. Ghaderzadeh, M. Ghorbani-Asl, L. Gammelgaard, P. Bøggild, K. S. Thygesen, A. V. Krasheninnikov, S. Xiao, M. Wubs, and N. Stenger, "Controlled generation of luminescent centers in hexagonal boron nitride by irradiation engineering," Sci. Adv. **7**, eabe7138 (2021).
[80]M. Fischer, A. Sajid, J. Iles-Smith, A. Hötger, D. I. Miakota, M. K. Svendsen, C. Kastl, S. Canulescu, S. Xiao, M. Wubs, K. S. Thygesen, A. W. Holleitner, and N. Stenger, "Combining experiments on luminescent centres in hexagonal boron nitride with the polaron model and ab initio methods towards the identification of their microscopic origin," Nanoscale **15**, 14215–14226 (2023).
[81]I. Zhigulin, J. Horder, V. Ivády, S. J. U. White, A. Gale, C. Li, C. J. Lobo, M. Toth, I. Aharonovich, and M. Kianinia, "Stark effect of blue quantum emitters in hexagonal boron nitride," Phys. Rev. Appl. **19**, 044011 (2023).
[82]F. Hayee, L. Yu, J. L. Zhang, C. J. Ciccarino, M. Nguyen, A. F. Marshall, I. Aharonovich, J. Vučković, P. Narang, T. F. Heinz, and J. A. Dionne, "Revealing multiple classes of stable quantum emitters in hexagonal boron nitride with correlated optical and electron microscopy," Nat. Mater. **19**, 534–539 (2020).
[83]S. Kundu, T. Amit, H. R. Krishnamurthy, M. Jain, and S. Refaely-Abramson, "Exciton fine structure in twisted transition metal dichalcogenide heterostructures," npj Comput. Mater. **9**, 186 (2023).
[84]C. Attaccalite, M. Bockstedte, A. Marini, A. Rubio, and L. Wirtz, "Coupling of excitons and defect states in boron-nitride nanostructures," Phys. Rev. B **83**, 144115 (2011).
[85]D. Wigger, R. Schmidt, O. Del Pozo-Zamudio, J. A. Preuß, P. Tonndorf, R. Schneider, P. Steeger, J. Kern, Y. Khodaei, J. Sperling, S. M. de Vasconcellos, R. Bratschitsch, and T. Kuhn, "Phonon-assisted emission and absorption of individual color centers in hexagonal boron nitride," 2D Mater. **6**, 035006 (2019).
[86]F. Paleari, H. P. C. Miranda, A. Molina-Sánchez, and L. Wirtz, "Exciton-phonon coupling in the ultraviolet absorption and emission spectra of bulk hexagonal boron nitride," Phys. Rev. Lett. **122**, 187401 (2019).
[87]H.-Y. Chen, D. Sangalli, and M. Bernardi, "Exciton-phonon interaction and relaxation times from first principles," Phys. Rev. Lett. **125**, 107401 (2020).
[88]Y.-H. Chan, M. H. Naik, J. B. Haber, J. B. Neaton, S. G. Louie, D. Y. Qiu, and F. H. da Jornada, "Exciton–phonon coupling induces a new pathway for ultrafast intralayer-to-interlayer exciton transition and interlayer charge transfer in WS_2-MoS_2 heterostructure: A first-principles study," Nano Lett. **24**, 7972–7978 (2024).
[89]K. Watanabe and T. Taniguchi, "Jahn-Teller effect on exciton states in hexagonal boron nitride single crystal," Phys. Rev. B **79**, 193104 (2009).
[90]F. Xiang, L. Huberich, P. A. Vargas, R. Torsi, J. Allerbeck, A. M. Z. Tan, C. Dong, P. Ruffieux, R. Fasel, O. Gröning, Y.-C. Lin, R. G. Hennig, J. A. Robinson, and B. Schuler, "Charge state-dependent symmetry breaking of atomic defects in transition metal dichalcogenides," Nat. Commun. **15**, 2738 (2024).
[91]A. M. Z. Tan, C. Freysoldt, and R. G. Hennig, "Stability of charged sulfur vacancies in 2D and bulk MoS_2 from plane-wave density functional theory with electrostatic corrections," Phys. Rev. Mater. **4**, 64004 (2020).
[92]D. Jansen, T. Tounsi, J. Fischer, A. V. Krasheninnikov, T. Michely, H.-P. Komsa, and W. Jolie, "Tip-induced creation and Jahn-Teller distortions of sulfur vacancies in single-layer MoS_2," Phys. Rev. B **109**, 195430 (2024).
[93]G. Grosso, H. Moon, C. J. Ciccarino, J. Flick, N. Mendelson, L. Mennel, M. Toth, I. Aharonovich, P. Narang, and D. R. Englund, "Low-temperature electron-phonon interaction of quantum emitters in hexagonal boron nitride," ACS Photonics **7**, 1410–1417 (2020).
[94]J. A. Preuß, D. Groll, R. Schmidt, T. Hahn, R. Machnikowski Paweland Bratschitsch, T. Kuhn, S. Michaelis de Vasconcellos, and D. Wigger, "Resonant and phonon-assisted ultrafast coherent control of a single hBN color center," Optica **9**, 522 (2022).
[95]F. Sigger, I. Amersdorffer, A. Hötger, M. Nutz, J. Kiemle, T. Taniguchi, K. Watanabe, M. Förg, J. Noe, J. J. Finley, A. Högele, A. W. Holleitner, T. Hümmer, D. Hunger, and C. Kastl, "Ultra-sensitive extinction measurements of optically active defects in monolayer MoS_2," J. Phys. Chem. Lett. **13**, 10291–10296 (2022).
[96]E. S. Snow, P. M. Campbell, and D. S. Katzer, "Optical absorption spectroscopy of single defects in $GaAs/Al_xGa_{1-x}As$ tunnel structures," Phys. Rev. B **47**, 16032–16035 (1993).
[97]M. Paur, A. J. Molina-Mendoza, D. Polyushkin, S. Michaelis de Vasconcellos, R. Bratschitsch, and T. Mueller, "Resonant photocurrent from a single quantum emitter in tungsten diselenide," 2D Mater. **7**, 045021 (2020).
[98]A. Hötger, W. Männer, T. Amit, D. Hernangómez-Pérez, T. Taniguchi, K. Watanabe, U. Wurstbauer, J. J. Finley, S. Refaely-Abramson, C. Kastl, and A. W. Holleitner, "Photovoltage and photocurrent absorption spectra of sulfur vacancies locally patterned in monolayer MoS_2," Nano Lett. **23**, 11655–11661 (2023).
[99]R. E. Fishman, R. N. Patel, D. A. Hopper, T.-Y. Huang, and L. C. Bassett, "Photon-emission-correlation spectroscopy as an analytical tool for solid-state quantum defects," PRX Quantum **4**, 010202 (2023).
[100]T. P. Darlington, C. Carmesin, M. Florian, E. Yanev, O. Ajayi, J. Ardelean, D. A. Rhodes, A. Ghiotto, A. Krayev, K. Watanabe, T. Taniguchi, J. W. Kysar, A. N. Pasupathy, J. C. Hone, F. Jahnke, N. J. Borys, and P. J. Schuck, "Imaging strain-localized excitons in nanoscale bubbles of monolayer WSe_2 at room temperature," Nat. Nanotechnol. **15**, 854–860 (2020).
[101]E. S. Yanev, T. P. Darlington, S. A. Ladyzhets, M. C. Strasbourg, C. Trovatello, S. Liu, D. A. Rhodes, K. Hall, A. Sinha, N. J. Borys, J. C. Hone, and P. J. Schuck, "Programmable nanowrinkle-induced room-temperature exciton localization in monolayer WSe_2," Nat. Commun. **15**, 1543 (2024).
[102]I. Niehues, D. Wigger, K. Kaltenecker, A. Klein-Hitpass, P. Roelli, A. K. Da˛browska, K. Ludwiczak, P. Tatarczak, J. O. Becker, R. Schmidt, M. Schnell, J. Binder, A. Wysmołek, and R. Hillenbrand, "Nanoscale resolved mapping of the dipole emission of hBN color centers with a scattering-type scanning near-field optical microscope," Nanophotonics **14**, 335–342 (2025).
[103]B. Shevitski, S. M. Gilbert, C. T. Chen, C. Kastl, E. S. Barnard, E. Wong, D. F. Ogletree, K. Watanabe, T. Taniguchi, A. Zettl, and S. Aloni, "Blue-light-emitting color centers in high-quality hexagonal boron nitride," Phys. Rev. B **100**, 155419 (2019).
[104]J. A. Robinson and B. Schuler, "Engineering and probing atomic quantum defects in 2D semiconductors: A perspective," Appl. Phys. Lett. **119**, 140501 (2021).
[105]Y. Yu, I. C. Seo, M. Luo, K. Lu, B. Son, J. K. Tan, and D. Nam, "Tunable single-photon emitters in 2D materials," Nanophotonics **13**, 3615–3629 (2024).
[106]S. Vaidya, X. Gao, S. Dikshit, I. Aharonovich, and T. Li, "Quantum sensing and imaging with spin defects in hexagonal boron nitride," Adv. Phys. X **8**, 2206049 (2023).
[107]H.-H. Fang, X.-J. Wang, X. Marie, and H.-B. Sun, "Quantum sensing with optically accessible spin defects in van der Waals layered materials," Light. Sci. Appl. **13**, 303 (2024).
[108]S. Hou, H. Hu, M. Xu, J. Zhang, H. Xiao, Z. Liu, W. Xing, X. Liu, S. You, B. Liu, Y. Zhang, J. Yu, Z. Xie, X. He, J. Zhang, and Y. Hao, "Engineering quantum emitters in 2D materials," Adv. Opt. Mater. **13**, 2500693 (2025).
[109]I. Niehues, E. D. S. Nysten, R. Schmidt, M. Weiß, and D. Wigger, "Excitons in quantum technologies: The role of strain engineering," MRS Bull. **49**, 958–967 (2024).
[110]S. Im, S. Moon, J. Kim, J. Song, C. Ji, S. Pak, and J. K. Kim, "Quantum emitters based on hexagonal boron nitride for next-generation quantum technology," Prog. Quantum Electron. **102**, 100576 (2025).
[111]L. C. Bassett, A. Alkauskas, A. L. Exarhos, and K.-M. C. Fu, "Quantum defects by design," Nanophotonics **8**, 1867–1888 (2019).
[112]Y. Ping and T. J. Smart, "Computational design of quantum defects in two-dimensional materials," Nat. Comput. Sci. **1**, 646–654 (2021).
[113]V. Ivády, G. Barcza, G. Thiering, S. Li, H. Hamdi, J.-P. Chou, Ö. Legeza, and A. Gali, "*Ab initio* theory of the negatively charged boron vacancy qubit in hexagonal boron nitride," npj Comput. Mater. **6**, 41 (2020).
[114]M. Abdi, J.-P. Chou, A. Gali, and M. B. Plenio, "Color centers in hexagonal boron nitride monolayers: A group theory and *ab initio* analysis," ACS Photonics **5**, 1967–1976 (2018).
[115]H. L. Stern, Q. Gu, J. Jarman, S. Eizagirre Barker, N. Mendelson, D. Chugh, S. Schott, H. H. Tan, H. Sirringhaus, I. Aharonovich, and M. Atatüre, "Room-temperature optically detected magnetic resonance of single defects in hexagonal boron nitride," Nat. Commun. **13**, 618 (2022).
[116]A. Gottscholl, M. Kianinia, V. Soltamov, S. Orlinskii, G. Mamin, C. Bradac, C. Kasper, K. Krambrock, A. Sperlich, M. Toth, I. Aharonovich, and V.

02 July 2026 15:24:17

© Author(s) 2025

Dyakonov, "Initialization and read-out of intrinsic spin defects in a van der Waals crystal at room temperature," Nat. Mater. **19**, 540–545 (2020).
[117]N. Chejanovsky, A. Mukherjee, J. Geng, Y. C. Chen, Y. Kim, A. Denisenko, A. Finkler, T. Taniguchi, K. Watanabe, D. B. R. Dasari, P. Auburger, A. Gali, J. H. Smet, and J. Wrachtrup, "Single-spin resonance in a van der Waals embedded paramagnetic defect," Nat. Mater. **20**, 1079–1084 (2021).
[118]N. J. Guo, S. Li, W. Liu, Y. Z. Yang, X. D. Zeng, S. Yu, Y. Meng, Z. P. Li, Z. A. Wang, L. K. Xie, R. C. Ge, J. F. Wang, Q. Li, J. S. Xu, Y. T. Wang, J. S. Tang, A. Gali, C. F. Li, and G. C. Guo, "Coherent control of an ultrabright single spin in hexagonal boron nitride at room temperature," Nat. Commun. **14**, 2893 (2023).
[119]A. Gottscholl, M. Diez, V. Soltamov, C. Kasper, A. Sperlich, M. Kianinia, C. Bradac, I. Aharonovich, and V. Dyakonov, "Room temperature coherent control of spin defects in hexagonal boron nitride," Sci. Adv. **7**, eabf3630 (2021).
[120]R. Rizzato, M. Schalk, S. Mohr, J. C. Hermann, J. P. Leibold, F. Bruckmaier, G. Salvitti, C. Qian, P. Ji, G. V. Astakhov, U. Kentsch, M. Helm, A. V. Stier, J. J. Finley, and D. B. Bucher, "Extending the coherence of spin defects in hBN enables advanced qubit control and quantum sensing," Nat. Commun. **14**, 5089 (2023).
[121]P. Khatri, I. J. Luxmoore, and A. J. Ramsay, "Phonon sidebands of color centers in hexagonal boron nitride," Phys. Rev. B **100**, 125305 (2019).
[122]M. A. Feldman, A. Puretzky, L. Lindsay, E. Tucker, D. P. Briggs, P. G. Evans, R. F. Haglund, and B. J. Lawrie, "Phonon-induced multicolor correlations in hBN single-photon emitters," Phys. Rev. B **99**, 020101 (2019).
[123]C. F. Klingshirn, *Semiconductor Optics*, Graduate Texts in Physics (Springer Berlin Heidelberg, Berlin, Heidelberg, 2012), pp. 11–37.
[124]E. Mostaani, M. Szyniszewski, C. H. Price, R. Maezono, M. Danovich, R. J. Hunt, N. D. Drummond, and V. I. Fal'ko, "Diffusion quantum Monte Carlo study of excitonic complexes in two-dimensional transition-metal dichalcogenides," Phys. Rev. B **96**, 75431 (2017).
[125]V. Carozo, Y. Wang, K. Fujisawa, B. R. Carvalho, A. McCreary, S. Feng, Z. Lin, C. Zhou, N. Perea-López, A. L. Elías, B. Kabius, V. H. Crespi, and M. Terrones, "Optical identification of sulfur vacancies: Bound excitons at the edges of monolayer tungsten disulfide," Sci. Adv. **3**, e1602813 (2017).
[126]L. Loh, Y. W. Ho, F. Xuan, A. G. del Águila, Y. Chen, S. Y. Wong, J. Zhang, Z. Wang, K. Watanabe, T. Taniguchi, P. J. Pigram, M. Bosman, S. Y. Quek, M. Koperski, and G. Eda, "Nb impurity-bound excitons as quantum emitters in monolayer WS_2," Nat. Commun. **15**, 10035 (2024).
[127]I. Kylänpää and H.-P. Komsa, "Binding energies of exciton complexes in transition metal dichalcogenide monolayers and effect of dielectric environment," Phys. Rev. B **92**, 205418 (2015).
[128]R. Rosati, R. Schmidt, S. Brem, R. Perea-Causín, I. Niehues, J. Kern, J. A. Preuß, R. Schneider, S. Michaelis de Vasconcellos, R. Bratschitsch, and E. Malic, "Dark exciton anti-funneling in atomically thin semiconductors," Nat. Commun. **12**, 7221 (2021).
[129]A. Ben Mhenni, D. Van Tuan, L. Geilen, M. M. Petrić, M. Erdi, K. Watanabe, T. Taniguchi, S. A. Tongay, K. Müller, N. P. Wilson, J. J. Finley, H. Dery, and M. Barbone, "Breakdown of the static dielectric screening approximation of Coulomb interactions in atomically thin semiconductors," ACS Nano **19**, 4269–4278 (2025).
[130]S. Zhao, Z. Li, X. Huang, A. Rupp, J. Göser, I. A. Vovk, S. Y. Kruchinin, K. Watanabe, T. Taniguchi, I. Bilgin, A. S. Baimuratov, and A. Högele, "Excitons in mesoscopically reconstructed moiré heterostructures," Nat. Nanotechnol. **18**, 572–579 (2023).
[131]M. M. Glazov, F. Dirnberger, V. M. Menon, T. Taniguchi, K. Watanabe, D. Bougeard, J. D. Ziegler, and A. Chernikov, "Exciton fine structure splitting and linearly polarized emission in strained transition-metal dichalcogenide monolayers," Phys. Rev. B **106**, 125303 (2022).
[132]K. Höflich, G. Hobler, F. I. Allen, T. Wirtz, G. Rius, L. McElwee-White, A. V. Krasheninnikov, M. Schmidt, I. Utke, N. Klingner, M. Osenberg, R. Córdoba, F. Djurabekova, I. Manke, P. Moll, M. Manoccio, J. M. De Teresa, L. Bischoff, J. Michler, O. De Castro, A. Delobbe, P. Dunne, O. V. Dobrovolskiy, N. Frese, A. Gölzhäuser, P. Mazarov, D. Koelle, W. Möller, F. Pérez-Murano, P. Philipp, F. Vollnhals, and G. Hlawacek, "Roadmap for focused ion beam technologies," Appl. Phys. Rev. **10**, 041311 (2023).
[133]A. V. Krasheninnikov and K. Nordlund, "Ion and electron irradiation-induced effects in nanostructured materials," J. Appl. Phys. **107**, 71301 (2010).
[134]Z. Li and F. Chen, "Ion beam modification of two-dimensional materials: Characterization, properties, and applications," Appl. Phys. Rev. **4**, 011103 (2017).
[135]M. Schleberger and J. Kotakoski, "2D material science: Defect engineering by particle irradiation," Materials **11**, 1885 (2018).
[136]G.-Y. Zhao, H. Deng, N. Tyree, M. Guy, A. Lisfi, Q. Peng, J.-A. Yan, C. Wang, and Y. Lan, "Recent progress on irradiation-induced defect engineering of two-dimensional 2H-MoS_2 few layers," Appl. Sci. **9**, 678 (2019).
[137]M. Telkhozhayeva and O. Girshevitz, "Roadmap toward controlled ion beam-induced defects in 2D materials," Adv. Funct. Mater. **34**, 2404615 (2024).
[138]R. Zan, Q. M. Ramasse, U. Bangert, and K. S. Novoselov, "Graphene reknits its holes," Nano Lett. **12**, 3936–3940 (2012).
[139]T. Susi, J. C. Meyer, and J. Kotakoski, "Quantifying transmission electron microscopy irradiation effects using two-dimensional materials," Nat. Rev. Phys. **1**, 397–405 (2019).
[140]R. Egerton, "Control of radiation damage in the TEM," Ultramicroscopy **127**, 100–108 (2013).
[141]X. Zhao, J. Kotakoski, J. C. Meyer, E. Sutter, P. Sutter, A. V. Krasheninnikov, U. Kaiser, and W. Zhou, "Engineering and modifying two-dimensional materials by electron beams," MRS Bull. **42**, 667–676 (2017).
[142]S. Kretschmer, T. Lehnert, U. Kaiser, and A. V. Krasheninnikov, "Formation of defects in two-dimensional MoS_2 in the transmission electron microscope at electron energies below the knock-on threshold: The role of electronic excitations," Nano Lett. **20**, 2865–2870 (2020).
[143]T. Lehnert, O. Lehtinen, G. Algara-Siller, and U. Kaiser, "Electron radiation damage mechanisms in 2D $MoSe_2$," Appl. Phys. Lett. **110**, 033106 (2017).
[144]M. N. Bui, S. Rost, M. Auge, L. Zhou, C. Friedrich, S. Blügel, S. Kretschmer, A. V. Krasheninnikov, K. Watanabe, T. Taniguchi, H. C. Hofsäss, D. Grützmacher, and B. E. Kardynał, "Optical properties of $MoSe_2$ monolayer implanted with ultra-low-energy Cr ions," ACS Appl. Mater. Interfaces **15**, 35321–35331 (2023).
[145]C. Speckmann, J. Lang, J. Madsen, M. R. A. Monazam, G. Zagler, G. T. Leuthner, N. McEvoy, C. Mangler, T. Susi, and J. Kotakoski, "Combined electronic excitation and knock-on damage in monolayer MoS_2," Phys. Rev. B **107**, 094112 (2023).
[146]E. H. Åhlgren, A. Markevich, S. Scharinger, B. Fickl, G. Zagler, F. Herterich, N. McEvoy, C. Mangler, and J. Kotakoski, "Atomic-scale oxygen-mediated Etching of 2D MoS_2 and $MoTe_2$," Adv. Mater. Interfaces **9**, 2200987 (2022).
[147]A. K. Dash, H. Swaminathan, E. Berger, M. Mondal, T. Lehenkari, P. R. Prasad, K. Watanabe, T. Taniguchi, H.-P. Komsa, and A. Singh, "Evidence of defect formation in monolayer MoS_2 at ultralow accelerating voltage electron irradiation," 2D Mater. **10**, 035002 (2023).
[148]A. K. Dash, S. K. Yadav, S. Roux, M. P. Singh, K. Watanabe, T. Taniguchi, A. Naik, C. Robert, X. Marie, and A. Singh, "Quantum light generation with ultra-high spatial resolution in 2D semiconductors via ultra-low energy electron irradiation," Adv. Funct. Mater. **35**, 2421684 (2025).
[149]Y.-C. Lin, T. Björkman, H.-P. Komsa, P.-Y. Teng, C.-H. Yeh, F.-S. Huang, K.-H. Lin, J. Jadczak, Y.-S. Huang, P.-W. Chiu, A. V. Krasheninnikov, and K. Suenaga, "Three-fold rotational defects in two-dimensional transition metal dichalcogenides," Nat. Commun. **6**, 6736 (2015).
[150]J. F. Ziegler and J. P. Biersack, "The stopping and range of ions in matter," in *Treatise on Heavy-Ion Science*, edited by D. A. Bromley (Springer US, Boston, MA, 1985), pp. 93–129.
[151]T. A. Bui, G. T. Leuthner, J. Madsen, M. R. A. Monazam, A. I. Chirita, A. Postl, C. Mangler, J. Kotakoski, and T. Susi, "Creation of single vacancies in hBN with electron irradiation," Small **19**, 2301926 (2023).
[152]X. Wei, D.-M. Tang, Q. Chen, Y. Bando, and D. Golberg, "Local Coulomb explosion of boron nitride nanotubes under electron beam irradiation," ACS Nano **7**, 3491–3497 (2013).
[153]M. Jain, S. Kretschmer, J. Meyer, and A. V. Krasheninnikov, "Adatom-mediated damage of two-dimensional materials under the electron beam in a transmission electron microscope," Phys. Rev. Mater. **8**, 054004 (2024).
[154]D. Yagodkin, K. Greben, A. Eljarrat, S. Kovalchuk, M. Ghorbani-Asl, M. Jain, S. Kretschmer, N. Severin, J. P. Rabe, A. V. Krasheninnikov, C. T. Koch, and K. I. Bolotin, "Extrinsic localized excitons in patterned 2D semiconductors," Adv. Funct. Mater. **32**, 2203060 (2022).

02 July 2026 15:24:17

© Author(s) 2025

[155]O. Dyck, A. R. Lupini, P. D. Rack, J. Fowlkes, and S. Jesse, "Controlling hydrocarbon transport and electron beam induced deposition on single layer graphene: Toward atomic scale synthesis in the scanning transmission electron microscope," Nano Select **3**, 643–654 (2022).
[156]M. Huth, F. Porrati, C. Schwalb, M. Winhold, R. Sachser, M. Dukic, J. Adams, and G. Fantner, "Focused electron beam induced deposition: A perspective," Beilstein J. Nanotechnol. **3**, 597–619 (2012).
[157]M. Nastasi, J. Mayer, and J. K. Hirvonen, *Ion-Solid Interactions* (Cambridge University Press, 1996).
[158]U. Bangert, W. Pierce, D. M. Kepaptsoglou, Q. Ramasse, R. Zan, M. H. Gass, J. A. Van den Berg, C. B. Boothroyd, J. Amani, and H. Hofsäss, "Ion implantation of graphene—Toward IC compatible technologies," Nano Lett. **13**, 4902–4907 (2013).
[159]T. Susi, T. P. Hardcastle, H. Hofsäss, A. Mittelberger, T. J. Pennycook, C. Mangler, R. Drummond-Brydson, A. J. Scott, J. C. Meyer, and J. Kotakoski, "Single-atom spectroscopy of phosphorus dopants implanted into graphene," 2D Mater. **4**, 021013 (2017).
[160]M. Tripathi, A. Markevich, R. Böttger, S. Facsko, E. Besley, J. Kotakoski, and T. Susi, "Implanting germanium into graphene," ACS Nano **12**, 4641–4647 (2018).
[161]M. N. Bui, S. Rost, M. Auge, J.-S. Tu, L. Zhou, I. Aguilera, S. Blügel, M. Ghorbani-Asl, A. V. Krasheninnikov, A. Hashemi, H.-P. Komsa, L. Jin, L. Kibkalo, E. N. O'Connell, Q. M. Ramasse, U. Bangert, H. C. Hofsäss, D. Grützmacher, and B. E. Kardynal, "Low-energy Se ion implantation in MoS_2 monolayers," npj 2D Mater. Appl. **6**, 42 (2022).
[162]R. Villarreal, Z. Zarkua, S. Kretschmer, V. Hendriks, J. Hillen, H. C. Tsai, F. Junge, M. Nissen, T. Saha, S. Achilli, H. C. Hofsäss, M. Martins, G. De Ninno, P. Lacovig, S. Lizzit, G. Di Santo, L. Petaccia, S. De Feyter, S. De Gendt, S. Brems, J. Van de Vondel, A. V. Krasheninnikov, and L. M. C. Pereira, "Achieving high substitutional incorporation in Mn-doped graphene," ACS Nano **18**, 17815–17825 (2024).
[163]P. Willke, J. A. Amani, A. Sinterhauf, S. Thakur, T. Kotzott, T. Druga, S. Weikert, K. Maiti, H. Hofsäss, and M. Wenderoth, "Doping of graphene by low-energy ion beam implantation: Structural, electronic, and transport properties," Nano Lett. **15**, 5110–5115 (2015).
[164]M. Telychko, K. Noori, H. Biswas, D. Dulal, Z. Chen, P. Lyu, J. Li, H.-Z. Tsai, H. Fang, Z. Qiu, Z. W. Yap, K. Watanabe, T. Taniguchi, J. Wu, K. P. Loh, M. F. Crommie, A. Rodin, and J. Lu, "Gate-tunable resonance state and screening effects for proton-like atomic charge in graphene," Nano Lett. **22**, 8422–8429 (2022).
[165]H. Wang, Q. Wang, Y. Cheng, K. Li, Y. Yao, Q. Zhang, C. Dong, P. Wang, U. Schwingenschlögl, W. Yang, and X. X. Zhang, "Doping monolayer graphene with single atom substitutions," Nano Lett. **12**, 141–144 (2012).
[166]Q. Ma, M. Isarraraz, C. S. Wang, E. Preciado, V. Klee, S. Bobek, K. Yamaguchi, E. Li, P. M. Odenthal, A. Nguyen, D. Barroso, D. Sun, G. von Son Palacio, M. Gomez, A. Nguyen, D. Le, G. Pawin, J. Mann, T. F. Heinz, T. S. Rahman, and L. Bartels, "Postgrowth tuning of the bandgap of single-layer molybdenum disulfide films by sulfur/selenium exchange," ACS Nano **8**, 4672–4677 (2014).
[167]A. V. Krasheninnikov, "Are two-dimensional materials radiation tolerant?," Nanoscale Horiz. **5**, 1447–1452 (2020).
[168]S. Ghaderzadeh, S. Kretschmer, M. Ghorbani-Asl, G. Hlawacek, and A. V. Krasheninnikov, "Atomistic simulations of defect production in monolayer and bulk hexagonal boron nitride under low- and high-fluence ion irradiation," Nanomaterials **11**, 1214 (2021).
[169]E. Akcöltekin, S. Akcöltekin, O. Osmani, A. Duvenbeck, H. Lebius, and M. Schleberger, "Swift heavy ion irradiation of $SrTiO_3$ under grazing incidence," New J. Phys. **10**, 053007 (2008).
[170]S. Kretschmer, M. Maslov, S. Ghaderzadeh, M. Ghorbani-Asl, G. Hlawacek, and A. V. Krasheninnikov, "Supported two-dimensional materials under ion irradiation: The substrate governs defect production," ACS Appl. Mater. Interfaces **10**, 30827–30836 (2018).
[171]A. Paralikis, C. Piccinini, A. A. Madigawa, P. Metuh, L. Vannucci, N. Gregersen, and B. Munkhbat, "Tailoring polarization in WSe_2 quantum emitters through deterministic strain engineering," npj 2D Mater. Appl. **8**, 59 (2024).
[172]D. Tedeschi, E. Blundo, M. Felici, G. Pettinari, B. Liu, T. Yildrim, E. Petroni, C. Zhang, Y. Zhu, S. Sennato, Y. Lu, and A. Polimeni, "Controlled micro/nanodome formation in proton-irradiated bulk transition-metal dichalcogenides," Adv. Mater. **31**, 1903795 (2019).
[173]M. R. Rosenberger, C. K. Dass, H.-J. Chuang, S. V. Sivaram, K. M. McCreary, J. R. Hendrickson, and B. T. Jonker, "Quantum calligraphy: Writing single-photon emitters in a two-dimensional materials platform," ACS Nano **13**, 904–912 (2019).
[174]G. D. Shepard, O. A. Ajayi, X. Li, X.-Y. Zhu, J. Hone, and S. Strauf, "Nanobubble induced formation of quantum emitters in monolayer semiconductors," 2D Mater. **4**, 021019 (2017).
[175]A. V. Tyurnina, D. A. Bandurin, E. Khestanova, V. G. Kravets, M. Koperski, F. Guinea, A. N. Grigorenko, A. K. Geim, and I. V. Grigorieva, "Strained bubbles in van der Waals heterostructures as local emitters of photoluminescence with adjustable wavelength," ACS Photonics **6**, 516–524 (2019).
[176]A. Mukherjee, C. Chakraborty, L. Qiu, and A. N. Vamivakas, "Electric field tuning of strain-induced quantum emitters in WSe_2," AIP Adv. **10**, 075310 (2020).
[177]O. Iff, N. Lundt, S. Betzold, L. N. Tripathi, M. Emmerling, S. Tongay, Y. J. Lee, S.-H. Kwon, S. Höfling, and C. Schneider, "Deterministic coupling of quantum emitters in WSe_2 monolayers to plasmonic nanocavities," Opt. Express **26**, 25944 (2018).
[178]M. Chhaperwal, H. M. Tongale, P. Hays, K. Watanabe, T. Taniguchi, S. A. Tongay, and K. Majumdar, "Simultaneously enhancing brightness and purity of WSe_2 single photon emitter using high-aspect-ratio nanopillar array on metal," Nano Lett. **24**, 12461–12468 (2024).
[179]P. Singh, G. R. Wilbur, E. Yeung, J. K. Jagde, M. Jain, D. B. Northeast, S. J. Mohammed, J. Lapointe, D. Dalacu, and K. C. Hall, "Exploring quantum emission in bilayer WSe_2: Strain effects from nanopillars," Phys. Status Solidi B **262**, 2400616 (2025).
[180]Y. Yu, J. Ge, M. Luo, I. C. Seo, Y. Kim, J. J. H. Eng, K. Lu, T.-R. Wei, S. W. Lee, W. Gao, H. Li, and D. Nam, "Dynamic tuning of single-photon emission in monolayer WSe_2 via localized strain engineering," Nano Lett. **25**, 3438–3444 (2025).
[181]H. Zhao, L. Zhu, X. Li, V. Chandrasekaran, J. K. Baldwin, M. T. Pettes, A. Piryatinski, L. Yang, and H. Htoon, "Manipulating interlayer excitons for near-infrared quantum light generation," Nano Lett. **23**, 11006–11012 (2023).
[182]A. Ripin, R. Peng, X. Zhang, S. Chakravarthi, M. He, X. Xu, K.-M. Fu, T. Cao, and M. Li, "Tunable phononic coupling in excitonic quantum emitters," Nat. Nanotechnol. **18**, 1020–1026 (2023).
[183]T. Cai, S. Dutta, S. Aghaeimeibodi, Z. Yang, S. Nah, J. T. Fourkas, and E. Waks, "Coupling emission from single localized defects in two-dimensional semiconductor to surface plasmon polaritons," Nano Lett. **17**, 6564–6568 (2017).
[184]J.-P. So, K.-Y. Jeong, J. M. Lee, K.-H. Kim, S.-J. Lee, W. Huh, H.-R. Kim, J.-H. Choi, J. M. Kim, Y. S. Kim, C.-H. Lee, S. Nam, and H.-G. Park, "Polarization control of deterministic single-photon emitters in monolayer WSe_2," Nano Lett. **21**, 1546–1554 (2021).
[185]S. I. Azzam, K. Parto, and G. Moody, "Purcell enhancement and polarization control of single-photon emitters in monolayer WSe_2 using dielectric nanoantennas," Nanophotonics **12**, 477–484 (2023).
[186]C. Errando-Herranz, E. Schöll, R. Picard, M. Laini, S. Gyger, A. W. Elshaari, A. Branny, U. Wennberg, S. Barbat, T. Renaud, M. Sartison, M. Brotons-Gisbert, C. Bonato, B. D. Gerardot, V. Zwiller, and K. D. Jöns, "Resonance fluorescence from waveguide-coupled, strain-localized, two-dimensional quantum emitters," ACS Photonics **8**, 1069–1076 (2021).
[187]X. Li, W. Wang, and X. Ma, "Quantum photon sources in WSe_2 monolayers induced by weakly localized strain fields," J. Phys. Chem. C **126**, 20057–20064 (2022).
[188]F. C. M. Wu, S.-H. Wu, B. Fang, X. Li, J. Zheng, J. A. C. Incorvia, and E. T. Yu, "Modulation of single photon emission from suspended 1L WSe_2 under electrostatically induced strain," Nano Lett. **25**, 10983–10989 (2025).
[189]H. Kim, J. S. Moon, G. Noh, J. Lee, and J.-H. Kim, "Position and frequency control of strain-induced quantum emitters in WSe_2 monolayers," Nano Lett. **19**, 7534–7539 (2019).
[190]W. Wu, A. Strasser, Z. Xiu, K. Ngan, T. D. Hoang, S. Liu, H. Shen, L. N. Holtzman, J. H. Edgar, J. C. Hone, V. Perebeinos, S. Sun, J. Kono, X. Qian, and S. Huang, "Ultrahigh-purity single-photon emission from 2D WSe_2 via

02 July 2026 15:24:17

© Author(s) 2025

effective suppression of classical emission," Nano Lett. **25**, 11226–11233 (2025).
[191]R. S. Daveau, T. Vandekerckhove, A. Mukherjee, Z. Wang, J. Shan, K. F. Mak, A. N. Vamivakas, and G. D. Fuchs, "Spectral and spatial isolation of single tungsten diselenide quantum emitters using hexagonal boron nitride wrinkles," APL Photonics **5**, 096105 (2020).
[192]L. Peng, H. Chan, P. Choo, T. W. Odom, S. K. R. S. Sankaranarayanan, and X. Ma, "Creation of single-photon emitters in WSe_2 monolayers using nanometer-sized gold tips," Nano Lett. **20**, 5866–5872 (2020).
[193]M. I. B. Utama, H. Zeng, T. Sadhukhan, A. Dasgupta, S. C. Gavin, R. Ananth, D. Lebedev, W. Wang, J.-S. Chen, K. Watanabe, T. Taniguchi, T. J. Marks, X. Ma, E. A. Weiss, G. C. Schatz, N. P. Stern, and M. C. Hersam, "Chemomechanical modification of quantum emission in monolayer WSe_2," Nat. Commun. **14**, 2193 (2023).
[194]S.-J. Lee, J.-P. So, R. M. Kim, K.-H. Kim, H.-H. Rha, G. Na, J. H. Han, K.-Y. Jeong, K. T. Nam, and H.-G. Park, "Spin angular momentum-encoded single-photon emitters in a chiral nanoparticle-coupled WSe_2 monolayer," Sci. Adv. **10**, eadn7210 (2024).
[195]M. Pandey, R. Ahuja, and R. Kumar, "Electron beam irradiation-induced atomically thin domes of two-dimensional materials: Graphene and MoS_2," Surf. Interfaces **51**, 104654 (2024).
[196]A. N. Abramov, I. Y. Chestnov, E. S. Alimova, T. Ivanova, I. S. Mukhin, D. N. Krizhanovskii, I. A. Shelykh, I. V. Iorsh, and V. Kravtsov, "Photoluminescence imaging of single photon emitters within nanoscale strain profiles in monolayer WSe_2," Nat. Commun. **14**, 5737 (2023).
[197]J.-P. So, H.-R. Kim, H. Baek, K.-Y. Jeong, H.-C. Lee, W. Huh, Y. S. Kim, K. Watanabe, T. Taniguchi, J. Kim, C.-H. Lee, and H.-G. Park, "Electrically driven strain-induced deterministic single-photon emitters in a van der Waals heterostructure," Sci. Adv. **7**, eabj3176 (2021).
[198]H.-J. Chuang, C. E. Stevens, M. R. Rosenberger, S.-J. Lee, K. M. McCreary, J. R. Hendrickson, and B. T. Jonker, "Enhancing single photon emission purity via design of van der Waals heterostructures," Nano Lett. **24**, 5529–5535 (2024).
[199]S.-J. Lee, H.-J. Chuang, A. L. Yeats, K. M. McCreary, D. J. O'Hara, B. T. Jonker, D. J. O'Hara, B. T. Jonker, D. J. O'Hara, B. T. Jonker, D. J. O'Hara, and B. T. Jonker, "Ferroelectric modulation of quantum emitters in monolayer WS_2," ACS Nano **18**, 25349–25358 (2024).
[200]N. V. Proscia, Z. Shotan, H. Jayakumar, P. Reddy, C. Cohen, M. Dollar, A. Alkauskas, M. Doherty, C. A. Meriles, and V. M. Menon, "Near-deterministic activation of room-temperature quantum emitters in hexagonal boron nitride," Optica **5**, 1128 (2018).
[201]S. Karankova, Y. Lee, C. Jang, Y. Song, and H. Moon, "One-step creation of quantum emitter arrays in hexagonal boron nitride by local stress application," Adv. Opt. Mater. **13**, 2403018 (2025).
[202]D. Yim, M. Yu, G. Noh, J. Lee, and H. Seo, "Polarization and localization of single-photon emitters in hexagonal boron nitride wrinkles," ACS Appl. Mater. Interfaces **12**, 36362–36369 (2020).
[203]M. A. Sakib, B. Triplett, W. Harris, N. Hussain, A. Senichev, M. Momenzadeh, J. Bocanegra, P. Vabishchevich, R. Wu, A. Boltasseva, V. M. Shalaev, and M. R. Shcherbakov, "Purcell-induced bright single photon emitters in hexagonal boron nitride," Nano Lett. **24**, 12390–12397 (2024).
[204]Y. Chen, H. Huang, M. Ge, W. Li, L. Zhang, W. Du, and T. Wang, "Electrically driven strain-activated defect emission from hexagonal boron nitride at room temperature," Phys. Status Solidi RRL **19**, 2400421 (2025).
[205]P. Santra, S. Ghaderzadeh, M. Ghorbani-Asl, H.-P. Komsa, E. Besley, and A. V. Krasheninnikov, "Strain-modulated defect engineering of two-dimensional materials," npj 2D Mater. Appl. **8**, 33 (2024).
[206]L. Zeng, S. Zhang, J. Meng, J. Chen, J. Jiang, Y. Shi, J. Huang, Z. Yin, J. Wu, and X. Zhang, "Single-photon emission from point defects in hexagonal boron nitride induced by plasma treatment," ACS Appl. Mater. Interfaces **16**, 24899–24907 (2024).
[207]T. Vogl, G. Campbell, B. C. Buchler, Y. Lu, and P. K. Lam, "Fabrication and deterministic transfer of high-quality quantum emitters in hexagonal boron nitride," ACS Photonics **5**, 2305–2312 (2018).
[208]Z.-Q. Q. Xu, C. Elbadawi, T. T. Tran, M. Kianinia, X. Li, D. Liu, T. B. Hoffman, M. Nguyen, S. Kim, J. H. Edgar, X. Wu, L. Song, S. Ali, M. Ford, M. Toth, and I. Aharonovich, "Single photon emission from plasma treated 2D hexagonal boron nitride," Nanoscale **10**, 7957–7965 (2018).
[209]P. K. Chow, R. B. Jacobs-Gedrim, J. Gao, T.-M. Lu, B. Yu, H. Terrones, and N. Koratkar, "Defect-induced photoluminescence in monolayer semiconducting transition metal dichalcogenides," ACS Nano **9**, 1520–1527 (2015).
[210]Z. Wu, W. Zhao, J. Jiang, T. Zheng, Y. You, J. Lu, and Z. Ni, "Defect activated photoluminescence in WSe_2 monolayer," J. Phys. Chem. C **121**, 12294–12299 (2017).
[211]Q. Qian, W. Wu, L. Peng, Y. Wang, A. M. Z. Tan, L. Liang, S. M. Hus, K. Wang, T. H. Choudhury, J. M. Redwing, A. A. Puretzky, D. B. Geohegan, R. G. Hennig, X. Ma, and S. Huang, "Photoluminescence induced by substitutional nitrogen in single-layer tungsten disulfide," ACS Nano **16**, 7428–7437 (2022).
[212]A. Hötger, J. Klein, K. Barthelmi, L. Sigl, F. Sigger, W. Männer, S. Gyger, M. Florian, M. Lorke, F. Jahnke, T. Taniguchi, K. Watanabe, K. D. Jöns, U. Wurstbauer, C. Kastl, K. Müller, J. J. Finley, and A. W. Holleitner, "Gate-switchable arrays of quantum light emitters in contacted monolayer MoS_2 van der Waals heterodevices," Nano Lett. **21**, 1040–1046 (2021).
[213]H. Liang, Y. Chen, C. Yang, K. Watanabe, T. Taniguchi, G. Eda, and A. A. Bettiol, "High sensitivity spin defects in hBN created by high-energy He beam irradiation," Adv. Opt. Mater. **11**, 1–7 (2023).
[214]K. Sasaki, Y. Nakamura, H. Gu, M. Tsukamoto, S. Nakaharai, T. Iwasaki, K. Watanabe, T. Taniguchi, S. Ogawa, Y. Morita, and K. Kobayashi, "Magnetic field imaging by hBN quantum sensor nanoarray," Appl. Phys. Lett. **122**, 244003 (2023).
[215]G. Liu, X. Wu, P. Jing, Z. Cheng, D. Zhan, Y. Bao, J. Yan, H. Xu, L. Zhang, B. Li, K. Liu, L. Liu, and D. Shen, "Single photon emitters in hexagonal boron nitride fabricated by focused helium ion beam," Adv. Opt. Mater. **12**, 2302083 (2024).
[216]J. Klein, A. Kuc, A. Nolinder, M. Altzschner, J. Wierzbowski, F. Sigger, F. Kreupl, J. J. Finley, U. Wurstbauer, A. W. Holleitner, and M. Kaniber, "Robust valley polarization of helium ion modified atomically thin MoS_2," 2D Mater. **5**, 011007 (2017).
[217]J. Klein, L. Sigl, S. Gyger, K. Barthelmi, M. Florian, S. Rey, T. Taniguchi, K. Watanabe, F. Jahnke, C. Kastl, V. Zwiller, K. D. Jöns, K. Müller, U. Wurstbauer, J. J. Finley, and A. W. Holleitner, "Engineering the luminescence and generation of individual defect emitters in atomically thin MoS_2," ACS Photonics **8**, 669–677 (2021).
[218]K. Barthelmi, T. Amit, L. Sigl, M. Troue, T. Klokkers, A. Herrmann, T. Taniguchi, K. Watanabe, J. Finley, C. Kastl, S. Refaely-Abramson, and A. Holleitner, "Spectrally resolved far-field emission pattern of single photon emitters in MoS_2," Phys. Rev. Mater. **9**, 016201 (2025).
[219]V. Iberi, L. Liang, A. V. Ievlev, M. G. Stanford, M.-W. Lin, X. Li, M. Mahjouri-Samani, S. Jesse, B. G. Sumpter, S. V. Kalinin, D. C. Joy, K. Xiao, A. Belianinov, and O. S. Ovchinnikova, "Nanoforging single layer $MoSe_2$ through defect engineering with focused helium ion beams," Sci. Rep. **6**, 30481 (2016).
[220]F. Sarcan, N. J. Fairbairn, P. Zotev, T. Severs-Millard, D. J. Gillard, X. Wang, B. Conran, M. Heuken, A. Erol, A. I. Tartakovskii, T. F. Krauss, G. J. Hedley, and Y. Wang, "Understanding the impact of heavy ions and tailoring the optical properties of large-area monolayer WS_2 using focused ion beam," npj 2D Mater. Appl. **7**, 23 (2023).
[221]Y. Chen, H. Liang, L. Loh, Y. Ho, I. Verzhbitskiy, K. Watanabe, T. Taniguchi, M. Bosman, A. A. Bettiol, and G. Eda, "Gate-tunable bound exciton manifolds in monolayer $MoSe_2$," Nano Lett. **23**, 4456–4463 (2023).
[222]A. J. Healey, S. C. Scholten, T. Yang, J. A. Scott, G. J. Abrahams, I. O. Robertson, X. F. Hou, Y. F. Guo, S. Rahman, Y. Lu, M. Kianinia, I. Aharonovich, and J.-P. P. Tetienne, "Quantum microscopy with van der Waals heterostructures," Nat. Phys. **19**, 87–91 (2023).
[223]X. Gao, S. Vaidya, K. Li, P. Ju, B. Jiang, Z. Xu, A. E. L. Allcca, K. Shen, T. Taniguchi, K. Watanabe, S. A. Bhave, Y. P. Chen, Y. Ping, and T. Li, "Nuclear spin polarization and control in hexagonal boron nitride," Nat. Mater. **21**, 1024–1028 (2022).
[224]I. Schwartz, J. Scheuer, B. Tratzmiller, S. Müller, Q. Chen, I. Dhand, Z.-Y. Wang, C. Müller, B. Naydenov, F. Jelezko, and M. B. Plenio, "Robust optical polarization of nuclear spin baths using Hamiltonian engineering of nitrogen-vacancy center quantum dynamics," Sci. Adv. **4**, eaat8978 (2018).
[225]M. Hennessey, B. Whitefield, A. Gale, M. Kianinia, J. A. Scott, I. Aharonovich, and M. Toth, "Framework for engineering of spin defects in hexagonal boron nitride by focused ion beams," Adv. Quantum Tech. **8**, 2300459 (2025).

02 July 2026 15:24:17

© Author(s) 2025

[226]J. E. Fröch, L. P. Spencer, M. Kianinia, D. D. Totonjian, M. Nguyen, A. Gottscholl, V. Dyakonov, M. Toth, S. Kim, and I. Aharonovich, "Coupling spin defects in hexagonal boron nitride to monolithic bullseye cavities," Nano Lett. **21**, 6549–6555 (2021).
[227]S. Sarkar, Y. Xu, S. Mathew, M. Lal, J.-Y. Chung, H. Y. Lee, K. Watanabe, T. Taniguchi, T. Venkatesan, and S. Gradečak, "Identifying luminescent boron vacancies in h-BN generated using controlled He^+ ion irradiation," Nano Lett. **24**, 43–50 (2024).
[228]X. Gao, B. Jiang, A. E. Llacsahuanga Allcca, K. Shen, M. A. Sadi, A. B. Solanki, P. Ju, Z. Xu, P. Upadhyaya, Y. P. Chen, S. A. Bhave, and T. Li, "High-contrast plasmonic-enhanced shallow spin defects in hexagonal boron nitride for quantum sensing," Nano Lett. **21**, 7708–7714 (2021).
[229]F. Ren, Y. Wu, and Z. Xu, "Creation and repair of luminescence defects in hexagonal boron nitride by irradiation and annealing for optical neutron detection," J. Lumin. **261**, 119911 (2023).
[230]F. Ren, Z. Xu, Y. Wu, X. Wang, Y. Guo, L. Chen, Y. Song, and B. Dong, "Color centers in hexagonal boron nitride nanosheet-based heterojunctions: implications for quantum emitters and ultrathin sensors," ACS Appl. Nano Mater. **7**, 3436–3444 (2024).
[231]N.-J. Guo, W. Liu, Z.-P. Li, Y.-Z. Yang, S. Yu, Y. Meng, Z.-A. Wang, X.-D. Zeng, F.-F. Yan, Q. Li, J.-F. Wang, J.-S. Xu, Y.-T. Wang, J.-S. Tang, C.-F. Li, and G.-C. Guo, "Generation of spin defects by ion implantation in hexagonal boron nitride," ACS Omega **7**, 1733–1739 (2022).
[232]J. Zhou, H. Lu, D. Chen, M. Huang, G. Q. Yan, F. Al-matouq, J. Chang, D. Djugba, Z. Jiang, H. Wang, and C. R. Du, "Sensing spin wave excitations by spin defects in few-layer-thick hexagonal boron nitride," Sci. Adv. **10**, eadk8495 (2024).
[233]A. Carbone, I. D. Breev, J. Figueiredo, S. Kretschmer, L. Geilen, A. Ben Mhenni, J. Arceri, A. V. Krasheninnikov, M. Wubs, A. W. Holleitner, A. Huck, C. Kastl, and N. Stenger, "Quantifying the creation of negatively charged boron vacancies in He-ion irradiated hexagonal boron nitride," Phys. Rev. Mater. **9**, 056203 (2025).
[234]T. Clua-Provost, A. Durand, Z. Mu, T. Rastoin, J. Fraunié, E. Janzen, H. Schutte, J. H. Edgar, G. Seine, A. Claverie, X. Marie, C. Robert, B. Gil, G. Cassabois, and V. Jacques, "Isotopic control of the boron-vacancy spin defect in hexagonal boron nitride," Phys. Rev. Lett. **131**, 126901 (2023).
[235]T. Clua-Provost, Z. Mu, A. Durand, C. Schrader, J. Happacher, J. Bocquel, P. Maletinsky, J. Fraunié, X. Marie, C. Robert, G. Seine, E. Janzen, J. H. Edgar, B. Gil, G. Cassabois, and V. Jacques, "Spin-dependent photodynamics of boron-vacancy centers in hexagonal boron nitride," Phys. Rev. B **110**, 014104 (2024).
[236]M. Kianinia, S. White, J. E. Fröch, C. Bradac, and I. Aharonovich, "Generation of spin defects in hexagonal boron nitride," ACS Photonics **7**, 2147–2152 (2020).
[237]L. Sortino, A. Gale, L. Kühner, C. Li, J. Biechteler, F. J. Wendisch, M. Kianinia, H. Ren, M. Toth, S. A. Maier, I. Aharonovich, and A. Tittl, "Optically addressable spin defects coupled to bound states in the continuum metasurfaces," Nat. Commun. **15**, 2008 (2024).
[238]Z. Mu, H. Cai, D. Chen, J. Kenny, Z. Jiang, S. Ru, X. Lyu, T. S. Koh, X. Liu, I. Aharonovich, and W. Gao, "Excited-state optically detected magnetic resonance of spin defects in hexagonal boron nitride," Phys. Rev. Lett. **128**, 216402 (2022).
[239]S. Baber, R. N. E. Malein, P. Khatri, P. S. Keatley, S. Guo, F. Withers, A. J. Ramsay, and I. J. Luxmoore, "Excited state spectroscopy of boron vacancy defects in hexagonal boron nitride using time-resolved optically detected magnetic resonance," Nano Lett. **22**, 461–467 (2022).
[240]E. Glushkov, M. Macha, E. Räth, V. Navikas, N. Ronceray, C. Y. Cheon, A. Ahmed, A. Avsar, K. Watanabe, T. Taniguchi, I. Shorubalko, A. Kis, G. Fantner, and A. Radenovic, "Engineering optically active defects in hexagonal boron nitride using focused ion beam and water," ACS Nano **16**, 3695–3703 (2022).
[241]J. R. Toledo, D. B. de Jesus, M. Kianinia, A. S. Leal, C. Fantini, L. A. Cury, G. A. M. Sáfar, I. Aharonovich, and K. Krambrock, "Electron paramagnetic resonance signature of point defects in neutron-irradiated hexagonal boron nitride," Phys. Rev. B **98**, 155203 (2018).
[242]A. Gottscholl, M. Diez, V. Soltamov, C. Kasper, D. Krauße, A. Sperlich, M. Kianinia, C. Bradac, I. Aharonovich, and V. Dyakonov, "Spin defects in hBN as promising temperature, pressure and magnetic field quantum sensors," Nat. Commun. **12**, 4480 (2021).
[243]P. Kumar, F. Fabre, A. Durand, T. Clua-Provost, J. Li, J. H. Edgar, N. Rougemaille, J. Coraux, X. Marie, P. Renucci, C. Robert, I. Robert-Philip, B. Gil, G. Cassabois, A. Finco, and V. Jacques, "Magnetic imaging with spin defects in hexagonal boron nitride," Phys. Rev. Appl. **18**, L061002 (2022).
[244]A. Durand, T. Clua-Provost, F. Fabre, P. Kumar, J. Li, J. H. Edgar, P. Udvarhelyi, A. Gali, X. Marie, C. Robert, J. M. Gérard, B. Gil, G. Cassabois, and V. Jacques, "Optically active spin defects in few-layer thick hexagonal boron nitride," Phys. Rev. Lett. **131**, 116902 (2023).
[245]P. Udvarhelyi, T. Clua-Provost, A. Durand, J. Li, J. H. Edgar, B. Gil, G. Cassabois, V. Jacques, and A. Gali, "A planar defect spin sensor in a two-dimensional material susceptible to strain and electric fields," npj Comput. Mater. **9**, 150 (2023).
[246]T. Clua-Provost, A. Durand, J. Fraunié, C. Robert, X. Marie, J. Li, J. H. Edgar, B. Gil, J.-M. Gérard, G. Cassabois, and V. Jacques, "Impact of thickness-dependent nanophotonic effects on the optical response of color centers in hexagonal boron nitride," Nano Lett. **24**, 12915–12920 (2024).
[247]Z. Mu, J. Fraunié, A. Durand, S. Clément, A. Finco, J. Rouquette, A. Hadj-Azzem, N. Rougemaille, J. Coraux, J. Li, T. Poirier, J. H. Edgar, I. C. Gerber, X. Marie, B. Gil, G. Cassabois, C. Robert, and V. Jacques, "Magnetic imaging under high pressure with a spin-based quantum sensor integrated in a van der Waals heterostructure," arXiv:2501.03640 (2025).
[248]X. Gao, S. Pandey, M. Kianinia, J. Ahn, P. Ju, I. Aharonovich, N. Shivaram, and T. Li, "Femtosecond laser writing of spin defects in hexagonal boron nitride," ACS Photonics **8**, 994–1000 (2021).
[249]X. Xu, Z. O. Martin, D. Sychev, A. S. Lagutchev, Y. P. Chen, T. Taniguchi, K. Watanabe, V. M. Shalaev, and A. Boltasseva, "Creating quantum emitters in hexagonal boron nitride deterministically on chip-compatible substrates," Nano Lett. **21**, 8182–8189 (2021).
[250]T. Suzuki, Y. Yamazaki, T. Taniguchi, K. Watanabe, Y. Nishiya, Y-i Matsushita, K. Harii, Y. Masuyama, Y. Hijikata, and T. Ohshima, "Spin property improvement of boron vacancy defect in hexagonal boron nitride by thermal treatment," Appl. Phys. Express **16**, 032006 (2023).
[251]N. Mendelson, R. Ritika, M. Kianinia, J. Scott, S. Kim, J. E. Fröch, C. Gazzana, M. Westerhausen, L. Xiao, S. S. Mohajerani, S. Strauf, M. Toth, I. Aharonovich, and Z. Xu, "Coupling spin defects in a layered material to nanoscale plasmonic cavities," Adv. Mater. **34**, 2106046 (2022).
[252]X. Xu, A. B. Solanki, D. Sychev, X. Gao, S. Peana, A. S. Baburin, K. Pagadala, Z. O. Martin, S. N. Chowdhury, Y. P. Chen, T. Taniguchi, K. Watanabe, I. A. Rodionov, A. V. Kildishev, T. Li, P. Upadhyaya, A. Boltasseva, and V. M. Shalaev, "Greatly enhanced emission from spin defects in hexagonal boron nitride enabled by a low-loss plasmonic nanocavity," Nano Lett. **23**, 25–33 (2023).
[253]C. Qian, V. Villafañe, M. Schalk, G. V. Astakhov, U. Kentsch, M. Helm, P. Soubelet, N. P. Wilson, R. Rizzato, S. Mohr, A. W. Holleitner, D. B. Bucher, A. V. Stier, and J. J. Finley, "Unveiling the zero-phonon line of the boron vacancy center by cavity-enhanced emission," Nano Lett. **22**, 5137–5142 (2022).
[254]T. T. H. Do, M. Nonahal, C. Li, V. Valuckas, H. H. Tan, A. I. Kuznetsov, H. S. Nguyen, I. Aharonovich, and S. T. Ha, "Room-temperature strong coupling in a single-photon emitter-metasurface system," Nat. Commun. **15**, 2281 (2024).
[255]R. Gong, G. He, X. Gao, P. Ju, Z. Liu, B. Ye, E. A. Henriksen, T. Li, and C. Zu, "Coherent dynamics of strongly interacting electronic spin defects in hexagonal boron nitride," Nat. Commun. **14**, 3299 (2023).
[256]F. Ren, Z. Xu, and Y. Wu, "Optimization of carbon irradiation parameters for creating spin defects in hexagonal boron nitride," Nanotechnol. Precis. Eng. **8**, 033014 (2025).
[257]D. Zhong, S. Gao, M. Saccone, J. R. Greer, M. Bernardi, S. Nadj-Perge, and A. Faraon, "Carbon-related quantum emitter in hexagonal boron nitride with homogeneous energy and 3-fold polarization," Nano Lett. **24**, 1106–1113 (2024).
[258]P. Rivera, M. He, B. Kim, S. Liu, C. Rubio-Verdú, H. Moon, L. Mennel, D. A. Rhodes, H. Yu, T. Taniguchi, K. Watanabe, J. Yan, D. G. Mandrus, H. Dery, A. Pasupathy, D. Englund, J. Hone, W. Yao, and X. Xu, "Intrinsic donor-bound excitons in ultraclean monolayer semiconductors," Nat. Commun. **12**, 871 (2021).

02 July 2026 15:24:17

© Author(s) 2025

[259]H. Liu, N. Mendelson, I. H. Abidi, S. Li, Z. Liu, Y. Cai, K. Zhang, J. You, M. Tamtaji, H. Wong, Y. Ding, G. Chen, I. Aharonovich, and Z. Luo, "Rational control on quantum emitter formation in carbon-doped monolayer hexagonal boron nitride," ACS Appl. Mater. Interfaces **14**, 3189–3198 (2022).
[260]U. Bangert, A. Stewart, E. O'Connell, E. Courtney, Q. Ramasse, D. Kepaptsoglou, H. Hofsäss, J. Amani, J.-S. Tu, and B. Kardynal, "Ion-beam modification of 2D materials—Single implant atom analysis via annular dark-field electron microscopy," Ultramicroscopy **176**, 31–36 (2017).
[261]X. Gao, S. Vaidya, S. Dikshit, P. Ju, K. Shen, Y. Jin, S. Zhang, and T. Li, "Nanotube spin defects for omnidirectional magnetic field sensing," Nat. Commun. **15**, 7697 (2024).
[262]D. I. Badrtdinov, C. Rodriguez-Fernandez, M. Grzeszczyk, Z. Qiu, K. Vaklinova, P. Huang, A. Hampel, K. Watanabe, T. Taniguchi, L. Jiong, M. Potemski, C. E. Dreyer, M. Koperski, and M. Rösner, "Dielectric environment sensitivity of carbon centers in hexagonal boron nitride," Small **19**, 2300144 (2023).
[263]S. C. Scholten, P. Singh, A. J. Healey, I. O. Robertson, G. Haim, C. Tan, D. A. Broadway, L. Wang, H. Abe, T. Ohshima, M. Kianinia, P. Reineck, I. Aharonovich, and J.-P. Tetienne, "Multi-species optically addressable spin defects in a van der Waals material," Nat. Commun. **15**, 6727 (2024).
[264]H. L. Stern, C. M. Gilardoni, Q. Gu, S. Eizagirre Barker, O. F. J. Powell, X. Deng, S. A. Fraser, L. Follet, C. Li, A. J. Ramsay, H. H. Tan, I. Aharonovich, and M. Atatüre, "A quantum coherent spin in hexagonal boron nitride at ambient conditions," Nat. Mater. **23**, 1379–1385 (2024).
[265]F. Ren and Z. Xu, "Atomistic simulations of carbon implantation into hBN for creating color centers," J. Phys. Chem. C **129**, 5054–5064 (2025).
[266]S. A. Tawfik, S. Ali, M. Fronzi, M. Kianinia, T. T. Tran, C. Stampfl, I. Aharonovich, M. Toth, and M. J. Ford, "First-principles investigation of quantum emission from hBN defects," Nanoscale **9**, 13575–13582 (2017).
[267]A. Sajid, J. R. Reimers, and M. J. Ford, "Defect states in hexagonal boron nitride: Assignments of observed properties and prediction of properties relevant to quantum computation," Phys. Rev. B **97**, 064101 (2018).
[268]M. Mackoit-Sinkevičienė, M. Maciaszek, C. G. Van de Walle, and A. Alkauskas, "Carbon dimer defect as a source of the 4.1 eV luminescence in hexagonal boron nitride," Appl. Phys. Lett. **115**, 212101 (2019).
[269]J. Horder, D. Scognamiglio, N. Coste, A. Gale, K. Watanabe, T. Taniguchi, M. Kianinia, M. Toth, and I. Aharonovich, "Optical coherence of B center quantum emitters in hexagonal boron nitride," ACS Photonics **12**, 1284–1290 (2025).
[270]C. Jara, T. Rauch, S. Botti, M. A. L. Marques, A. Norambuena, R. Coto, J. E. Castellanos-Águila, J. R. Maze, and F. Munoz, "First-principles identification of single photon emitters based on carbon clusters in hexagonal boron nitride," J. Phys. Chem. A **125**, 1325–1335 (2021).
[271]C. Cholsuk, S. Suwanna, and T. Vogl, "Tailoring the emission wavelength of color centers in hexagonal boron nitride for quantum applications," Nanomaterials **12**, 2427 (2022).
[272]C. Cholsuk, A. Zand, A. Çakan, and T. Vogl, "The hBN defects database: a theoretical compilation of color centers in hexagonal boron nitride," J. Phys. Chem. C **128**, 12716–12725 (2024).
[273]A. Chatterjee, A. Biswas, A. S. Fuhr, T. Terlier, B. G. Sumpter, P. M. Ajayan, I. Aharonovich, and S. Huang, "Room-temperature high-purity single-photon emission from carbon-doped boron nitride thin films," Sci. Adv. **11**, 2899 (2025).
[274]M. Koperski, D. Vaclavkova, K. Watanabe, T. Taniguchi, K. S. Novoselov, and M. Potemski, "Midgap radiative centers in carbon-enriched hexagonal boron nitride," Proc. Natl. Acad. Sci. U. S. A. **117**, 13214–13219 (2020).
[275]V. Karanikolas, T. Iwasaki, J. Henzie, N. Ikeda, Y. Yamauchi, Y. Wakayama, T. Kuroda, K. Watanabe, and T. Taniguchi, "Plasmon-triggered ultrafast operation of color centers in hexagonal boron nitride layers," ACS Omega **8**, 14641–14647 (2023).
[276]G. I. López-Morales, M. Li, A. Hampel, S. Satapathy, N. V. Proscia, H. Jayakumar, A. Lozovoi, D. Pagliero, G. E. Lopez, V. M. Menon, J. Flick, and C. A. Meriles, "Investigation of photon emitters in Ce-implanted hexagonal boron nitride," Opt. Mater. Express **11**, 3478 (2021).
[277]M. Hua, W.-Y. Chen, H. Hou, V. S. C. Kolluru, M. Chan, H. Liu, T. E. E. Gage, J.-M. Zuo, B. T. Diroll, and J. Wen, "Deterministic fabrication of highly reproducible monochromatic quantum emitters in hexagonal boron nitride," Nanoscale **17**, 20081–20088 (2025).
[278]X. Gao, S. Vaidya, K. Li, Z. Ge, S. Dikshit, S. Zhang, P. Ju, K. Shen, Y. Jin, Y. Ping, and T. Li, "Single nuclear spin detection and control in a van der Waals material," Nature **643**, 943–949 (2025).
[279]A. Gritsch, L. Weiss, J. Früh, S. Rinner, and A. Reiserer, "Narrow optical transitions in erbium-implanted silicon waveguides," Phys. Rev. X **12**, 041009 (2022).
[280]G. García-Arellano, G. I. López Morales, Z. Shotan, R. Kumar, B. Murdin, C. E. Dreyer, and C. A. Meriles, "Erbium-implanted WS_2 flakes with room-temperature photon emission at telecom wavelengths," Nano Lett. **25**, 9070–9076 (2025).
[281]S. Nedić, K. Yamamura, A. Gale, I. Aharonovich, and M. Toth, "Electron beam restructuring of quantum emitters in hexagonal boron nitride," Adv. Opt. Mater. **12**, 2400908 (2024).
[282]O. Cretu, H.-P. Komsa, O. Lehtinen, G. Algara-Siller, U. Kaiser, K. Suenaga, and A. V. Krasheninnikov, "Experimental observation of boron nitride chains," ACS Nano **8**, 11950–11957 (2014).
[283]R. Bourrellier, S. Meuret, A. Tararan, O. Stéphan, M. Kociak, L. H. G. Tizei, and A. Zobelli, "Bright UV single photon emission at point defects in h-BN," Nano Lett. **16**, 4317–4321 (2016).
[284]A. Kumar, C. Cholsuk, A. Zand, M. N. Mishuk, T. Matthes, F. Eilenberger, S. Suwanna, and T. Vogl, "Localized creation of yellow single photon emitting carbon complexes in hexagonal boron nitride," APL Mater. **11**, 071108 (2023).
[285]C. Piccinini, A. Paralikis, J. F. Neto, A. A. Madigawa, P. Wyborski, V. Remesh, L. Vannucci, N. Gregersen, and B. Munkhbat, "High-purity and stable single-photon emission in bilayer WSe_2 via phonon-assisted excitation," Commun. Phys. **8**, 158 (2025).
[286]A. Branny, G. Wang, S. Kumar, C. Robert, B. Lassagne, X. Marie, B. D. Gerardot, and B. Urbaszek, "Discrete quantum dot like emitters in monolayer $MoSe_2$: Spatial mapping, magneto-optics, and charge tuning," Appl. Phys. Lett. **108**, 142101 (2016).
[287]M. R. Rosenberger, H.-J. J. Chuang, K. M. McCreary, A. T. Hanbicki, S. V. Sivaram, and B. T. Jonker, "Nano-squeegee for the creation of clean 2D material interfaces," ACS Appl. Mater. Interfaces **10**, 10379–10387 (2018).
[288]T. Grünleitner, A. Henning, M. Bissolo, M. Zengerle, L. Gregoratti, M. Amati, P. Zeller, J. Eichhorn, A. V. Stier, A. W. Holleitner, J. J. Finley, and I. D. Sharp, "Real-time investigation of sulfur vacancy generation and passivation in monolayer molybdenum disulfide via *in situ* x-ray photoelectron spectromicroscopy," ACS Nano **16**, 20364–20375 (2022).
[289]W. Wang, L. O. Jones, J. S. Chen, G. C. Schatz, and X. Ma, "Utilizing ultraviolet photons to generate single-photon emitters in semiconductor monolayers," ACS Nano **16**, 21240–21247 (2022).
[290]N. S. McIntyre, P. A. Spevack, G. Beamson, and D. Briggs, "Effects of argon ion bombardment on basal plane and polycrystalline MoS_2," Surf. Sci. **237**, L390–L397 (1990).
[291]B. Huang, F. Tian, Y. Shen, M. Zheng, Y. Zhao, J. Wu, Y. Liu, S. J. Pennycook, and J. T. L. Thong, "Selective engineering of chalcogen defects in MoS_2 by low-energy helium plasma," ACS Appl. Mater. Interfaces **11**, 24404–24411 (2019).
[292]M. Donarelli, F. Bisti, F. Perrozzi, and L. Ottaviano, "Tunable sulfur desorption in exfoliated MoS_2 by means of thermal annealing in ultra-high vacuum," Chem. Phys. Lett. **588**, 198–202 (2013).
[293]X. Zhang, S. Wang, C.-K. Lee, C.-M. Cheng, J.-C. Lan, X. Li, J. Qiao, and X. Tao, "Unravelling the effect of sulfur vacancies on the electronic structure of the MoS_2 crystal," Phys. Chem. Chem. Phys. **22**, 21776–21783 (2020).
[294]C. Kastl, R. J. Koch, C. T. Chen, J. Eichhorn, S. Ulstrup, A. Bostwick, C. Jozwiak, T. R. Kuykendall, N. J. Borys, F. M. Toma, S. Aloni, A. Weber-Bargioni, E. Rotenberg, and A. M. Schwartzberg, "Effects of defects on band structure and excitons in WS_2 revealed by nanoscale photoemission spectroscopy," ACS Nano **13**, 1284–1291 (2019).
[295]J. Klein, A. Kerelsky, M. Lorke, M. Florian, F. Sigger, J. Kiemle, M. C. Reuter, T. Taniguchi, K. Watanabe, J. J. Finley, A. N. Pasupathy, A. W. Holleitner, F. M. Ross, and U. Wurstbauer, "Impact of substrate induced band tail states on the electronic and optical properties of MoS_2," Appl. Phys. Lett. **115**, 261603 (2019).

02 July 2026 15:24:17

© Author(s) 2025

[296]A. Hötger, T. Amit, J. Klein, K. Barthelmi, T. Pelini, A. Delhomme, S. Rey, M. Potemski, C. Faugeras, G. Cohen, D. Hernangómez-Pérez, T. Taniguchi, K. Watanabe, C. Kastl, J. J. Finley, S. Refaely-Abramson, A. W. Holleitner, and A. V. Stier, "Spin-defect characteristics of single sulfur vacancies in monolayer MoS_2," npj 2D Mater. Appl. **7**, 30 (2023).

[297]S. Varghese, S. Wang, B. Neupane, B. Bhandari, Y. Jiang, R. Gonzalez Rodriguez, S. Krylyuk, A. V. Davydov, H. Yan, Y. Wang, A. B. Kaul, J. Cui, and Y. Lin, "Quantum emitters induced by high pressure and UV laser irradiation in multilayer GaSe," ACS Omega **10**, 7466–7473 (2025).

[298]J. Strand, L. Larcher, and A. L. Shluger, "Properties of intrinsic point defects and dimers in hexagonal boron nitride," J. Phys.:Condens. Matter **32**, 055706 (2020).

[299]T. Vogl, M. W. Doherty, B. C. Buchler, Y. Lu, and P. K. Lam, "Atomic localization of quantum emitters in multilayer hexagonal boron nitride," Nanoscale **11**, 14362–14371 (2019).

[300]T. Zabelotsky, S. Singh, G. Haim, R. Malkinson, S. Kadkhodazadeh, I. P. Radko, I. Aharonovich, H. Steinberg, K. Berg-Sørensen, A. Huck, T. Taniguchi, K. Watanabe, and N. Bar-Gill, "Creation of boron vacancies in hexagonal boron nitride exfoliated from bulk crystals for quantum sensing," ACS Appl. Nano Mater. **6**, 21671–21678 (2023).

[301]R. Klaiss, J. Ziegler, D. Miller, K. Zappitelli, K. Watanabe, T. Taniguchi, and B. Alemán, "Uncovering the morphological effects of high-energy Ga+focused ion beam milling on hBN single-photon emitter fabrication," J. Chem. Phys. **157**, 074703 (2022).

[302]S. Li and A. Gali, "Identification of an oxygen defect in hexagonal boron nitride," J. Phys. Chem. Lett. **13**, 9544–9551 (2022).

[303]H. Liang, Y. Chen, L. Loh, N. L. Q. Cheng, D. Litvinov, C. Yang, Y. Chen, Z. Zhang, K. Watanabe, T. Taniguchi, M. Koperski, S. Y. Quek, M. Bosman, G. Eda, and A. A. Bettiol, "Site-selective creation of blue emitters in hexagonal boron nitride," ACS Nano **19**, 15130–15138 (2025).

[304]F. Murzakhanov, B. Yavkin, G. Mamin, S. Orlinskii, I. Mumdzhi, I. Gracheva, B. Gabbasov, A. Smirnov, V. Davydov, and V. Soltamov, "Creation of negatively charged boron vacancies in hexagonal boron nitride crystal by electron irradiation and mechanism of inhomogeneous broadening of boron vacancy-related spin resonance lines," Nanomaterials **11**, 1373 (2021).

[305]T. T. Tran, C. Elbadawi, D. Totonjian, C. J. Lobo, G. Grosso, H. Moon, D. R. Englund, M. J. Ford, I. Aharonovich, and M. Toth, "Robust multicolor single photon emission from point defects in hexagonal boron nitride," ACS Nano **10**, 7331–7338 (2016).

[306]C. Fournier, K. Watanabe, T. Taniguchi, J. Barjon, S. Buil, J.-P. Hermier, and A. Delteil, "Investigating the fast spectral diffusion of a quantum emitter in hBN using resonant excitation and photon correlations," Phys. Rev. B **107**, 195304 (2023).

[307]D. Gérard, S. Buil, J-p Hermier, and A. Delteil, "Crossover from inhomogeneous to homogeneous response of a resonantly driven hBN quantum emitter," Phys. Rev. B **111**, 085304 (2025).

[308]J. Horder, S. J. U. White, A. Gale, C. Li, K. Watanabe, T. Taniguchi, M. Kianinia, I. Aharonovich, and M. Toth, "Coherence properties of electron-beam-activated emitters in hexagonal boron nitride under resonant excitation," Phys. Rev. Appl. **18**, 064021 (2022).

[309]D. Wong, J. Velasco, L. Ju, J. Lee, S. Kahn, H.-Z. Tsai, C. Germany, T. Taniguchi, K. Watanabe, A. Zettl, F. Wang, and M. F. Crommie, "Characterization and manipulation of individual defects in insulating hexagonal boron nitride using scanning tunnelling microscopy," Nat. Nanotechnol. **10**, 949–953 (2015).

[310]F. Libbi, P. M. M. C. De Melo, Z. Zanolli, M. J. Verstraete, and N. Marzari, "Phonon-assisted luminescence in defect centers from many-body perturbation theory," Phys. Rev. Lett. **128**, 167401 (2022).

[311]L. Weston, D. Wickramaratne, M. Mackoit, A. Alkauskas, and C. G. Van de Walle, "Native point defects and impurities in hexagonal boron nitride," Phys. Rev. B **97**, 214104 (2018).

[312]J. Fraunié, T. Clua-Provost, S. Roux, Z. Mu, A. Delpoux, G. Seine, D. Lagarde, K. Watanabe, T. Taniguchi, X. Marie, T. Poirier, J. H. Edgar, J. Grisolia, B. Lassagne, A. Claverie, V. Jacques, and C. Robert, "Charge state tuning of spin defects in hexagonal boron nitride," Nano Lett. **25**, 5836–5842 (2025).

[313]J. R. Reimers, J. Shen, M. Kianinia, C. Bradac, I. Aharonovich, M. J. Ford, and P. Piecuch, "Photoluminescence, photophysics, and photochemistry of the V_B^- defect in hexagonal boron nitride," Phys. Rev. B **102**, 144105 (2020).

[314]N. Mathur, A. Mukherjee, X. Gao, J. Luo, B. A. McCullian, T. Li, A. N. Vamivakas, and G. D. Fuchs, "Excited-state spin-resonance spectroscopy of V_B^- defect centers in hexagonal boron nitride," Nat. Commun. **13**, 3233 (2022).

[315]P. Yu, H. Sun, M. Wang, T. Zhang, X. Ye, J. Zhou, H. Liu, C.-J. Wang, F. Shi, Y. Wang, and J. Du, "Excited-state spectroscopy of spin defects in hexagonal boron nitride," Nano Lett. **22**, 3545–3549 (2022).

[316]B. Whitefield, M. Toth, I. Aharonovich, J. Tetienne, and M. Kianinia, "Magnetic field sensitivity optimization of negatively charged boron vacancy defects in hBN," Adv. Quantum Tech. **8**, 2300118 (2025).

[317]A. Haykal, R. Tanos, N. Minotto, A. Durand, F. Fabre, J. Li, J. H. Edgar, V. Ivády, A. Gali, T. Michel, A. Dréau, B. Gil, G. Cassabois, and V. Jacques, "Decoherence of V_B^- spin defects in monoisotopic hexagonal boron nitride," Nat. Commun. **13**, 4347 (2022).

[318]P. Konrad, M. Kianinia, L. Spencer, A. Sperlich, L. Hein, S. Steinicke, I. Aharonovich, and V. Dyakonov, "Intermediate excited state relaxation dynamics of boron-vacancy spin defects in hexagonal boron nitride," arXiv:2503.22815 (2025).

[319]S. S. Mohajerani, S. Chen, A. Alaei, T. Chou, N. Liu, Y. Ma, L. Xiao, S. S. Lee, E.-H. Yang, and S. Strauf, "Narrowband quantum light emission from oxygen-related color centers in hexagonal boron nitride," ACS Photonics **11**, 2359–2367 (2024).

[320]K. Li, T. J. Smart, and Y. Ping, "Carbon trimer as a 2 eV single-photon emitter candidate in hexagonal boron nitride: A first-principles study," Phys. Rev. Mater. **6**, L042201 (2022).

[321]O. Golami, K. Sharman, R. Ghobadi, S. C. Wein, H. Zadeh-Haghighi, C. Gomes da Rocha, D. R. Salahub, and C. Simon, "*Ab initio* and group theoretical study of properties of a carbon trimer defect in hexagonal boron nitride," Phys. Rev. B **105**, 184101 (2022).

[322]A. Sajid and K. S. Thygesen, "V_NC_B defect as source of single photon emission from hexagonal boron nitride," 2D Mater. **7**, 031007 (2020).

[323]A. Nazir and D. P. S. McCutcheon, "Modelling exciton–phonon interactions in optically driven quantum dots," J. Phys.:Condens. Matter **28**, 103002 (2016).

[324]J. Iles-Smith, D. P. S. McCutcheon, A. Nazir, and J. Mørk, "Phonon scattering inhibits simultaneous near-unity efficiency and indistinguishability in semiconductor single-photon sources," Nat. Photonics **11**, 521–526 (2017).

[325]P. Tieben and A. W. Schell, "Fingerprinting defects in hexagonal boron nitride via multi-phonon excitation," Adv. Opt. Mater. **12**, 2302700 (2024).

[326]S. X. Li, T. Ichihara, H. Park, G. He, D. Kozawa, Y. Wen, V. B. Koman, Y. Zeng, M. Kuehne, Z. Yuan, S. Faucher, J. H. Warner, and M. S. Strano, "Prolonged photostability in hexagonal boron nitride quantum emitters," Commun. Mater. **4**, 19 (2023).

[327]T. W. Tang, R. Ritika, M. Tamtaji, H. Liu, Y. Hu, Z. Liu, P. R. Galligan, M. Xu, J. Shen, J. Wang, J. You, Y. Li, G. Chen, I. Aharonovich, and Z. Luo, "Structured-defect engineering of hexagonal boron nitride for identified visible single-photon emitters," ACS Nano **19**, 8509–8519 (2025).

[328]H. L. Stern, R. Wang, Y. Fan, R. Mizuta, J. C. Stewart, L.-M. Needham, T. D. Roberts, R. Wai, N. S. Ginsberg, D. Klenerman, S. Hofmann, and S. F. Lee, "Spectrally resolved photodynamics of individual emitters in large-area monolayers of hexagonal boron nitride," ACS Nano **13**, 4538–4547 (2019).

[329]M. Neumann, X. Wei, L. Morales-Inostroza, S. Song, S.-G. Lee, K. Watanabe, T. Taniguchi, S. Götzinger, and Y. H. Lee, "Organic molecules as origin of visible-range single photon emission from hexagonal boron nitride and mica," ACS Nano **17**, 11679–11691 (2023).

[330]C. Toninelli, I. Gerhardt, A. S. Clark, A. Reserbat-Plantey, S. Götzinger, Z. Ristanović, M. Colautti, P. Lombardi, K. D. Major, I. Deperasińska, W. H. Pernice, F. H. L. Koppens, B. Kozankiewicz, A. Gourdon, V. Sandoghdar, and M. Orrit, "Single organic molecules for photonic quantum technologies," Nat. Mater. **20**, 1615–1628 (2021).

[331]C. Eggeling, J. Widengren, R. Rigler, and C. A. M. Seidel, "Photobleaching of fluorescent dyes under conditions used for single-molecule detection: evidence of two-step photolysis," Anal. Chem. **70**, 2651–2659 (1998).

[332]C. Fournier, S. Roux, K. Watanabe, T. Taniguchi, S. Buil, J. Barjon, J.-P. Hermier, and A. Delteil, "Two-photon interference from a quantum emitter in hexagonal boron nitride," Phys. Rev. Appl. **19**, L041003 (2023).

02 July 2026 15:24:17

© Author(s) 2025

[333]T. Taniguchi and K. Watanabe, "Synthesis of high-purity boron nitride single crystals under high pressure by using Ba–BN solvent," J. Cryst. Growth **303**, 525–529 (2007).
[334]T. Pelini, C. Elias, R. Page, L. Xue, S. Liu, J. Li, J. H. Edgar, A. Dréau, V. Jacques, P. Valvin, B. Gil, and G. Cassabois, "Shallow and deep levels in carbon-doped hexagonal boron nitride crystals," Phys. Rev. Mater. **3**, 94001 (2019).
[335]T. Q. P. Vuong, G. Cassabois, P. Valvin, A. Ouerghi, Y. Chassagneux, C. Voisin, and B. Gil, "Phonon-photon mapping in a color center in hexagonal boron nitride," Phys. Rev. Lett. **117**, 97402 (2016).
[336]M. Winter, M. H. E. Bousquet, D. Jacquemin, I. Duchemin, and X. Blase, "Photoluminescent properties of the carbon-dimer defect in hexagonal boron-nitride: A many-body finite-size cluster approach," Phys. Rev. Mater. **5**, 095201 (2021).
[337]P. Auburger and A. Gali, "Towards ab initio identification of paramagnetic substitutional carbon defects in hexagonal boron nitride acting as quantum bits," Phys. Rev. B **104**, 75410 (2021).
[338]J. Horder, D. Scognamiglio, Á. Ganyecz, V. Ivadáy, M. Kianinia, M. Toth, I. Aharonovich, V. Ivády, N. Coste, M. Kianinia, M. Toth, and I. Aharonovich, "Near-coherent quantum emitters in hexagonal boron nitride with discrete polarization axes," ACS Photonics **11**, 3954–3959 (2024).
[339]Á. Ganyecz, R. Babar, Z. Benedek, I. Aharonovich, G. Barcza, and V. Ivády, "First-principles theory of the nitrogen interstitial in hBN: A plausible model for the blue emitter," Nanoscale **16**, 4125–4139 (2024).
[340]A. Gale, M. Kianinia, J. Horder, C. Tweedie, M. Singhal, D. Scognamiglio, J. Qi, K. Li, C. Verdi, I. Aharonovich, M. Toth, K. Liu, C. Verdi, I. Aharonovich, and M. Toth, "Quantum emitters in rhombohedral boron nitride," Adv. Opt. Mater. e00593 (published online, 2025).
[341]M. Maciaszek and L. Razinkovas, "Blue quantum emitter in hexagonal boron nitride and a carbon chain tetramer: A first-principles study," ACS Appl. Nano Mater. **7**, 18979–18985 (2024).
[342]W. Luo, A. A. Puretzky, B. J. Lawrie, Q. Tan, H. Gao, Z. Chen, A. V. Sergienko, A. K. Swan, L. Liang, and X. Ling, "Deterministic localization of strain-induced single-photon emitters in multilayer GaSe," ACS Photonics **10**, 2530–2539 (2023).
[343]H. Geng, J. Tang, Y. Wu, Y. Yu, J. R. Guest, and R. Zhang, "Imaging valley excitons in a 2D semiconductor with scanning tunneling microscope-induced luminescence," ACS Nano **18**, 8961–8970 (2024).
[344]L. E. P. López, A. Rosławska, F. Scheurer, S. Berciaud, and G. Schull, "Tip-induced excitonic luminescence nanoscopy of an atomically resolved van der Waals heterostructure," Nat. Mater. **22**, 482–488 (2023).
[345]R. Gutzler, M. Garg, C. R. Ast, K. Kuhnke, and K. Kern, "Light–matter interaction at atomic scales," Nat. Rev. Phys. **3**, 441–453 (2021).
[346]A. Rosławska, C. C. Leon, A. Grewal, P. Merino, K. Kuhnke, and K. Kern, "Atomic-scale dynamics probed by photon correlations," ACS Nano **14**, 6366–6375 (2020).
[347]J. H. Coombs, J. K. Gimzewski, B. Reihl, J. K. Sass, and R. R. Schlittler, "Photon emission experiments with the scanning tunnelling microscope," J. Microsc. **152**, 325–336 (1988).
[348]R. Berndt, R. Gaisch, J. K. Gimzewski, B. Reihl, R. R. Schlittler, W. D. Schneider, and M. Tschudy, "Photon emission at molecular resolution induced by a scanning tunneling microscope," Science **262**, 1425–1427 (1993).
[349]G. V. Nazin, X. H. Qiu, and W. Ho, "Atomic engineering of photon emission with a scanning tunneling microscope," Phys. Rev. Lett. **90**, 216110 (2003).
[350]X. H. Qiu, G. V. Nazin, W. Ho, and W. Hot, "Vibrationally resolved fluorescence excited with submolecular precision," Science **299**, 542–546 (2003).
[351]F.-F. Kong, X.-J. Tian, Y. Y. Zhang, Y.-J. Yu, S.-H. Jing, Y. Y. Zhang, G.-J. Tian, Y. Luo, J.-L. Yang, Z.-C. Dong, and J. G. Hou, "Probing intramolecular vibronic coupling through vibronic-state imaging," Nat. Commun. **12**, 1280 (2021).
[352]J. Doležal, A. Sagwal, R. C. de Campos Ferreira, and M. Švec, "Single-molecule time-resolved spectroscopy in a tunable STM nanocavity," Nano Lett. **24**, 1629–1634 (2024).
[353]L. Zhang, Y.-J. Yu, L.-G. Chen, Y. Y. Luo, B. Yang, F.-F. Kong, G. Chen, Y. Zhang, Q. Zhang, Y. Y. Luo, J.-L. Yang, Z.-C. Dong, and J. G. Hou, "Electrically driven single-photon emission from an isolated single molecule," Nat. Commun. **8**, 580 (2017).
[354]C. C. Leon, O. Gunnarsson, D. G. de Oteyza, A. Rosławska, P. Merino, A. Grewal, K. Kuhnke, and K. Kern, "Single photon emission from a plasmonic light source driven by a local field-induced coulomb blockade," ACS Nano **14**, 4216–4223 (2020).
[355]Q. Schaeverbeke, R. Avriller, T. Frederiksen, and F. Pistolesi, "Single-photon emission mediated by single-electron tunneling in plasmonic nanojunctions," Phys. Rev. Lett. **123**, 246601 (2019).
[356]K. Kaiser, L.-A. Lieske, J. Repp, and L. Gross, "Charge-state lifetimes of single molecules on few monolayers of NaCl," Nat. Commun. **14**, 4988 (2023).
[357]L. Bobzien, J. Allerbeck, N. Krane, A. Ortega-Guerrero, Z. Wang, D. E. C. Figueroa, C. Dong, C. A. Pignedoli, J. A. Robinson, and B. Schuler, "Layer-dependent charge-state lifetime of single Se vacancies in WSe_2," Phys. Rev. Lett. **134**, 076201 (2025).
[358]K. Nisi, J. C. Thomas, S. Levashov, E. Mitterreiter, T. Taniguchi, K. Watanabe, S. Aloni, T. R. Kuykendall, J. Eichhorn, A. W. Holleitner, A. Weber-Bargioni, and C. Kastl, "Scanning probe spectroscopy of sulfur vacancies and MoS_2 monolayers in side-contacted van der Waals heterostructures," 2D Mater. **12**, 015023 (2025).
[359]K. Miwa, H. Imada, M. Imai-Imada, K. Kimura, M. Galperin, and Y. Kim, "Many-body state description of single-molecule electroluminescence driven by a scanning tunneling microscope," Nano Lett. **19**, 2803–2811 (2019).
[360]S. Susarla, M. H. Naik, D. D. Blach, J. Zipfel, T. Taniguchi, K. Watanabe, L. Huang, R. Ramesh, F. H. da Jornada, S. G. Louie, P. Ercius, and A. Raja, "Hyperspectral imaging of exciton confinement within a moiré unit cell with a subnanometer electron probe," Science **378**, 1235–1239 (2022).
[361]H. Sun, Q. Yang, J. Wang, M. Ding, M. Cheng, L. Liao, C. Cai, Z. Chen, X. Huang, Z. Wang, Z. Xu, W. Wang, K. Liu, L. Liu, X. Bai, J. Chen, S. Meng, and L. Wang, "Unveiling sulfur vacancy pairs as bright and stable color centers in monolayer WS_2," Nat. Commun. **15**, 9476 (2024).
[362]M. Ziatdinov, O. Dyck, A. Maksov, X. Li, X. Sang, K. Xiao, R. R. Unocic, R. Vasudevan, S. Jesse, and S. V. Kalinin, "Deep learning of atomically resolved scanning transmission electron microscopy images: Chemical identification and tracking local transformations," ACS Nano **11**, 12742–12752 (2017).
[363]C.-H. Lee, A. Khan, D. Luo, T. P. Santos, C. Shi, B. E. Janicek, S. Kang, W. Zhu, N. A. Sobh, A. Schleife, B. K. Clark, and P. Y. Huang, "Deep learning enabled strain mapping of single-atom defects in two-dimensional transition metal dichalcogenides with sub-picometer precision," Nano Lett. **20**, 3369–3377 (2020).
[364]S. Yang, W. Choi, B. W. Cho, F. O. Agyapong-Fordjour, S. Park, S. J. Yun, H. Kim, Y. Han, Y. H. Lee, K. K. Kim, and Y. Kim, "Deep learning-assisted quantification of atomic dopants and defects in 2D materials," Adv. Sci. **8**, 2101099 (2021).
[365]K. M. Roccapriore, M. G. Boebinger, J. Klein, M. Weile, F. Ross, M. Ziatdinov, R. R. Unocic, and S. V. Kalinin, "AI-enabled automation of atomic manipulation and characterization in the STEM," Microsc. Microanal. **29**, 1366–1367 (2023).
[366]M. Weile, S. Grytsiuk, A. Penn, D. G. Chica, X. Roy, K. Mosina, Z. Sofer, J. Schiøtz, S. Helveg, M. Rösner, F. M. Ross, and J. Klein, "Defect complexes in CrSBr revealed through electron microscopy and deep learning," Phys. Rev. X **15**, 021080 (2025).
[367]K. M. Roccapriore, F. M. Ross, and J. Klein, "Quantitative electron beam-single atom interactions enabled by sub-20-pm precision targeting," Adv. Sci. e02551 (published online, 2025).
[368]A. Dietrich, M. Bürk, E. S. Steiger, L. Antoniuk, T. T. Tran, M. Nguyen, I. Aharonovich, F. Jelezko, and A. Kubanek, "Observation of Fourier transform limited lines in hexagonal boron nitride," Phys. Rev. B **98**, 081414 (2018).
[369]A. Dietrich, M. W. Doherty, I. Aharonovich, and A. Kubanek, "Solid-state single photon source with Fourier transform limited lines at room temperature," Phys. Rev. B **101**, 81401 (2020).
[370]H. Akbari, S. Biswas, P. K. Jha, J. Wong, B. Vest, and H. A. Atwater, "Lifetime-limited and tunable quantum light emission in h-BN via electric field modulation," Nano Lett. **22**, 7798–7803 (2022).
[371]A. L. Exarhos, D. A. Hopper, R. N. Patel, M. W. Doherty, and L. C. Bassett, "Magnetic-field-dependent quantum emission in hexagonal boron nitride at room temperature," Nat. Commun. **10**, 222 (2019).
[372]I. Gasparutti, S. H. Song, M. Neumann, X. Wei, K. Watanabe, T. Taniguchi, and Y. H. Lee, "How clean is clean? Recipes for van der Waals heterostructure cleanliness assessment," ACS Appl. Mater. Interfaces **12**, 7701–7709 (2020).

02 July 2026 15:24:17

© Author(s) 2025

[373]H. Wang, N. Stenger, P. Lyngby, M. Kuisma, J. Schiøtz, and K. S. Thygesen, "Two-dimensional materials as ideal substrates for molecular quantum emitters," Nano Lett. **25**, 9952–9959 (2025).
[374]R. Smit, A. Tebyani, J. Hameury, S. J. van der Molen, and M. Orrit, "Sharp zero-phonon lines of single organic molecules on a hexagonal boron-nitride surface," Nat. Commun. **14**, 7960 (2023).
[375]J. C. Thomas, W. Chen, Y. Xiong, B. A. Barker, J. Zhou, W. Chen, A. Rossi, N. Kelly, Z. Yu, D. Zhou, S. Kumari, E. S. Barnard, J. A. Robinson, M. Terrones, A. Schwartzberg, D. F. Ogletree, E. Rotenberg, M. M. Noack, S. Griffin, A. Raja, D. A. Strubbe, G.-M. Rignanese, A. Weber-Bargioni, and G. Hautier, "A substitutional quantum defect in WS_2 discovered by high-throughput computational screening and fabricated by site-selective STM manipulation," Nat. Commun. **15**, 3556 (2024).
[376]D. Groll, T. Kuhn, P. Machnikowski, D. Wigger, and T. Kuhn, "Controlling photoluminescence spectra of hBN color centers by selective phonon-assisted excitation: A theoretical proposal," Mater. Quantum Technol. **1**, 015004 (2021).
[377]M. K. Svendsen, S. Ali, N. Stenger, K. S. Thygesen, and J. Iles-Smith, "Signatures of non-Markovianity in cavity QED with color centers in two-dimensional materials," Phys. Rev. Res. **5**, L032037 (2023).
[378]T. K. Bracht, M. Cosacchi, T. Seidelmann, M. Cygorek, A. Vagov, V. M. Axt, T. Heindel, and D. E. Reiter, "Swing-up of quantum emitter population using detuned pulses," PRX Quantum **2**, 40354 (2021).
[379]Y. Karli, F. Kappe, V. Remesh, T. K. Bracht, J. Münzberg, S. Covre da Silva, T. Seidelmann, V. M. Axt, A. Rastelli, D. E. Reiter, and G. Weihs, "SUPER scheme in action: Experimental demonstration of red-detuned excitation of a quantum emitter," Nano Lett. **22**, 6567–6572 (2022).
[380]L. Vannucci, J. F. Neto, C. Piccinini, A. Paralikis, N. Gregersen, and B. Munkhbat, "Single-photon emitters in WSe_2: Critical role of phonons on excitation schemes and indistinguishability," Phys. Rev. B **109**, 245304 (2024).
[381]S. White, C. Stewart, A. S. Solntsev, C. Li, M. Toth, M. Kianinia, and I. Aharonovich, "Phonon dephasing and spectral diffusion of quantum emitters in hexagonal boron nitride," Optica **8**, 1153 (2021).
[382]K.-M. C. Fu, C. Santori, P. E. Barclay, L. J. Rogers, N. B. Manson, and R. G. Beausoleil, "Observation of the dynamic Jahn-Teller effect in the excited states of nitrogen-vacancy centers in diamond," Phys. Rev. Lett. **103**, 256404 (2009).
[383]D. Gérard, S. Buil, K. Watanabe, T. Taniguchi, J.-P. Hermier, and A. Delteil, "Resonance fluorescence and indistinguishable photons from a coherently driven B centre in hBN," arXiv:2506.16980 (2025).
[384]O. L. Krivanek, T. C. Lovejoy, N. Dellby, T. Aoki, R. W. Carpenter, P. Rez, E. Soignard, J. Zhu, P. E. Batson, M. J. Lagos, R. F. Egerton, and P. A. Crozier, "Vibrational spectroscopy in the electron microscope," Nature **514**, 209–212 (2014).
[385]C. A. Gadre, X. Yan, Q. Song, J. Li, L. Gu, H. Huyan, T. Aoki, S.-W. Lee, G. Chen, R. Wu, and X. Pan, "Nanoscale imaging of phonon dynamics by electron microscopy," Nature **606**, 292–297 (2022).
[386]Y.-J. Kim, L. D. Palmer, W. Lee, N. J. Heller, and S. K. Cushing, "Using electron energy-loss spectroscopy to measure nanoscale electronic and vibrational dynamics in a TEM," J. Chem. Phys. **159**, 50901 (2023).
[387]K. Venkatraman, B. D. A. Levin, K. March, P. Rez, and P. A. Crozier, "Vibrational spectroscopy at atomic resolution with electron impact scattering," Nat. Phys. **15**, 1237–1241 (2019).
[388]J. Madsen, P. Liu, J. Kling, J. B. Wagner, T. W. Hansen, O. Winther, and J. Schiøtz, "A deep learning approach to identify local structures in atomic-resolution transmission electron microscopy images," Adv. Theory Simul. **1**, 1800037 (2018).
[389]D. Propst, W. Joudi, M. Längle, J. Madsen, C. Kofler, B. M. Mayer, D. Lamprecht, C. Mangler, L. Filipovic, T. Susi, and J. Kotakoski, "Automated image acquisition and analysis of graphene and hexagonal boron nitride from pristine to highly defective and amorphous structures," Sci. Rep. **14**, 26939 (2024).
[390]A. M. Fox, "Solid-state quantum emitters," Adv. Quantum Tech. **8**, 2300390 (2025).
[391]L. Wang, I. Meric, P. Y. Huang, Q. Gao, Y. Gao, H. Tran, T. Taniguchi, K. Watanabe, L. M. Campos, D. A. Muller, J. Guo, P. Kim, J. Hone, K. L. Shepard, and C. R. Dean, "One-dimensional electrical contact to a two-dimensional material," Science **342**, 614–617 (2013).
[392]U. Chandni, K. Watanabe, T. Taniguchi, and J. P. Eisenstein, "Evidence for defect-mediated tunneling in hexagonal boron nitride-based junctions," Nano Lett. **15**, 7329–7333 (2015).
[393]S. Guo, S. Germanis, T. Taniguchi, K. Watanabe, F. Withers, and I. J. Luxmoore, "Electrically driven site-controlled single photon source," ACS Photonics **10**, 2549–2555 (2023).
[394]M. Grzeszczyk, K. Vaklinova, K. Watanabe, T. Taniguchi, K. S. Novoselov, and M. Koperski, "Electroluminescence from pure resonant states in hBN-based vertical tunneling junctions," Light. Sci. Appl. **13**, 155 (2024).
[395]G. Park, I. Zhigulin, H. Jung, J. Horder, K. Yamamura, Y. Han, H. Cho, H.-W. Jeong, K. Watanabe, T. Taniguchi, M. Oh, G.-H. Lee, M.-H. Jo, I. Aharonovich, and J. Kim, "Narrowband electroluminescence from color centers in hexagonal boron nitride," Nano Lett. **24**, 15268–15274 (2024).
[396]S. J. U. White, T. Yang, N. Dontschuk, C. Li, Z.-Q. Xu, M. Kianinia, A. Stacey, M. Toth, and I. Aharonovich, "Electrical control of quantum emitters in a Van der Waals heterostructure," Light. Sci. Appl. **11**, 186 (2022).
[397]S.-B. Song, S. Yoon, S. Y. Kim, S. Yang, S.-Y. Seo, S. Cha, H.-W. Jeong, K. Watanabe, T. Taniguchi, G.-H. Lee, J. S. Kim, M.-H. Jo, and J. Kim, "Deep-ultraviolet electroluminescence and photocurrent generation in graphene/hBN/graphene heterostructures," Nat. Commun. **12**, 7134 (2021).
[398]C. Steiner, R. Rahmel, F. Volmer, R. Windisch, L. H. Janssen, P. Pesch, K. Watanabe, T. Taniguchi, F. Libisch, B. Beschoten, C. Stampfer, and A. Kurzmann, "Current-induced brightening of vacancy-related emitters in hexagonal boron nitride," Phys. Rev. Res. **7**, L032037 (2025).
[399]M. Yu, D. Yim, H. Seo, and J. Lee, "Electrical charge control of h-BN single photon sources," 2D Mater. **9**, 035020 (2022).
[400]S. Wang, J. Wang, W. Zhao, F. Giustiniano, L. Chu, I. Verzhbitskiy, J. Zhou Yong, and G. Eda, "Efficient carrier-to-exciton conversion in field emission tunnel diodes based on MIS-type van der Waals heterostack," Nano Lett. **17**, 5156–5162 (2017).
[401]G. Noh, D. Choi, J.-H. Kim, D.-G. Im, Y.-H. Kim, H. Seo, and J. Lee, "Stark tuning of single-photon emitters in hexagonal boron nitride," Nano Lett. **18**, 4710–4715 (2018).
[402]A. Gale, D. Scognamiglio, I. Zhigulin, B. Whitefield, M. Kianinia, I. Aharonovich, and M. Toth, "Manipulating the charge state of spin defects in hexagonal boron nitride," Nano Lett. **23**, 6141–6147 (2023).
[403]I. Zhigulin, G. Park, K. Yamamura, K. Watanabe, T. Taniguchi, M. Toth, J. Kim, and I. Aharonovich, "Electrical generation of color centers in hexagonal boron nitride," ACS Appl. Mater. Interfaces **17**, 24129–24136 (2025).

02 July 2026 15:24:17

© Author(s) 2025